ADVANCES IN ATOMIC, MOLECULAR, AND OPTICAL PHYSICS, VOL. 47

FORMATION OF ULTRACOLD MOLECULES ($T \leq 200\ \mu K$) VIA PHOTOASSOCIATION IN A GAS OF LASER-COOLED ATOMS

FRANÇOISE MASNOU-SEEUWS and PIERRE PILLET
Laboratoire Aimé Cotton, Bât. 505, Campus d'Orsay, 91405 Orsay Cedex, France

Copyright © 2001 by Academic Press
All rights of reproduction in any form reserved.
ISBN 0-12-003847-1/ISSN 1049-250X/01 $35.00

I. Introduction

Interest in making cold ($T < 1$ K) and ultracold (T well below 1 mK) molecules has long been recognized; among the possible applications, we may cite ultrahigh-resolution spectroscopy measurements and metrology. Other applications can be considered, for instance the search for an elementary dipole moment in a paramagnetic molecule as a test of time-reversal symmetry (Kozlov and Ezhov, 1994; Hinds and Sangster, 1992; Sauer *et al.,* 1994). Threshold laws for molecular collisions at very low energies could also be investigated (Gray and Rice, 1985; Forrey *et al.,* 1989). More recently, the creation of a Bose–Einstein condensate of molecules has appeared as a new challenge (Timmermans *et al.,* 1999a,b, Wynar *et al.,* 2000, Koŝtrun *et al.,* 2000) while Julienne *et al.* (1998) have proposed creating a "molecular laser."

In 2000, an extensive review written by Bahns *et al.* on the formation of cold ($T \leq 1$ K) molecules gave a detailed description of possible applications to high-resolution spectroscopy, manipulation of molecules, cold collisions, production of cold trimers and larger clusters, and finally Bose–Einstein condensation. Non-optical cooling techniques were reviewed, including free-jet expansion and helium buffer gas cooling, leading to subkelvin temperatures. To reach the ultracold domain, i.e., submillikelvin temperatures, optical cooling techniques need to be considered. However, direct laser cooling of molecules does not seem a promising technique, and it appears more efficient first to cool the atoms and then make a molecule out of cold atoms.

Indeed, laser cooling and trapping of atoms is now a well-mastered technique, used in many applications such as atomic clocks. Temperatures below 10^{-6} K are "easily" reached. Among the very few attempts to generalize optical cooling to molecules, one may cite the deflection of a molecular beam achieved by Herman *et al.* in 1979, and the demonstration, by Djeu and Whitney (1981), of laser cooling by continuous anti-Stokes scattering, introduced long ago by Kastler (1950) as "luminorefrigeration." As discussed by Bahns *et al.* (1996), the main obstacle in this research direction is that a molecule is essentially a multilevel system whereas direct optical cooling requires a closed two-level system to recycle population. Cooling of an atom takes place via a large number of optical pumping cycles in which absorption and spontaneous emission transfer population from a lower level to an upper one and back, as indicated in Fig. 1 for the case of $Cs(6s) \rightarrow Cs(6p_{3/2})$

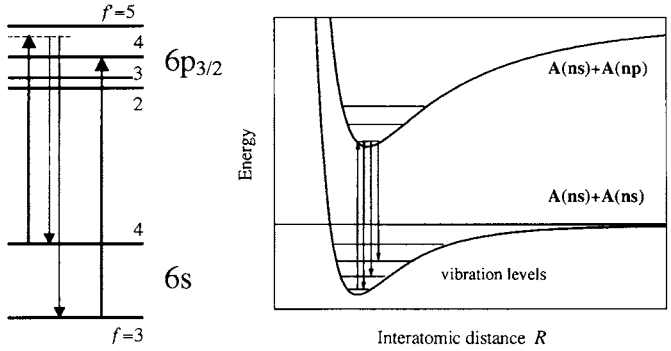

FIG. 1. (Left) Optical pumping scheme for cooling an atomic cesium sample, using the $6s \rightarrow 6p_{3/2}$ D_2 resonance line. In order to cool the atom, many cycles of absorption–spontaneous emission must be performed between the set of two ($6s$, $f = 4$) and ($6p_{3/2}$, $f = 5$) hyperfine sublevels, varying the red detuning of the laser. As the spontaneous emission may also be populating the ($6s$, $f = 3$) sublevel, a repumping laser is used to put the atoms back in the upper state. (Right) The difficulty of generalizing a direct cooling scheme to a molecule comes from the very large number of levels.

transition. The presence of neighboring levels, for instance, hyperfine sublevels, is a nuisance, as absorption can populate another level, causing population loss by spontaneous emission to the wrong lower level. When the number of neighboring levels is limited, as in the chosen example, this inconvenience is corrected for by use of repumping lasers. However, the number of repumping lasers has to stay within reasonable limits, so the procedure cannot be easily generalized to a multilevel system such as a molecule (Bahns *et al.*, 1996, 2000).

An alternative is to take advantage of the efficiency of laser cooling techniques for atoms: the idea is to cool free atoms in a first step, and then create ultracold molecules by photoassociation of atomic pairs. This reaction in the cold regime was first proposed by Thorsheim *et al.* (1987), and is indeed efficient to form cold molecules in excited electronic states. Photoassociation has already been demonstrated for all alkali atoms from Li to Cs: the first studies were for Na_2 (Lett *et al.*, 1993), followed by Rb_2 (Miller *et al.*, 1993), Li_2 (Abraham *et al.*, 1995), K_2 (Wang *et al.*, 1996), Cs_2 (Fioretti *et al.*, 1998), and NaK (Shaffer *et al.*, 1999). Photoassociation has been further demonstrated for hydrogen (Mosk *et al.*, 1999), helium (Herschbach *et al.*, 2000), and very recently for calcium (Zinner *et al.*, 2000), opening the way to photoassociation of other alkaline earth atoms. However, the lifetime of a photoassociated molecule is short, and after a few nanoseconds it decays by spontaneous emission, usually giving back a pair of atoms. The route to long-lived ultracold molecules depends on the occurrence of particular stabilization schemes in which spontaneous (or stimulated) emission also transfers population toward bound levels of the ground singlet or triplet state. Theoretical models have been proposed by Band and Julienne (1995), and by Côté and Dalgarno (1997, 1999). Other schemes have been found in experiments, and up

to now long-lived ultracold molecules have been observed for three alkali dimers Cs_2 (Fioretti *et al.*, 1998, 1999; Comparat *et al.*, 2000), K_2 (Nikolov *et al.*, 1999, 2000), and Rb_2 (Gabbanini *et al.*, 2000). Besides, Takekoshi *et al.* (1998, 1999) have observed and trapped ultracold Cs_2 molecules formed by a mechanism which may not be photoassociation and could be three-body collisions. Very recently, photoassociation experiments in a condensate have also been performed (Wynar *et al.*, 2000).

The field of cold molecules is experiencing very rapid evolution, both optical and nonoptical cooling techniques being developed: the fact that it is possible to write the present review chapter only one year after the previous one is a shining manifestation of this activity. We may say that spectacular progress has been accomplished during the last three years in three main directions, two with nonoptical techniques and one with optical techniques.

At present (autumn 2000), the most efficient ways of cooling molecules to a subkelvin temperatures *below 1 K but still above 100 mK,* with the perspective of reaching a few millikelvin in a near future are as follow:

- The *helium buffer gas cooling* technique developed by the Harvard team (Doyle *et al.*, 1995; Friedrich *et al.*, 1998, 1999; Weinstein *et al.*, 1998), together with magnetic trapping of molecules, as already described in the review of Bahns *et al.* (2000). CaH molecules, produced via laser ablation of solid CaH_2, are cooled by cryogenic ^{3}He down to a temperature of 400 mK, and a typical number of 10^8 molecules are currently loaded in a magnetic trap (deCarvalho *et al.*, 1999).
- The new *Stark decelerator* technique introduced by Gerard Meijer and his group in Nijmegen. They have demonstrated that a beam of neutral dipolar molecules (CO, ND_3) can be decelerated with a time-varying electric field (Bethlem *et al.*, 1999), bringing them to temperatures down to 350 mK. The ND_3 molecules are then trapped in a traveling potential well (Bethlem *et al.*, 2000a,b), with a density of $\sim 10^6$ cm^{-3} molecules in a volume of ~ 0.25 cm^3, so that the total number of trapped molecules is $\sim$400,000.

For the formation of *ultracold* molecules, i.e., at temperatures *well below 1 mK,* the photoassociation scheme in a sample of laser-cooled ultracold atoms is presently the best route, yielding a few millions of molecules at a translational temperature in the microkelvin range, which very recently were successfully trapped. The present review chapter will focus on this subject. The photoassociation reaction being a crucial step in the process, we shall first review the concept of photoassociation in Section II, emphasizing the physical ideas behind it. The next step is the formation of ground-state ultracold molecules by spontaneous emission, which requires a favorable branching ratio between bound–bound and bound–free transitions. This is a key point of the experiments, which will be described in Section III. Then the new theoretical methods developed to interpret such experiments will be described in Section IV. Finally, we shall report on the present status

of the comparison between theory and experiment in Section V, new possible schemes and the perspectives in the field being discussed in Section VI.

II. Physical Concepts in Photoassociation and Formation of Molecules

In photoassociation experiments, first suggested by Thorsheim *et al.* (1987), a pair of ultracold ground-state atoms absorbs a photon slightly ($\sim$ a fraction of cm^{-1} to 1000 cm^{-1}) red-detuned relative to the resonance line. Considering alkali atoms A(ns), and a laser red-detuned either to the D_1 or the D_2 resonance line, the reaction reads

$$A(ns) + A(ns) + E_c + \hbar(\omega_0^i - \delta_L) \rightarrow A_2^* * (\Omega_{u,g}(ns + np\,^2P_{1/2,3/2}); v, J). \quad (1)$$

In Eq. (1), we have considered excitation to an electronic potential curve, $\Omega_{u,g}$ in Hund's case c representation, hereafter labeled i. This curve is correlated to one of the two asymptotes $(ns + np_{1/2})$ and $(ns + np_{3/2})$, and $2\pi\omega_0$ is the frequency of the corresponding resonance line. $\hbar\delta_L$ is the energy detuning of the laser and $E_c \simeq k_B T$ the kinetic energy of the pair of atoms, where we have introduced the Boltzman constant k_B. In the present review, we shall not consider coupling between various excited potential curves, and we shall not include effects linked to the hyperfine structure of the atoms, therefore assuming a detuning larger than the hyperfine splitting both in the ground state and in the excited state.

From the conservation of energy and angular momentum, taking as the energy origin the asymptotic energy $E(ns + ns)$ of the ground-state potential, we may write (Pillet *et al.*, 1997) the resonant condition for population of a bound level with energy $E^i_{v,J}$ in an electronically excited potential curve i as

$$E_c + \hbar(\omega_0 - \delta_L) = E_{\text{Doppler}} + E_{\text{recoil}} + E^i_{v,J}. \quad (2)$$

In Eq. (2), E_c is the kinetic energy associated with the relative motion of the two atoms, $E_{\text{Doppler}} = \mathbf{V} \cdot \hbar\mathbf{k}_L$ is the energy associated with the first-order non-relativistic effect, and $E_{\text{recoil}} = (\hbar k_L)^2/8\mu$ is the recoil energy. We have introduced the reduced mass μ of the two atoms, the velocity $\mathbf{V}$ of the center of mass, and the wavevector $\mathbf{k}_L$ of the laser.

In the following, considering the energy D^i of the asymptote of the potential curve i, we shall often use the binding energy

$$\Delta^i_{v,J} = D^i - E^i(v, J), \quad (3)$$

$$\Delta^i_v = D^i - E^i(v, J = 0) = E^i_v. \quad (4)$$

The *resonance condition* can be written

$$\hbar\delta_L - \Delta_v^i = E_c - E_{\text{Doppler}} - E_{\text{recoil}}. \tag{5}$$

In this chapter, we shall consider temperatures of ~20 to 200 μK, so that $E_c \approx 1.4 \times 10^{-5}$ to 1.4×10^{-4} cm^{-1}, while in the case of cesium and for a red-detuning of 1 cm^{-1} = 29.9792458 GHz, the two other quantities are $E_{\text{Doppler}} \simeq 100$ kHz, $E_{\text{recoil}} \simeq 1$ kHz.

As we shall see below, since the typical accuracy of the photoassociation experiments is at present of the order of 150 MHz or 5×10^{-3} cm^{-1}, it is justified to neglect the right-hand side of Eq. (5) and write

$$\hbar\delta_L \approx \Delta_v^i. \tag{6}$$

The resonance condition is then an approximate equality between the binding energy of the vibrational level and the energy shift of the laser relative to the resonance line; this is why in photoassociation spectroscopy it is common to use the word "detuning" for the binding energy Δ_v^i of a level. This free–bound transition takes place under conditions somewhat unusual with respect to conventional molecular spectroscopy:

- Due to the ultracold conditions, the width of the statistical distribution of the kinetic energy E_c is markedly reduced. For a gas of atoms at thermal equilibrium with a temperature T, this width is of the order of $k_B T$. It corresponds to ~200 cm^{-1} at room temperature (300 K), yielding the well-known appearance of diffuse spectra, but only to ~2 MHz or 7×10^{-5} cm^{-1}, at 100 μK yielding well-resolved spectral lines, similar to bound–bound transitions. Besides, only a few partial waves have to be considered in the description of the initial continuum state, so the rotational structure is most often limited to $J < 7$–10, in contrast with conventional molecular spectra where a much larger number of rotational levels are usually observed. The interest of photoassociation as a new spectroscopic technique was reviewed by Stwalley and Wang (1999).
- In the final state, the vibrational motion extends up to very large internuclear distances, typically a few tens or even 100 a_0. At small detunings, detailed spectroscopic information has been obtained in the last decade on long-range molecular states correlated to the $(ns + np)$ dissociation limit of the alkali dimers, as described in the reviews by Stwalley and Wang (1999) and by Weiner *et al.* (1999).

In the present chapter, we shall not describe spectroscopy results but, rather, concentrate on the determination of the number of molecules formed in a given experiment. The first question is how many excited molecules are formed

per second by photoassociation. The absorption coefficient, and therefore the reaction rate, is expected to depend on the electric dipole matrix element between the wavefunctions in the initial and final states. We shall analyze the final state and the structure of the excited potential curves with asymptotic $-C_3^i/R^3$ behavior (see Section II.A). Close to the dissociation limit, vibrational levels in such potentials can be described with the Le Roy–Bernstein analytical law, presented in Section II.B, from which we shall deduce scaling laws for various matrix elements. The theoretical predictions for the photoassociation rate at low laser intensity will be summarized in Section II.C, and shown to be indeed proportional to the square of the overlap integral between the wavefunctions in the initial and final states. This integral will then be estimated by use of the reflection principle (Section II.D): within a Franck–Condon picture, reaction (1) can be understood as a vertical transition at a large distance $R_L = (C_3^i/\hbar\delta_L)^{1/3}$ from the continuum of the ground state to a vibrational level of the excited electronic state. In Section II.E, we shall discuss the variation of the amplitude of the ground-state wavefunction at $R = R_L$, and the presence of nodes. The efficiency of the photoassociation process will be estimated (Section II.F) as a function of physical parameters such as the detuning and the temperature. Then, in Section II.G we shall introduce the problem of controlling the decay of this short-lived excited molecule into a bound vibrational level of the ground state rather than into a pair of atoms.

A. Long-Range Alkali Dimer Molecules: A Pair of Atoms

The alkali atoms have been a benchmark for studies of thermal energy collisions, line broadening, and laser cooling; for alkali dimers, besides the photoassociation spectroscopy experiments quoted above, there exist much data obtained by conventional molecular spectroscopy experiments. Therefore the features of the long-range potentials correlated to the first asymptote have been investigated by many authors, starting with Dashevskaya *et al.* (1969), then Movre and Pichler (1977) as well as Bussery and Aubert-Frécon (1985a, 1985b), Julienne and Vigué (1991), Marinescu and Dalgarno (1995, 1996), Aubert-Frécon *et al.* (1998), all of them quoted in the review of Stwalley and Wang (1999). A few *ab initio* calculations exist at shorter distances (Foucrault *et al.,* 1992; Spies, 1989; Magnier *et al.,* 1993; Magnier and Millié, 1996).

One important feature is the existence of long-range wells: we shall focus on their particular behavior for the heavy alkali dimers. The concept of a "pure long-range molecule," in which the motion of the two atoms is confined to the region of large distances where only electrostatic interactions are active, any chemical interaction being negligible, was introduced by Stwalley *et al.* in 1978.

As an example, we reproduce in Fig. 2 the potential curves for interaction between two ground-state cesium atoms or, alternatively, a pair of Cs(6*s*) + Cs ($6p_{1/2,3/2}$) atoms. The hyperfine structure being neglected, such figures were

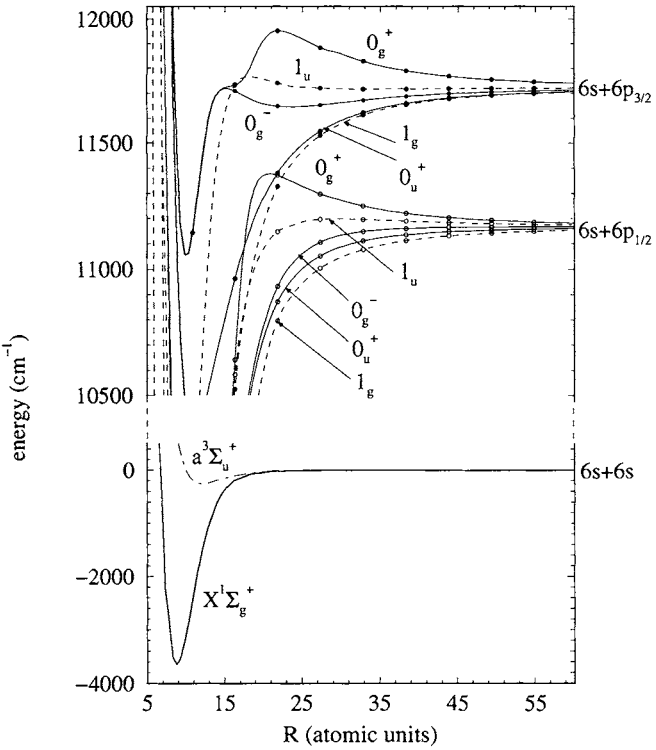

FIG. 2. Potentials of the Cs_2 molecule correlated to the $(6s + 6s)$ and $(6s + 6p^2P_{1/2,3/2})$ asymptotes. Hund's case c representation is used for the excited potentials, the $2g$ and $2u$ curves being not represented.

obtained by matching the *ab initio* potential curves from Meyer's group (Spies, 1989) with the long-range asymptotic expansion of Marinescu and Dalgarno (1995). Two facts are striking:

- Due to the dipole–dipole R^{-3} asymptotic interaction, the excited potential curves extend at much larger range than the ground-state curves with asymptotic R^{-6} behavior. This feature is general for homonuclear dimers, but would not exist for heteronuclear dimers where the excited curves also display R^{-6} behavior at long range. Let us note for homonuclear dimers the exception of the 0_g^- $(p_{1/2})$ curve for which the C_3^i coefficient is zero, so that the asymptote varies as R^{-6}.
- Two curves, of 0_g^- and 1_u symmetry, both correlated to the $(6s + 6p_{3/2})$ asymptote, display a double-well structure, with $\sim R^{-3}$ behavior in the entire region of the outer well so that the external side of the barrier has a gentle slope. Such wells exist for all homonuclear dimers, but we shall see that,

for the heavier ones (Rb_2, Cs_2), they are located at intermediate internuclear distances and play a key role in the formation of ultracold molecules. All symmetries have an exponential short-range repulsive potential for $R \leq 7a_0$, with a steep slope.

What is the explanation for the existence of those long-range wells? In the absence of fine-structure coupling, the long-range interaction between a ground-state atom A (ns) and an atom in the first excited state A (np) is dominated by the dipole–dipole interaction $-C_3/R^3$. As only the excited atom has a permanent dipole, this interaction corresponds to transfer of excitation between the two distant atoms. The C_3 coefficient is inversely proportional to the radiative lifetime of the (np) excited atomic level and can be obtained from the square of the dipole moment matrix element:

$$C_3 = |\langle ns|d_z|np\rangle|^2. \tag{7}$$

This definition is chosen by Julienne and Vigué (1991), and by Marinescu and Dalgarno (1995). In the work of Aubert-Frécon *et al.* (1998), all coefficients are related to a quantity $M^2 = |\langle ns|\mathbf{d}|np\rangle|^2$, which is $3 \times C_3$. The C_3 values computed by Marinescu and Dalgarno (1995) are 5.503 for Li, 6.13 for Na, 8.665 for K, 9.202 for Rb, and 10.47 for Cs. In numerical examples, we note that for the heavy alkalis C_3 is of the order of 10 a.u. In such a model all exchange interaction is assumed to be negligible, justifying the denomination "a pair of atoms." Dashevskaya *et al.* (1969) have classified the electronic states by their symmetry relative to exchange of excitation between the two atoms as

$$v = (-1)^S w, \tag{8}$$

where $S = 0, 1$ for singlet and triplet states, respectively, while $w = 1, -1$ for g and u states, respectively. The long-range dipole–dipole interaction depends on the orientation of the dipoles relative to each other and to the molecular axis, and is found to be

$$+2\frac{C_3}{R^3} \text{ for symmetric } {}^1\Sigma_g^+, {}^3\Sigma_u^+ \text{ states, } (\rightarrow \quad \leftarrow)$$

$$-2\frac{C_3}{R^3} \text{ for antisymmetric } {}^1\Sigma_u^+, {}^3\Sigma_g^+ \text{ states, } (\rightarrow \quad \rightarrow)$$

$$-\frac{C_3}{R^3} \text{ for symmetric } {}^1\Pi_g, {}^3\Pi_u \text{ states, } (\uparrow \quad \downarrow)$$

$$+\frac{C_3}{R^3} \text{ for antisymmetric } {}^1\Pi_u, {}^3\Pi_g \text{ states, } (\uparrow \quad \uparrow).$$

When the fine-structure splitting is introduced, in the Hund's case c representation, the adiabatic $\Omega_{g,u}$ states for a given internuclear distance R at long and

intermediate range are obtained by diagonalization of the fine-structure effective operator in the subspace of states with the same quantum numbers w and Ω. (As already stated, we restrict ourselves to distances such that the nuclear spins can be considered as uncoupled.) Movre and Pichler (1977) have given the secular equations for all symmetries. This leads, close to the dissociation limit, to asymptotic coefficients that will hereafter be noted C_3^i, and are linked by some angular factor to the C_3 coefficient defined above for interaction between an (ns) and an (np) atom. This angular factor can readily be obtained by considering the asymptotic expansion of a given $i = \Omega_{g,u}$ state on various Hund's case a states for which the long-range coefficient is $C_3, -C_3, 2C_3, -2C_3$ according to the symmetry as described in Eq. (8).

As an example, we shall consider the two $0_g^-(p_{3/2})$ and $0_g^-(p_{1/2})$ states obtained by diagonalization within the subspace of the $(1)^3\Sigma_g^+$ and $(1)^3\Pi_g$ states. For heavy alkali dimers due to the large value of the fine-structure splitting $(E^{at}(p_{3/2})\text{-}E^{at}(p_{1/2}) = 237.60\ \text{cm}^{-1}$ for Rb, $554.11\ \text{cm}^{-1}$ for Cs), it is more convenient to use Hund's case c representation at all internuclear distances; for all dimers, the latter representation must be used at large distances to obtain the correct dissociation limits $(ns + np_{1/2})$ and $(ns + np_{3/2})$. At any distance R, the two 0_g^- potential curves are obtained (Marinescu and Dalgarno, 1996; Aubert-Frécon *et al.*, 1998; Fioretti *et al.*, 1999) by diagonalization of the potential matrix

$$\mathbf{V}(R) = \begin{bmatrix} E^{at}(p_{3/2}) + \frac{2}{3}V_\Sigma(R) + \frac{1}{3}V_\Pi(R) & \frac{\sqrt{2}}{3}(V_\Sigma(R) - V_\Pi(R)) \\ \frac{\sqrt{2}}{3}(V_\Sigma(R) - V_\Pi(R)) & E^{at}(p_{1/2}) + \frac{1}{3}V_\Sigma(R) + \frac{2}{3}V_\Pi(R) \end{bmatrix}, \tag{9}$$

where $V_\Sigma(R)$ and $V_\Pi(R)$ are the potential curves of the $(1)\ ^3\Sigma_g^+$ and $(1)\ ^3\Pi_g$ electronic states, displayed in Fig. 3 for Cs_2 and both correlated to the $(ns + np)$ dissociation limit. In Hund's case c representation, the correct dissociation limits are obtained at energies $E^{at}(p_{3/2})$ and $E^{at}(p_{1/2})$. The coupling between the two atomic fine-structure levels at finite distance, due to the anisotropy of the molecular potentials, is proportional to the splitting $[V_\Sigma(R) - V_\Pi(R)]$. The restriction to the subspace of states correlated to the $(ns + np)$ asymptote is no longer valid at small distances.

In the long-range region, where the dipole–dipole interaction dominates, the $V_\Sigma(R)$ and $V_\Pi(R)$ curves display their asymptotic $-2(C_3/R^3)$ and (C_3/R^3) behavior (see above) and the potential matrix can be approximated by

$$\mathbf{V}(R) \approx \begin{bmatrix} E^{at}(p_{3/2}) - \frac{C_3}{R^3} & -\frac{\sqrt{2}C_3}{R^3} \\ -\frac{\sqrt{2}C_3}{R^3} & E^{at}(p_{1/2}) \end{bmatrix}. \tag{10}$$

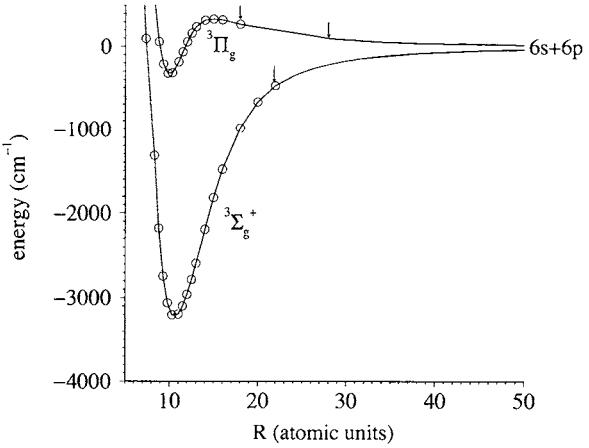

FIG. 3. $V_\Sigma(R)$ and $V_\Pi(R)$ potential curves (see text) for the Hund's case $a\ ^3\Sigma_g^+$ and $^3\Pi_g$ states of the Cs_2 molecule. The open circles correspond to *ab initio* calculations by Spies (1989). Arrows indicate the distance where the matching with the asymptotic expansion is taking place, choosing C_3^i, C_6^i, C_8^i coefficients from Marinescu and Dalgarno (1995). In the upper curve, direct matching being not possible, an interpolation was performed in the region between the two arrows.

The two 0_g^- asymptotic curves are obtained by diagonalization of this matrix, and can be considered as R^{-3} curves with slowly R-varying C_3 coefficients. At very large distances, the upper curve $0_g^-(p_{3/2})$ is asymptotically attractive with $C_3^i = C_3$, while the lower curve is flat ($C_3^i = 0$). As the nondiagonal term $\sqrt{2}(C_3/R^3)$ is increasing when the atoms get closer, there is an avoided crossing at a distance $R_{\min}$ such that $E^{at}(p_{3/2}) - E^{at}(p_{1/2}) \approx (\sqrt{2}C_3/R_{\min}^3)$. This explains why the external well is located at shorter and shorter distances when the fine-structure splitting increases from the light alkali atoms (Li, Na) to the heavier ones (Rb, Cs). This also explains why the repulsive part of this external well, located on the left of this avoided crossing, is displaying typical R^{-3} behavior: for $R \leq R_{\min}$, the repulsive branch of the external well may be approximated by

$$U_{\text{up}}(0_g^-(p_{3/2})) \approx E(p_{3/2}) + (\sqrt{2} - 1)\frac{C_3}{R^3}. \tag{11}$$

For Rb_2 and Cs_2 molecules, higher-order R^{-6} and R^{-8} multipole terms, as well as asymptotic exchange terms, contribute to the repulsive branch (Aubert-Frécon *et al.*, 1998; Fioretti *et al.*, 1999), yielding corrections of a few cm^{-1}; nevertheless, the physics of the long-range external wells is dominated by the dipole–dipole interaction between a pair of separated atoms. This is why we may say that we

form "a pair of atoms" rather than a usual molecule; the same idea is expressed in the concept of a "pure long-range molecule" by Stwalley *et al.* (1978).

This concept is even more adapted for the long-range well in the $1_u(p_{3/2})$ curve, which is located at a distance so large that the hyperfine-structure coupling has to be explicitly considered. The first observation of a 1_u pure long-range molecule was done by Wang *et al.* (1998) for K_2 ($D_e = 0.5394\ \text{cm}^{-1}$) and the Cs_2 state was analyzed recently by Comparat *et al.* (2000). (see Section III.C)

In contrast, for all attractive curves differing from $0_g^-(p_{3/2})$ and $1_u(p_{3/2})$ the vibrational motion extends from large to small internuclear distances, with reflection on the steep inner barrier. As we shall see later, the time spent in the inner region is comparatively very short.

B. The Le Roy–Bernstein Law for Bound Levels: Analogy with Rydberg Law, Scaling Laws

In this section, we shall neglect any rotation effect, assuming $J = 0$. Let us then consider a vibrational level with energy E_v^i close to dissociation limit D^i in a typical $i = \Omega_{g,u}$ excited potential curve $U^i(R)$ with asymptotic behavior

$$U^i(R) \approx D^i - \frac{C_3^i}{R^3}. \tag{12}$$

In the present section we shall also neglect the dynamical coupling with other channels i, so that the i label can safely be dropped to lighten the notation. A level will be characterized by its binding energy $\Delta_v^i = D_i - E_v^i$ hereafter denoted Δ_v. However, we shall keep the notation C_3^i for the long-range coefficient, as it differs from C_3 by an angular factor depending on the symmetry of the curve i.

The vibrational motion takes place both in the long-range region, where the motion in the asymptotic potential is very slow, and in the short-range region where, due to the attractive chemical potential, the motion is very quick. Besides, as the binding energy is negligible compared to the short-range potential, the local de Broglie wavelength at small internuclear distances is fairly independent of Δ_v, so that this rapid motion is similar for a wide range of levels. As an example, we display in Fig. 4 two vibrational wavefunctions, for the potential $Cs_2(1_g, 6s + 6p_{3/2})$, corresponding to binding energies $\Delta_v = 1$ and $10\ \text{cm}^{-1}$. Such functions have been computed according to the numerical method described in Section IV.A. It is clear that the probability density is concentrated at the outer turning point R_v, where the potential can safely be approximated by its asymptotic behavior given in Eq. (12). This corresponds to the physical idea of two atoms standing still most of the time at distance $R = R_v$. A look at the behavior of the two wavefunctions at small distances, displayed in Fig. 5, confirms that their nodal structure is similar, the only dependence on the binding energy appearing in their amplitude. This can

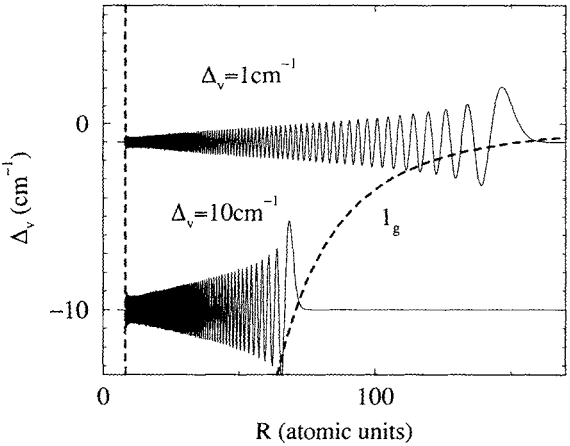

FIG. 4. Vibrational wavefunctions in the $^1\Sigma_g(6s+6p_{3/2})$ potential of the Cs_2 molecule, for two values of the binding energy, $\Delta_v = 1$ and 10 cm^{-1}.

be justified as stated above by the negligible value of Δ_v compared to the short-range potential, or alternatively, by the short time spent by the system in the inner region, leading through the uncertainty relation to a weak energy dependence. The physical interpretation is thus very similar to the description of the motion of a Rydberg electron in the potential of an atomic ion, where the effect of the

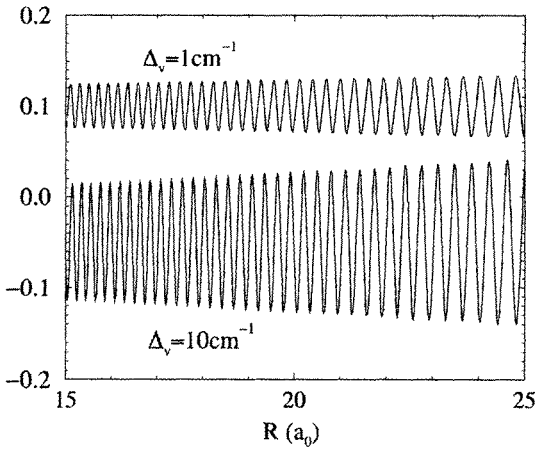

FIG. 5. Same as Fig. 4, concentrating on the short-range behavior of the wavefunctions for th two levels with binding energy $\Delta_v = 1$ and 10 cm^{-1}. The nodal structure of the two wavefunction is similar, the energy dependence being concentrated on the amplitude, which scales as $\Delta_v^{5/12}$, an therefore increases by ~2.6 when the detuning is multiplied by 10.

short-range non-Coulomb core is characterized by a quantum defect η in the Rydberg law,

$$\mathcal{E}(n,l) = \mathcal{I} - \frac{\text{Ryd}}{[n-\eta(l)]^2}, \tag{13}$$

linking the energy of a level to the principal quantum number n. In Eq. (13), $\mathcal{I}$ is the energy of the ionization threshold, and Ryd is the Rydberg constant. The quantum defect is weakly energy-dependent, but depends on the azimuthal quantum number l.

Considering motion in a potential with power-law asymptotic behavior R^{-n}, with $n \geq 3$, such as in Eq. (12), a generalization of Eq. (13) was derived in 1970 by Le Roy and Bernstein. This law was found to be such an important tool in the understanding of photoassociation spectroscopy that it seems worthwhile to recall the main steps of its demonstration (Le Roy and Bernstein, 1970; Stwalley, 1973). The scaling laws are discussed in the review of Vigué (1982), and the link with quantum defect theory analyzed by Ostrovsky *et al.* (2001).

Assuming the semiclassical picture to be valid, the vibrational wave function for a bound level with energy E_v in the single potential $U(R)$ may be written (Landau and Lifshitz, 1977) as

$$\Psi_v(R) = N_v \frac{1}{\sqrt{k(R)}} \sin\left(\int_{R_{\text{in}}^v}^{R} k(R')\,dR' + \frac{1}{4}\pi\right), \tag{14}$$

with the Bohr–Sommerfeld quantization condition on the phase,

$$\beta_{\text{BS}}(E_v) \equiv \int_{R_{\text{in}}^v}^{R_v} k(R')\,dR' = \left(v + \frac{1}{2}\right)\pi. \tag{15}$$

In Eqs. (14) and (15), R_{in}^v and R_v are, respectively, the inner and outer turning points of the vibrational motion. For a diatomic system with reduced mass μ, we have defined the local wavenumber $k_v(R)$ and local de Broglie wavelength $\lambda_v(R)$ as

$$k_v(R) = \frac{1}{\hbar}\sqrt{2\mu[E_v - U(R)]} = \frac{2\pi}{\lambda_v(R)}. \tag{16}$$

Therefore Eq. (14) is not valid close to a classical turning point, where $k_v(R_{\text{in}}^v) = k_v(R_v) = 0$. We shall give below a more general expression that is also valid close to a turning point. The normalization factor is linked to the classical period of motion (Landau and Lifshitz 1977) through

$$2[N_v]^{-2} = \int_{R_{\text{in}}^v}^{R_v} \frac{dR'}{k_v(R')} = \frac{\hbar T_{\text{vib}}}{2\mu}, \tag{17}$$

where T_{vib} is defined as the time necessary to go from the outer turning point to the inner one and back. The physical explanation given by Lefebvre-Brion and Field (1986) is that the probability amplitude in Eq. (14) is linked to the classical probability density, which is inversely proportional to the velocity times the period. From differentiation of the Bohr–Sommerfeld condition (15) over the quantum number, the same integral gives the inverse of spacing between the levels,

$$\hbar^2 \frac{\pi}{\mu} \left| \frac{dv}{dE} \right|_{E=E_v} = \int_{R_{\text{in}}^v}^{R_v} \frac{dR'}{k(R')}. \tag{18}$$

From this an important relation between the normalization factor and the level spacing,

$$\left. \frac{dE_v}{dv} \right|_{E=E_v} = \frac{\pi \hbar^2}{2\mu} N_v^2, \tag{19}$$

can be derived, which we shall use later to determine a scaling law.

For highly excited vibrational levels, the integral in Eqs. (15) and (18) is determined mostly by the outer domain of distances R, where the potential can be approximated by the general asymptotic formula $U(R) = D - C_n/R^n$; this allowed Le Roy and Bernstein (1970) to evaluate it in the limit $R_{\text{in}}^v/R_v \to 0$ with an analytical formula,

$$\int_{R_{\text{in}}^v}^{R_v} \frac{dR'}{k(R')} = \frac{2n}{n-2} \frac{\pi \hbar^2}{2\mu H_n} (D - E_v)^{-(n+2)/2n}, \tag{20}$$

$$H_n = \hbar \sqrt{\frac{2\pi}{\mu}} \frac{(n-2)\,\Gamma(1+1/n)}{2\Gamma(1/2+1/n)} C_n^{-1/n}. \tag{21}$$

By integration of Eq. (20), the Le Roy–Bernstein law is obtained, generalizing the Rydberg law to any potential in R^{-n}, $n \neq 2$,

$$E_v = D - [H_n(v_D - v)]^{2n/(n-2)}, \tag{22}$$

where the noninteger number v_D is the accumulated phase at the dissociation threshold divided by π. We may define an effective quantum number,

$$v_{\text{eff}} = v_D - v, \tag{23}$$

such that the levels are now numbered starting from the dissociation limit. In the spirit of the quantum defect theory (Seaton, 1983; Friedrich, 1998) it can be shown, as illustrated in Fig. 5, that for levels close to the dissociation limit, the wavefunctions exhibit the same nodal structure at short distances, the energy dependence

being concentrated in the normalization factor. Therefore any change in the short-range potential results into a modification of the phase in Eq. (15) equivalent for all such levels: whereas the total phase πv_D is modified, the difference $\pi (v_D - v)$ remains a constant.

In the case of photoassociation into an excited curve with long-range R^{-3} behavior as described by Eq. (12), the law giving the dissociation energy reads, using $\Gamma(4/3)/\Gamma(5/6) = 0.790903 = \gamma_3$ and

$$H_3 = 0.790903\hbar\sqrt{\frac{\pi}{2\mu}}\left(C_3^i\right)^{-1/3} = A_3\left(C_3^i\right)^{-1/3}, \tag{24}$$

and considering the cesium dimer, with $C_3^i \approx 10$ a.u. and atomic mass $M_A = 133$ as a reference,

$$\Delta_v = H_3^6(v_D - v)^6 = v_{\text{eff}}^6\left(\frac{133}{M_A}\right)^3\left(\frac{10}{C_3^i}\right)^2 \times 1.17\,10^{-12}\ \text{cm}^{-1}, \tag{25}$$

where M_A is the atomic mass so that $\mu = 1822.8885(M_A/2)$. Close to the dissociation limit there is a quasi-continuum of vibrational levels: for a detuning of 1 cm^{-1}, the numbering of a Cs_2 level from the dissociation limit is already $\sim 10^0$! This is why it is more convenient to analyze the present vibrational series by considering an energy scale rather than a numbering of levels. For a given dimer, the vibrational progression in Eq. (25) is a signature of the excited electronic state i populated by photoassociation, through the C_3^i coefficient. The vibrational spacing rapidly increases as a function of detuning, according to

$$\left.\frac{dE}{dv}\right|_{E=E_v} = -\frac{d\Delta v}{dv} = +6(H_3)^6(v_{\text{eff}})^5 = -6H_3(\Delta_v)^{5/6}. \tag{26}$$

We can give an estimate of the level spacing taking the cesium dimer as reference,

$$\left.\frac{d\Delta_v}{dv}\right|_{E=E_v} = -6.14 \times 10^{-2}\sqrt{\frac{133}{M_A}}\left(\frac{10}{C_3^i}\right)^{1/3}(\Delta_v)^{5/6}\,\text{cm}^{-1}. \tag{27}$$

In the case of Cs_2, choosing $C_3^i = 10.47$ from Marinescu and Dalgarno (1995), the level spacing is increasing from ~ 0.06 to ~ 0.4 cm^{-1} when the detuning varies from 1 to 10 cm^{-1}. The classical outer turning point,

$$R_v = \left(\frac{C_3^i}{\Delta_v}\right)^{1/3}, \tag{28}$$

then decreases from 131.9 to 61.5 a_0, verifying a $(\Delta_v)^{-1/3}$ or $(v_{\text{eff}})^{-2}$ scaling law, which, we shall see later, clearly manifested in the photoassociation spectra. The

scaling law verified by the normalization factor in Eq. (19), may be deduced from the vibrational spacing,

$$(N_v)^2([a_0]^{-2}) = 0.3516 \times \frac{M_A}{133}\left|\frac{d\Delta_v}{dv}\right|(\mathrm{cm}^{-1})\Big|_{E=E_v}. \tag{29}$$

We can verify in Figs. 4 and 5 that the inner part of the wavefunctions is indeed scaled by a factor ~2.6 when the detuning is varying from 1 to 10 cm^{-1}, corresponding to a change of $(N_v)^2$ by a factor $10^{5/6} \approx 6.8$. As this $(N_v)^2$ normalization factor scales any matrix element of a physical quantity corresponding to short-range coupling, the $(v_{\mathrm{eff}})^5$ or $(\Delta_v)^{5/6}$ scaling law is then equivalent to the well-known ν^{-3} scaling law for Rydberg states (Seaton, 1983; Friedrich, 1998). We should mention that in the case of an asymptotic R^{-5} potential, Gouédard *et al.* (1989) gave for the first time experimental verification of the corresponding scaling law near a dissociation limit of the Cl_2 molecule.

The formation of ground-state molecules in low enough vibrational levels can be considered as a short-range process, as it involves the overlap with short-range vibrational wavefunctions in the ground state. Therefore, *the corresponding probability is expected to scale as* $\Delta_v^{5/6}$ *as a function of the binding energy, and hence as* $\delta_L^{5/6}$ as a function of detuning. Thus, large detunings are expected to be more favorable. In contrast, we shall see later that, the photoassociation process is definitely more favorable at small detunings.

It is also interesting, within a time-dependent picture, to estimate the classical vibrational period in the $(ns + np)$ excited potential curve of a dimer A_2,

$$T_{\mathrm{vib}}[\mathrm{ps}] \approx \left(\frac{C_3^i[\mathrm{a.u.}]}{10}\right)^{1/3} \sqrt{\frac{M_A}{133}}(\Delta_v[\mathrm{cm}^{-1}])^{-5/6} \times 534\,\mathrm{ps}. \tag{30}$$

Assuming C_3^i values around 10 a.u., and for a 1-cm^{-1} detuning, the vibrational period has a magnitude of about 500 ps. At even smaller detunings, this classical vibration period becomes of the order of magnitude of the radiation lifetime (a few nanoseconds), so that a model neglecting spontaneous emission is no longer valid, and time-dependent models must be implemented.

To be thorough, we should give a correct expression for the semiclassical wavefunction in the vicinity of a turning point, where the approximation given in Eq. (14) is no longer valid. We shall follow the derivation proposed by Vigué (1982), Lefebvre-Brion and Field (1986), and Child (1991) and write the uniform semiclassical (USC) wavefunction (Miller, 1968), valid for all values of R, as

$$\Psi_v^{\mathrm{USC}}(R) = \frac{N}{\sqrt{\pi}}\left[\frac{Z(R)}{k(R)^2}\right]^{1/4} \mathrm{Ai}[-Z(R)], \tag{31}$$

where we have introduced an Airy function of the phase $Z(R) = [\frac{3}{2}\int_{R_{\text{in}}^v}^{R} k(R')\,dR']^{2/3}$. The sine behavior as a function of the phase is reached for $Z > 1.5$, where the uniform semiclassical function becomes equivalent to the sine function in Eq. (14). The factor multiplying the Airy function in Eq. (31) is then $N\sqrt{\pi}(\hbar[R_v]^2)^{1/3}[6\mu C_3^i]^{-1/6}$, where R_v is the outer turning point linked to the detuning through Eq. (28).

The semiclassical arguments developed in the present section, the choice for the norm, and therefore the derivation of the scaling laws, are no longer valid close to the dissociation limit, when the wavefunction has an important extension in the nonclassical region and behaves as an evanescent wave. Corrections to the semiclassical model have been proposed by many authors, and will be discussed in Section IV.A.3. Such corrections concern very few levels close to the dissociation limit. Besides numerical calculations are available in all cases.

Scaling laws offer an invaluable tool in the interpretation and fitting of experiments: the Le Roy–Bernstein formula has been widely used in order to identify the excited electronic states or to fit C_3^i coefficients to the observed spectrum [see the review of Stwalley and Wang (1999), and references therein]. Examples will be given in Section III.C.

Generalization of the present derivation to two coupled channels has been proposed recently by Kokoouline *et al.* (2000a) and Ostrovsky *et al.* (2001). The energies of the levels for two coupled vibrational series can be plotted as Lu Fano plots and fitted by three parameters, which are two generalized quantum defects and a reduced coupling parameter.

C. Theoretical Predictions for the Photoassociation Rates

The problem is to estimate how many excited molecules in a given ro-vibrational level will be created in a photoassociation experiment. Many different groups have been working on the theory of photoassociation, using both "time-independent" formalism, with stationary wavefunctions (Napolitano *et al.,* 1994; Pillet *et al.,* 1997; Côté and Dalgarno, 1998; Mackie and Javanainen, 1998), and "time-dependent" formalism, with wavepacket propagation (Mackholm *et al.,* 1994; Vardi *et al.,* 1997; Boesten *et al.,* 1999; Vala *et al.,* 2001; Vatasescu *et al.,* 2001). After some controversy, there is presently agreement between various approaches for "time-independent" calculations. Up to now, "time-dependent" calculations have focused on the presentation of new schemes rather than quantitative prediction of the photoassociation rates, and will be described in Section VI. A precise comparison between the predictions of "time-dependent" and "time- independent" approaches is still lacking.

The quantum formulation of the transition between a bound level and a continuum level of a molecule due to coupling by the electromagnetic field between two

electronic states was considered in the early days of quantum mechanics (Condon, 1928; Winans and Stueckelberg, 1928; James and Coolidge, 1939) using various approximations. Doyle (1968) has given a detailed derivation of the absorption coefficient in a sample of hydrogen atoms: the rate is then defined as the probability of absorption of a photon for an incident beam of one photon crossing unit area per second and per unit frequency interval.

Napolitano *et al.* (1994) as well as Côté and Dalgarno (1998) use this definition to compute the absorption rate coefficient for the inelastic process yielding a bound molecule out of two ground-state ^2S alkali atoms via absorption of a photon with energy $\hbar\omega_L = \hbar(\omega_0 - \delta_L)$ according to the reaction (1)

$$K(T, \omega_L, v) = (n_{\text{at}})^2 \left\langle \frac{\pi\hbar}{k} \sum_{J=0}^{\infty} (2J+1) |S(E, J; i, v, J; \omega_L)|^2 \right\rangle \tag{32}$$

where n_{at} is the atomic density and $S(E, J; i, v, J; \omega_L)$ is the free–bound transition amplitude between the initial continuum level at energy E and a bound level v, J in the excited potential curve i. Here, $\langle \ldots\ldots\ldots \rangle$ is an average over the distribution of initial velocities. If a Maxwellian distribution at temperature T is assumed, expression (32) yields for the absorption coefficient

$$K(T, \omega_L, v) = \sum_{J=0}^{\infty} (2J+1) \frac{n_{\text{at}}^2}{h Q_T} \times \int_0^{\infty} dE\, e^{-E/kT} |S(E, J; i, v, J; \omega_L)|^2, \tag{33}$$

where the translational partition function $Q_T = (2\pi\mu k_B T/h^2)^{3/2}$ has been introduced. In most papers, the numerical results are given for the quantity $K(T, \omega_L, v)$ divided by the incident photon flux and by the square of the atomic density.

Various approximations have been discussed to simplify the calculations. Although the S-matrix element has to be computed by solving coupled equations, Napolitano *et al.* (1994) show that their close-coupling calculations for sodium, in a temperature range from 0.01 to 10 mK, can be approximated by a very simple resonant scattering expression involving the width of the bound level defined as a function of the spontaneous emission rate and the stimulated emission rate back to the ground state. Such expression is similar to a Breit–Wigner formula, and Gardner *et al.* (1995) have generalized it taking account of the directional dependence. Photoassociation can then be viewed as an optically induced Feshbach resonance, and the richness of this point of view has been recently demonstrated by the experiments of Fatemi *et al.* (2000), who measured such resonances in a sodium sample. At low laser intensities, in the framework of a perturbative treatment, the widths factors in the Breit–Wigner formula involve the electronic transition moment between the unperturbed initial and final states. In the present work we shall

not discuss the shape of the photoassociation lines, assuming that the resonance condition(5) can be expressed by a δ function. By use of a Fermi-golden-rule type of approximation, Côté and Dalgarno (1998) find

$$S(E, J; i, v, J; \omega_L) \sim 8\pi^3 \frac{I}{c} \left|\langle \psi_{E,J}(R)|\mathcal{D}(R)|\phi^i_{v,J}(R)\rangle\right|^2 \delta(E - \hbar\delta_L + \Delta_v), \tag{34}$$

where we have introduced the coupling matrix element, proportional to the square root of the laser intensity and to the molecular transition dipole $\mathcal{D}(R)$, between the energy normalized ground-state scattering wavefunction $\psi_{E,J}(R)$ and the unperturbed vibrational function $\psi^i_{v,J}(R)$. With an R-centroid approximation (Lefebvre-Brion and Field, 1986), the electronic transition moment can be further approximated by

$$\langle \psi_{E,J}(R)|\mathcal{D}(R)|\phi^i_{v,J}(R)\rangle \approx \mathcal{D}(R_v)\langle \psi_{E,J}(R) \,|\, \phi^i_{v,J}(R)\rangle, \tag{35}$$

i.e., the product of $\mathcal{D}(R_v)$, value of the dipole moment at the outer classical turning point of the vibrational motion, and the overlap integral, the square root of the Franck–Condon factor. *Therefore, for a laser tuned at resonance, the photoassociation rate is controlled by the Franck–Condon factor between the radial wave functions in the initial continuum level and the final bound level.*

The approach developed by Pillet *et al.* (1997) uses an atomic physics point of view and a density-matrix description of a collection of N atoms, interacting by two-body interaction, in the presence of laser light at time t. The density matrix at time $t = 0$ is computed for an assembly of atoms when the laser is off, assuming a Maxwell–Boltzmann distribution at temperature T. The coupling matrix element is described by a δ function approximation in the spirit of Eq. (34), considering that the rotational quantum number may vary between the initial and final states. The time evolution equation of the density matrix, in interaction representation, is solved in a perturbative approach. For a low intensity I of the photoassociation laser tuned at resonance, the photoassociation rate $\mathcal{R}_{\mathrm{PA}}$ (in s^{-1}), defined as the number of photoassociated molecules, formed in an individual level (v, J), divided by the total number $N_{\mathrm{at}} = n_{at}\, V$ of atoms in a trap of volume V, is found as

$$\mathcal{R}_{\mathrm{PA}} = \mathcal{A}(J, J', \epsilon_{PA}) \left(\frac{3}{2\pi}\right)^{3/2} \frac{h}{2} n_{\mathrm{at}} \lambda^3_{\mathrm{th}}$$

$$\times \exp\left(\frac{-E_r}{k_B T}\right) K^2 \left|\langle \psi_{E,J}(R)|\phi^i_{v,J'}(R)\rangle\right|^2, \tag{36}$$

where $\mathcal{A}(J, J'), \epsilon_{PA})$ is an angular factor depending on J, J' and on the laser polarization. $\lambda_{th} = h\sqrt{1/(3\mu k_B T)}$ is the thermal de Broglie wavelength, and $2K$ is the atomic Rabi frequency. The latter is a function of the laser intensity I,

$$K^2 = \frac{\Gamma}{8}\frac{I}{I_0}, \tag{37}$$

where we have defined a saturation intensity $I_0 = \pi hc\Gamma/(3\lambda_{PA}^3)$ from the natural width of the atomic np level, $\Gamma/2\pi$. In the case of cesium, $\Gamma/2\pi = 5.22$ MHz, so the saturation intensity has a value of 1.1 mW/cm^2 at the PA laser wavelength $\lambda_{PA} = 2\pi c/\omega_0$. The rate $\mathcal{R}_{PA}$ in Eq. (36), divided by n_{at} and by the incident photon flux $\phi = I/\hbar\omega_{PA}$ yields a rate κ per photon and per unit density (its dimension is a length to the fifth power), which is similar to the expressions given by most other authors (Napolitano *et al.*, 1994; Julienne, 1996; Côté and Dalgarno, 1998). The quasi-continuum approach developed by Javanainen and Mackie (1998), Mackie and Javanainen (1999) avoids the use of delta functions and yields a similar result.

D. The Reflection Principle for Calculation of Franck–Condon Factors

The estimation of the photoassociation probability thus relies on knowledge of the Franck–Condon factor,

$$F(E \cong k_B T, J; i, v, J') = \left|\langle \psi_{E,J}(R) | \phi^i_{v,J'}(R)\rangle\right|^2. \tag{38}$$

In the following we shall consider $J = J'$ and drop the angular factor $\mathcal{A}(J, J', \epsilon_{PA})$.

Optical transitions between a bound and a continuum level of a molecule were studied in the early days of quantum mechanics and viewed as vertical transitions, at a given internuclear distance, between two electronic states (Franck, 1925; Condon, 1926, 1928). In his review on the Franck–Condon principle in bound–free transitions, Tellinghuisen (1985) gives an extensive discussion of the various approaches to the problem, through classical, semiclassical, or quantum methods.

In a semiclassical approach, the overlap integral can be estimated within a stationary phase approximation. Such a procedure, derived by Jablonski (1945), has been adapted to the photoassociation problem by Julienne (1996), and further discussed by Wang and Stwalley (1998) and Boisseau *et al.* (2000b). The main idea of this derivation is to write the product of two oscillating functions as the sum of two functions, and to neglect the high-frequency component, in order to keep only the low-frequency term. The approach is valid provided the two wavefunctions oscillate at frequencies that are not too different, so that the sum of

the frequencies is indeed much larger than their difference. When the continuum function is oscillating much more slowly, i.e., at very low temperatures, Pillet *et al.* (1997) consider for the vibrational function in the excited potential $\phi^i_{v,J}(R)$ an Airy function behavior in the vicinity of the outer classical turning point. We shall see later that the same formula is obtained by the two methods. The Franck–Condon factor obtained with the stationary-phase method is

$$F(E, J; i, v, J) \approx \frac{dE^i_{v,J}}{dv} \frac{1}{D(R^i_{v,J})} |\psi_{E,J}(R^i_{v,J})|^2, \tag{39}$$

proportional to the value $\psi_{E,J}(R^i_{v,J})$ of the continuum wavefunction at $R = R^i_{v,J}$, in accord with the image of a vertical transition where the vibrational motion is stopped. We shall use this formula for $J = 0$, and drop the J index hereafter.

The level spacing is introduced because of the normalization factor in the vibrational wavefunction [see Eq. (19)], while, as in the Landau–Zener formula, the quantity $D(R^i_v)$ is the difference between the slopes of the two potential curves at $R = R^i_v$,

$$D(R^i_v) = \frac{d}{dR}[U^i(R) - V_g(R)]|_{R=R^i_v}, \tag{40}$$

optimal conditions corresponding to a minimum of this quantity. The Condon point R^i_v has been defined in Eq. (28). $V_g(R)$ is the ground-state potential, which in the asymptotic region behaves as $\sim -C^g_6/R^6$ and therefore exhibits a much weaker slope than the excited potential $U^i(R)$. We may write

$$\frac{1}{D(R^i_v)} \approx \frac{[R^i_v]^4}{3C^i_3} \approx \frac{1}{3}(C^i_3)^{1/3}(\Delta_v)^{-4/3}. \tag{41}$$

A look at Eq. (39) shows that, as far as the choice of the final bound level is concerned, the efficiency of the photoassociation reaction involves the competition of two effects:

- In order to optimize the difference of slopes, which scales as $(\Delta_v)^{-4/3}$, or $(R^i_v)^4$, the photoassociation process should take place at small detunings, corresponding to a Condon point R^i_v located at large distances, where the two curves have similar slopes.
- In contrast, the normalization factor for the vibrational level v, related to the level spacing dE^i_v/dv, scales as $(\Delta_v)^{5/6}$, or $(R^i_v)^{-5/2}$, so that if we keep the

constraint of populating individual vibrational levels, this factor decreases when photoassociation is taking place at large distances R_v^i.

The competition of these two effects gives a $(\Delta_v)^{-1/2}$ dependence on the detuning. Of course, the Franck–Condon factor also depends on the behavior of the ground-state wavefunction, which, as discussed in the next section, favors excitation at small detunings, or vertical transition at a large distance R_v^i.

E. The Nodal Structure of the Zero-Energy Scattering Wavefunction

From Eq. (39), we see that the Franck-Condon factor reflects the nodal structure of the ground-state continuum wavefunction, in the sense that the s-wave contribution to the photoassociation signal will be zero when the Condon distance R_v^i is such that $\psi_E(R_v^i) = 0$. We display, in Figs. 6 and 7, an example of the wavefunctions $\psi_E(R)$ describing s-wave scattering of two ground-state cesium atoms, interacting through the ground $X^1\Sigma_g^+$ or lower-triplet $a^3\Sigma_u^+$ potential, for a collision energy of

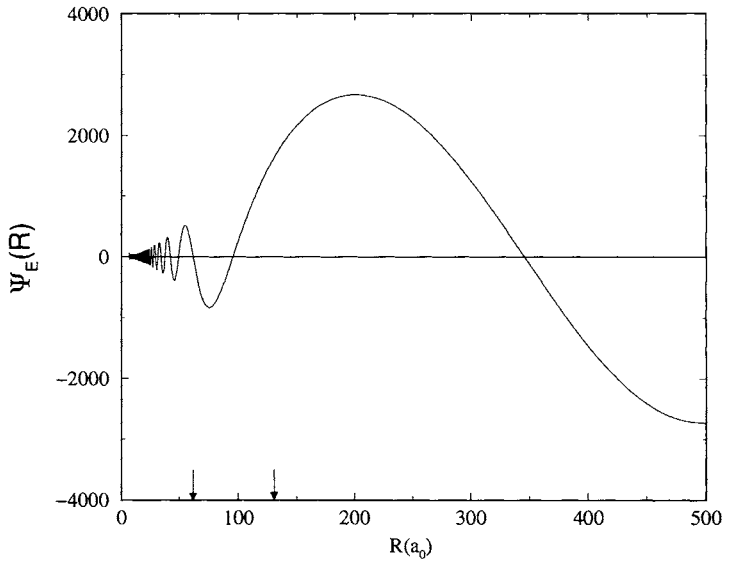

FIG. 6. Energy-normalized wavefunction $\Psi_E(R)$ for scattering of two ground-state cesium atoms in the $X^1\Sigma_g^+$ potential at a temperature of 140 μK. The computed wavefunction corresponds to a ground-state scattering length $a_S = -33a_0$. The two arrows indicate the distances $R_v^i = 131.9\ a_0$ and $R_v^i = 61.5\ a_0$ corresponding to photoassociation at detuning $\Delta_v = 1$ and 10 cm^{-1}, respectively, for an excited potential varying asymptotically as $-C_3^i/R^3$, with $C_3^i = 10.47$ a.u.

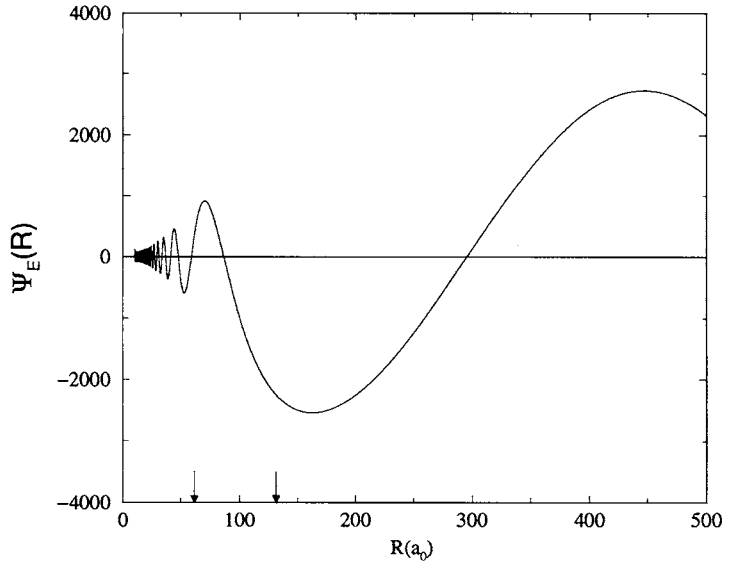

FIG. 7. Energy-normalized wavefunction $\Psi_E(R)$ for scattering of two ground-state cesium atoms in the $a^3\Sigma_u^+$ potential at a temperature of 140 μK. The computed wavefunction corresponds to a negative scattering length $a_T = -530a_0$. The two arrows indicate the distances $R_v^i = 131.9a_0$ and $R_v^i = 61.5a_0$ corresponding to photoassociation at detuning $\Delta_v = 1$ and 10 cm^{-1}, respectively, for an excited potential varying asymptotically as $-C_3^i/R^3$, with $C_3^i = 10.47$ a.u.

140 μK. The scattering lengths were chosen $a_S = -33a_0$ from Dion *et al.* (2001) and $a_T = 530a_0$ from Drag *et al.* (2000b). The main feature is the existence of two very different regions:

- At long range, when the ground-state potential is negligible, the wavefunction has sine behavior, with an amplitude inversely proportional to the square root of the wavenumber $k = \sqrt{(2\mu E/\hbar^2)}$ (or to $E^{1/4}$) and a phase depending on the scattering length $a_{S,T}$,

$$\Psi_E(R) = \left(\frac{2\mu}{\pi^2\hbar^2 E}\right)^{1/4} \sin[k(R-a)]. \tag{42}$$

It is expected that the photoassociation probability is enhanced at low collision energies as $E^{-1/2}$. If the scattering length is positive, a minimum in the photoassociation signal is observed for a Condon point located at distance a. At very low temperature, the Wigner threshold law behavior is reached, and in the asymptotic region $\Psi_E(R)$ is approximated by linear

behavior as a function of $(R - a)$ (Côté *et al.*, 1995; Julienne, 1996; Wang and Stwalley, 1998),

$$\Psi_0(R) \approx \sqrt{\frac{2\mu}{\pi\hbar^2 k}}\ \sin[\delta_0(k)]\left(\frac{R}{a} - 1\right) + O(k^2) \tag{43}$$

$$\approx \sqrt{\frac{2\mu k}{\pi\hbar^2}}\left[R\left(1 - \frac{a}{R}\right)\right], \tag{44}$$

where we have introduced the zero-energy s-wave phaseshift $\delta_0(k)$.

- At shorter distance, due to the presence of the ground-state potential and to quantum reflection effects, the amplitude of the wavefunction $\Psi_E(R)$ is dramatically decreased, leading to a loss of more than one order of magnitude in the photoassociation efficiency, and to the existence of minima in the photoassociation signal reflecting the nodal structure in the ground-state wavefunction. Such minima, predicted by Côté and Dalgarno, were observed for the first time by Hulet's group (Côté *et al.*, 1995) and then in many photoassociation experiments (Julienne, 1996), leading to accurate determination of the scattering length (Drag *et al.*, 2000b).

The two conclusions that we may draw are the following:

- First, the bottleneck in the photoassociation probability lies in the amplitude of the ground-state wavefunction, which depends on the scattering length and increases at low collision energies. It is more efficient to implement photoassociation in the long-distance region where the continuum wavefunction has reached asymptotic behavior. For instance, in the example of cesium photoassociation chosen in the present review, we may see in Figs. 6 and 7 that by increasing the detuning from 1 to 10 cm^{-1}, R_v^i is decreasing from 131.9_{a_0} to 61.5 a_0 and the amplitude of $\Psi_E(R_v^i)$ decreases by one order of magnitude, and hence the photoassociation probability decreases by two orders of magnitude.
- Second, accurate calculations of the overlap integrals should be performed, the analytical formulas being helpful only to estimate the orders of magnitude in the low-detuning region, for temperatures low enough that the linear approximation of the wavefunction in Eq. (44) is valid. We shall describe accurate numerical methods in Section IV.A.

F. A Simple Theory of Photoassociation

The perturbative approach adapted to the weak-laser-field regime, developed by Pillet *et al.* (1997), may be used for the calculation of photoassociation rates as

long as the saturation regime is not reached. We will assume $E = k_B T$ in the following. In a region where the ground-state potential is negligible, and at very low energies, the wavefunction $\Psi_E(R)$ can be approximated by a linear variation, so that the Franck–Condon factor may be written from Eqs. (39) and (12) as

$$F(E,\ J=0;i,v,\ J=0) \sim \frac{4\gamma_3}{\sqrt{\pi}\hbar^2}\left[C_3^i\right]^{2/3}\Delta_v^{-7/6}\mu E^{1/2}\left[1-\frac{a}{R_v}\right]^2, \qquad (45)$$

which is equivalent to the formula given by Wang and Stwalley (1998), in a paper where they compare homonuclear and heteronuclear systems. From Eqs. (19), (39) and (41) one may predict for the overlap integral a dependence in $\Delta_v^{-7/6}$, since the linear increase of the ground-state wavefunction as a function of distance R is introducing an extra $\Delta_v^{-2/3}$ factor. The $E^{1/2}$ energy dependence is linked to the linear approximation of the wavefunction, and would change to a $E^{-1/2}$ dependence if the asymptotic sine behavior of Eq. (42) was considered for the initial continuum wavefunction. Using Airy function representation for the excited-state wave function, as in the work of Pillet *et al.* (1997), the same formula is obtained for the estimation of the Franck–Condon overlap by analytical integration of the product of an Airy function and a sine function. Care must be taken to use the normalization of the vibrational wavefunction defined in Eq. (31), which is a factor 1.29 larger than the norm used by Pillet *et al.* (1997) from linearization of the potential. Numerical tests of the validity of the estimation in Eq. (39) are presented by Pillet *et al.* (1997) and by Boisseau *et al.* (2000b). In the latter case, the validity range of the reflection approximation is extensively discussed, and overlap integrals for p and d waves are given as well as for s waves. The conclusion is that the reflection approximation is valid in a large domain of physical situations, justifying the present discussion.

The conclusion of the paragraph is that photoassociation is much more efficient at large internuclear distances or at small detunings, creating excited molecules in loosely bound vibrational levels, which most of the time look like a pair of two atoms at large distance R_v^i. This molecule, being in an excited electronic state, decays by spontaneous emission, the lifetime being of the order of a few nanoseconds.

G. How to Make a Molecule in the Ground State or Lower Triplet State

The next problem is how to use those short-lived photoassociated molecules to create long-lived molecules in a bound level v_0 of the ground state or lower triplet state. The spontaneous emission process is most likely to take place through vertical transition at a large distance R_v^i. As the ground potential curves, with R^{-6} asymptotic

behavior, display a much narrower well (see Fig. 2), the vibrational motion does not extend that far, so spontaneous decay populates mainly continuum levels, and eventually a few of the uppermost bound levels. Once a photoassociated molecule is formed, it usually decays back into a pair of free ground-state atoms,

$$A_2[\Omega_{u,g}(ns + np_{1/2,3/2}); v, J], \rightarrow A(ns) + A(ns) + E_c' + \hbar(\omega_0 - \delta_2). \tag{46}$$

The gain in relative kinetic energy $[E_c' - E_c = \hbar(\delta_2 - \delta_L) > 0]$ generally allows both atoms to escape from the trap, so most photoassociation experiments have indeed been analyzed through trap-loss measurements.

In order to make ground-state molecules, several schemes have been proposed by theoretical goups. Côté and Dalgarno (1997, 1999) discuss how spontaneous decay of the photoassociated molecule populates the uppermost vibrational levels of the ground state.

$$A_2[\Omega_{u,g}(ns + np_{1/2,3/2}); v, J], \rightarrow A_2[^{1,3}\Sigma_{g,u}^{+}(ns + ns; v_0, J)] + \hbar(\omega_0 + \delta_3). \tag{47}$$

Their study for one excited potential curve of Li_2 confirms that the branching ratio between reactions (47) and (46) is very low, leading to a small population transfer into the last least-bound level of the ground $X\,^1\Sigma_g^+$ state, which is hardly a bound molecule. A similar conclusion has been obtained recently in the Cs_2 case by Dion *et al.* (2001). Therefore, Côté and Dalgarno (1997, 1999) propose implementing a Franck–Condon pumping scheme in order to transfer the population to lower vibrational levels. They consider sequences with absorption of laser light to a lower and lower vibrational level $v_1 < v$ of the $A^1\Sigma_u^+$ or $1^3\Sigma_g^+$ excited potential curves, followed by spontaneous emission. Detailed calculations of the absorption and spontaneous emission probabilities show that a large part of the population is lost at each step by spontaneous emission to the continuum [reaction (46)], and the authors conclude that the scheme is not efficient unless induced emission is considered instead of reaction (47).

Another scheme was proposed by Band and Julienne (1995), who suggested a two-photon sequence in which the photoassociation step is followed by absorption to a Rydberg state with good Franck–Condon overlap with low vibrational levels in the ground state. This scheme was implemented for K_2 in the experiments of Nikolov *et al.* (1999), and we shall see discuss its efficiency later.

Long-lived ultracold molecules were first observed in the cesium photoassociation experiment of Fioretti *et al.* (1998), owing to a formation scheme that was not originally considered by the theoreticians, and is clearly linked to the particular features of long-range wells in heavy alkali dimers. Indeed, we shall show that an

efficient mechanism has been found in situations where the vibrational motion of the photoassociated molecule is gradually slowed down at intermediate distances, leaving the possibility for vertical transition into a bound level of the ground (or lower-triplet)-state potential curve.

III. Ultracold Molecule Experiments

A. Introduction

In this section, we present the experimental results for the formation of ultracold molecules via photoassociation of laser-cooled atoms in a magnetooptical trap device (MOT). We give a detailed description of the experimental scheme in Orsay that led to the first observation of ultracold molecules in cesium (Fioretti *et al.,* 1998). Compared to the photoassociation spectroscopy experiments, the cold molecule experiments differ by the direct detection of the formed molecules, based on a photoionization process coupled with a time-of-flight mass spectrometer. Most of the time, the states studied in the photoassociation experiments do not give formation of cold molecules. This is due to the very weak branching ratio in favor of bound–bound transitions from the excited photoassociated molecules, which generally dissociate after spontaneous emission of one photon. We analyze carefully the mechanisms of formation of cold molecules in the case of cesium atoms, which are particularly efficient, making the cesium dimer a quite ideal case. We expose the precise measurements for the translational temperature in the molecular sample and for the rate of cold-molecule formation. We present finally the recent demonstration of the stimulated Raman photoassociation process to prepare state-selected cold molecules, so opening the way to the preparation of molecules, not only translationally cold but also vibrationally and rotationally cold. We discuss the other experimental schemes (Nikolov *et al.,* 1999, 2000; Gabbanini *et al.,* 2000). We briefly present the possible developments for trapping the formed cold molecules and analyze the experiment using a CO_2 laser quasi-electrostatic trap by Takekoshi *et al.* (1998). Finally, we mention very briefly the formation of cold molecules in a condensate (Wynar *et al.,* 2000), a subject which exceeds the frame of this review.

B. Experimental Setup in the Orsay Experiment

1. Cold Atomic Source

A scheme of the setup is shown in Fig. 8. Photoassociation (PA) experiments with cold alkali atoms are performed with the usual tools for providing cold atomic samples: a magnetooptical trap (MOT) (Raab *et al.,* 1987; Monroe *et al.,* 1990),

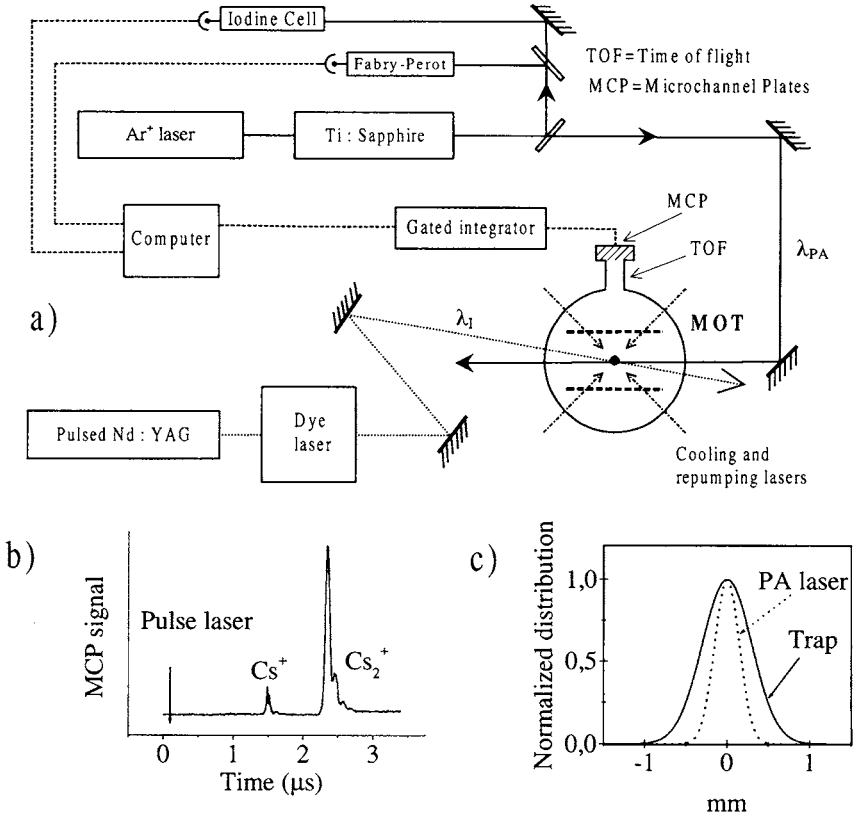

FIG. 8. (a) Scheme of the experimental setup. (b) Detection time sequence. The Cs^+ and Cs_2^+ ion pulses arrival times are in a ratio $\sqrt{2}$. (c) Overlap between the PA laser beam and the cold atomic sample.

dark SPOT (dark spontaneous force optical trap) (Ketterle *et al.*, 1993; Townsend *et al.*, 1996), or a dipole trap such as FORT (far off-resonance trap) (Miller *et al.*, 1993.) Very recently, PA experiments have also been developed by using a rubidium condensate (Wynar *et al.*, 2000). In the cesium experiments, the cold atom source is provided by the use of either a Cs vapor-loaded MOT or a dark SPOT. Details of the experimental setup have been published in several previous articles (Comparat *et al.*, 1999). Using a dark SPOT instead of a MOT implies a different initial state of the pair of atoms in the PA collisional process: the atoms are in the $6s_{1/2}$, $f = 3$ hyperfine level, instead of being in $f = 4$.

In a vapor-loaded MOT, the cold Cs atoms are produced at the intersection of three pairs of mutually orthogonal, counterpropagating $\sigma^+ - \sigma^-$ laser beams of intensity 1–2 mW/cm^2 and of diameter 6 mm, at the zero magnetic field point

of a pair of anti-Helmholtz coils with a magnetic field gradient of 15 gauss/cm. The residual pressure is 2×10^{-9} torr. The cooling and trapping laser beams are split from a slave diode laser (SDL 5422-H1, 150 mW, single mode, $\lambda \approx 852$ nm) injection locked to a master diode laser. The master laser (SDL 5412-H1, 100 mW) is stabilized by optical feedback from an extended, grating-ended cavity. Locking the master laser frequency to a saturated absorption line of a cesium vapor ensures its long-term stabilization. The trapping laser frequency is tuned about 13 MHz ($\simeq$2.5 natural linewidths) on the red of the frequency $\nu_{4\to5}$ of the $6s_{1/2}, f = 4 \to 6p_{3/2}, f' = 5$ atomic transition (see Fig. 1, left). A repumping laser beam (SDL 5712-H1, 100 mW, $\lambda \approx 852$ nm) of frequency $\nu_{3\to4}$ resonant with the $6_{1/2}, f = 3 \to 6p_{3/2}, f' = 4$ transition is superimposed with two of the beams of the cooling laser, preventing atoms from being optically pumped in the untrapped $f = 3$ hyperfine level of the ground state. The total number of cold atoms inside the trap is determined by using a calibrated photodiode to record the fluorescence signal due to the trapping laser. We use the expression for the detected power of fluorescence in the solid angle Ω, given by

$$P = N_{\text{at}} \frac{\Omega}{4\pi} h\nu_{\text{trap}} \frac{\Gamma}{2} \frac{C_1^2 \omega_{\text{tot}}^2/2}{\delta^2 + \Gamma^2/4 + C_2^2 \omega_{\text{tot}}^2/2}. \tag{48}$$

In Eq. (48), ω_{tot} is the total Rabi frequency due to the six trapping laser beams at the frequency ν_{trap}, Γ is the inverse of the characteristic time of spontaneous emission. C_1 and C_2 correspond to effective coefficients, $C_1^2 \simeq C_2^2 \simeq 0.73$, measured experimentally by Townsend *et al.* (1995). These coefficients do not correspond to those expected ($\simeq$0.4) by assuming an equirepartition on all the Zeeman sublevels of the atomic ground state $f = 4$. They indicate a larger population in the magnetic sublevels with maximum absolute quantum numbers.

Depending on the experimental conditions (laser detuning and intensity), the number of atoms lies in the range between 2 and 5×10^7 and the temperature T of the cold atomic sample ranges between 20 and 200 μK (Fioretti *et al.*, 1999). For a detuning of 14 MHz, an intensity of $\sim$1 mW/cm^2 for each laser beam, and a temperature of 140 ± 20 μK, the number of atoms is N_{at} of 4.7×10^7 estimated within a factor of 2. The atomic sample is approximately spherical. We assume that the density is proportional to a gaussian distribution $\exp(-r^2/2\sigma_R^2)$, with $\sigma_R = 300 \pm 50$ μm in the three space dimensions. The mean density is of the order of 4×10^{10} atoms/cm^3 ($\sim 10^{11}$ atoms/cm^3 for the peak density) and is known within a factor of 3. In these experimental conditions, the characteristic loading time for the trap has been measured in the range 600–800 ms, depending on day-to-day fluctuations of the experimental conditions. In the MOT and dark SPOT devices, atoms can be further cooled below the Doppler limit, down to $T \leq 30$ μK, by detuning, during 7 ms, the trapping laser to nine natural linewidths and simultaneously reducing the beam's intensity by a factor of 2 through a Pockels

cell. The MOT is shifted into a dark SPOT configuration by modifying the repumping arrangement to transfer most of the atoms (>90%) in the "dark" state $f = 3$ in the center of the trap. The repumping beam is now partly screened with a 3-mm-diameter black spot of insulating tape, stuck onto a microscope slide. The spot is imaged at the center of the trapping region using a lens of focal length $l = 400$ mm, placed at a distance $2l$ apart. Just after the lens, a beam splitter splits the repumping laser beam into two beams. They are superimposed with two cooling laser beams. The images of the spot for the two laser beams correspond to the center of the trapping zone. The difficulties in applying the dark SPOT technique to heavy atoms have already been noticed (Townsend *et al.*, 1996). To obtain a large fraction of the atoms in a "dark" state, we illuminate the cold atomic sample with a depumping laser beam of about 10 mW cm^{-2}, tuned about 25 MHz (~5 natural linewidths) on the blue of the frequency $\nu_{4\to3}$ of the $6s_{1/2}$, $f = 4 \to 6p_{3/2}$, $f' = 3$ atomic transition. For that purpose, the diode laser is locked on the level crossing $6s_{1/2}$, $f = 4 \to 6p_{3/2}$, $f' = 3$ and $6s_{1/2}$, $f = 4 \to 6p_{3/2}$, $f' = 5$ and the laser beam passes through an acoustooptic modulator which shifts its frequency by 200 MHz. We have verified by photoabsorption that more than 90% of the atoms in the center of the trapping zone are in the "dark" state $f = 3$.

2. Photoassociation Laser

The trapped, cold Cs atoms are illuminated with a continuous-wave (CW) laser with wavelength $\lambda_{PA} = \frac{2\pi c}{\omega_{PA}}$ to produce the photoassociation reaction; from Eqs. (1) and (6), neglecting the kinetic energy terms in Eq. (5), we consider two kinds of transitions, according to the hyperfine level in the initial state,

$$2\mathrm{Cs}\,(6s_{1/2},\, f = 4) + \hbar\omega_{PA} \to \mathrm{Cs}_2\,[\Omega_{u,g}(6s_{1/2} + 6p_{1/2,3/2};\, v,\, J)] \tag{49}$$

for the MOT experiments, and

$$2\mathrm{Cs}\,(6s_{1/2},\, f = 3) + \hbar\omega_{PA} \to \mathrm{Cs}_2\,[\Omega_{u,g}(6s_{1/2} + 6p_{1/2,3/2};\, v,\, J)] \tag{50}$$

for the dark SPOT experiments. The rovibrational level of a long-range molecular state $\Omega_{u,g}$—labeled here in Hund's case c notation—is thus populated. PA is achieved by continuously illuminating the cold Cs atoms with the beam ($\lambda_{PA} \gtrsim$ 852 or 894 nm) of a Ti:sapphire laser ("Coherent 899" ring laser) pumped by an argon-ion laser, red-detuned from the $6s(f = 4) \to 6p_{3/2}(f' = 5)$ atomic transition (11732.183 cm^{-1} (Avila *et al.*, 1986), or from the $6s(f = 4) \to 6p_{1/2}(f' = 3)$ atomic transition (11178.07 cm^{-1}). The frequency scale is calibrated using a Fabry–Perot interferometer, and the absorption lines of iodine (Gerstenkorn *et al.*, 1982). The maximum absolute uncertainty is estimated to be ± 150 MHz, mainly due

to the uncertainties on the position of the iodine lines. Thanks to the Perot–Fabry interferometer, which has a free spectral range of 750 MHz, the local uncertainty is reduced to about ± 10 MHz. The maximum available power of the laser beam is 650 mW. We approximate the intensity by a Gaussian profile, $\exp(-2\rho^2/w_0^2)$, with $w_0 = 300 \pm 50\,\mu$m, leading to a maximum intensity of 450 W cm^{-2} for the PA laser.

3. *Detection of the Molecules*

The Orsay experiment uses two kinds of detection schemes for the photoassociation process and the formation of molecules in the ground or lower triplet state.

- As in many photoassociation experiments (see Stwalley and Wang, 1999, and references therein), trap-loss analysis is performed recording the fluorescence yield from the trap, collected by a photodiode. The variations of the signal are interpreted as decrease of the number of atoms in the trap due both to dissociation of PA molecules into a pair of atoms that escape the trap [Eq. (46)] and possibly to the formation of cold ground-state molecules.
- Second, Cs_2^+ ions are detected through a time-of-flight mass spectrometer, after photoionization of the translationally cold Cs_2 molecules. The photons are provided by a pulsed dye laser ($\lambda_2 \sim 716$ nm, 7-ns duration) pumped by the second harmonic of a Nd-YAG laser; the ionization is a REMPI process, using as intermediate step the vibrational levels of an electronic molecular state correlated to the $(6s + 5d_{3/2,5/2}$ dissociation limits (Fioretti *et al.*, 1998) (see Fig. 9). There is a window of a few hundred wavenumbers around the wavelength $\lambda_I \approx 716$ nm and another window is observed for $\lambda'_I \approx 554$ nm, corresponding to the REMPI process via vibrational levels correlated to $6s + 7s$. The time-of-flight scheme discriminates atomic and molecular ions. The sensitivity of ion detection for probing the formation of molecules is a key point of these experiments. The upper vibrational levels of the ground state cannot be detected in the present scheme (Dion *et al.*, 2001), due to the selection rule forbidding $(6s \rightarrow 5d)$ atomic transitions. Estimations show that presently the detection efficiency is only about 5%.

C. Photoassociation Spectra

The fluorescence and the Cs_2^+ ion spectra are recorded as a function of the PA laser frequency. A summary of the Orsay data is shown in Fig. 10 with typical spectra obtained by using a MOT atomic sample. The origin of the energy scale is fixed at the $6s_{1/2}$, $f = 4 \rightarrow 6p_{3/2}$, $f' = 5$ atomic transition, which corresponds to an energy of 11732.183 cm^{-1} above the $6s_{1/2}$, $f = 4 + 6s_{1/2}$, $f = 4$ asymptote.

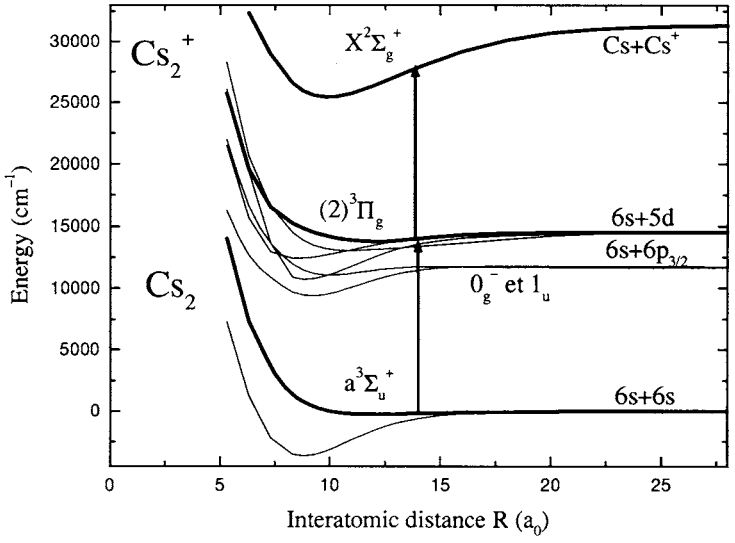

FIG. 9. The detection scheme in the Orsay experiment. It is a two-photon resonant process (REMPI) via vibrational levels in the (2) $^3\Pi_g$ potential curve correlated to the Cs$(6s)$ + Cs$(5d)$ dissociation limit. Ultracold molecules can be detected both in the ground $X\,^1\Sigma_g^+$ and metastable $a\,^3\Sigma_u^+$ states.

For detunings smaller than 0.1 cm^{-1}, the MOT is destroyed by the PA laser. The fluorescence and the Cs_2^+ ion spectra are quite different.

- First, we clearly observe resonance lines up to a PA laser detuning of 80 cm^{-1} in the ion spectrum, while the trap-loss spectrum stops beyond 40 cm^{-1}.
- Second, the density of resonance lines in the trap-loss spectrum is much more important.

1. Trap-Loss Spectrum

In the fluorescence spectrum, recorded as a function of the detuning of the photoassociation laser, we observe dips interpreted as vibrational progressions. The presence of a dip corresponds either to a photoassociation reaction followed by dissociation,

$$Cs_2\left[\Omega_{u,g}\left(6s + 6p\,^2P_{3/2}\right); v, J\right], \rightarrow Cs(6s) + Cs(6s) + E_c' + \hbar\left(\omega_0 - \delta_2\right), \quad (51)$$

where it is assumed that E_c' is large enough so that the two atoms live the trap, or to a photoassociation reaction followed by spontaneous emission into a bound

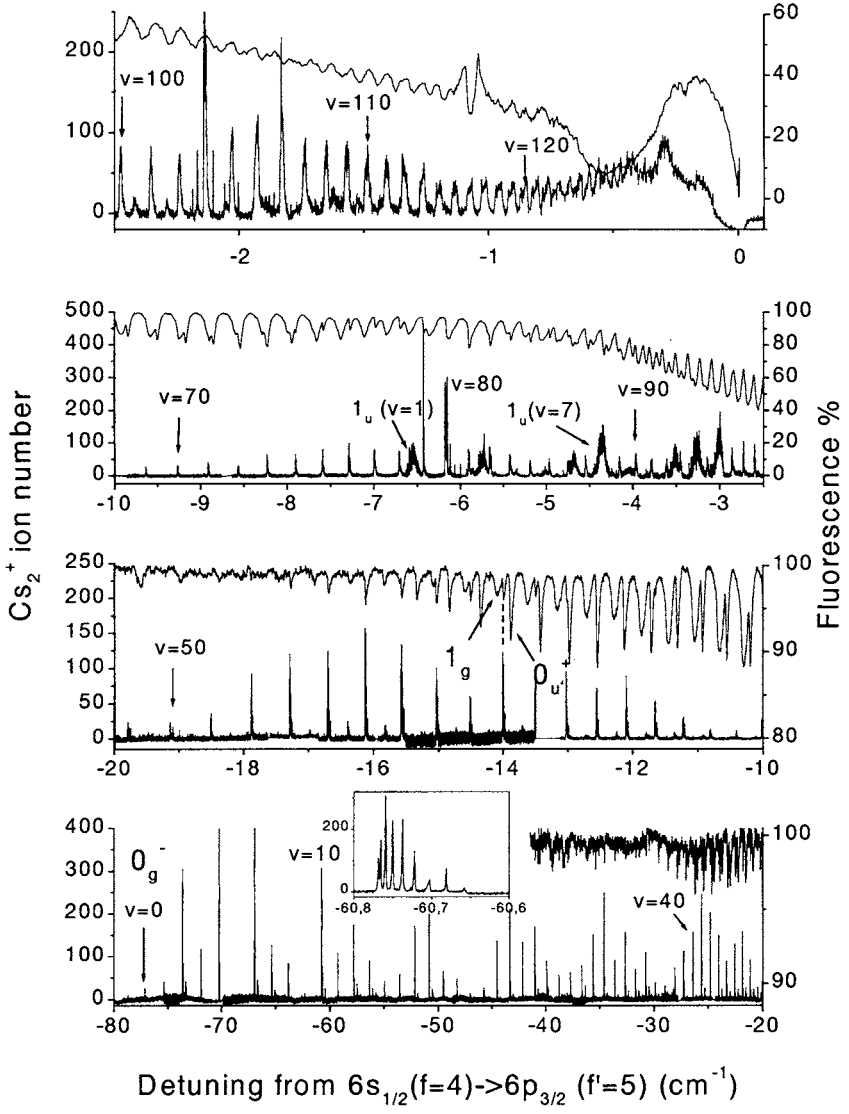

FIG. 10. Cs_2^+ ion signal (lower signal) and trap fluorescence yield (upper signal) versus detuning of the PA. In the inset, details of the rotational structure of the 0_g^- $v = 10$ level is shown. The dashed line indicates the correspondance of vibrational levels of the 0_g^- state on both spectra. Notice the different scales for the axis. The spectra are the results of a large number of scans.

level of the ground state,

$$Cs_2[\Omega_{u,g}(ns + np_{1/2,3/2}); v, J] \rightarrow Cs_2[^{1,3}\Sigma^+_{g,u}(6s + 6s; v_0, J)] + \hbar(\omega_0 + \delta_3). \tag{52}$$

The observed vibrational progressions can be assigned to the 1_g, 0^+_u, and 0^-_g $(6s_{1/2} + 6p_{3/2})$ states. About 80 lines for each vibrational progression are well resolved in the range 2–45 cm^{-1}. The 1_u state does not seem to be present in the fluorescence spectrum. The reason is that the dissociation of the photoassociated 1_u molecules after spontaneous emission do not produce "hot" enough atoms to escape the trap: in other words, E'_c is smaller than the trap depth. In the energy range of about 5 cm^{-1}, the observed linewidths are mostly due to the hyperfine structure and in qualitative agreement with the computed ones of about 6, 1.5, 0.6, and 6 GHz for the 1_g, 0^+_u, 0^-_g, and 1_u, respectively (Fioretti *et al.*, 1998).

To verify the identification of the lines, a fit can be performed with the semiclassical Le Roy–Bernstein law already discussed in Section II.B,

$$\left[D^i - E^i_v\right]^{1/6} = A_3(v_D - v)\left[C^i_3\right]^{-1/3}, \tag{53}$$

where the dissociation limit D^i, the constant A_3, and quantum number v_D have been defined in Eqs. (24) and (25). The relation between C^i_3 and $C_3 = \langle 6s|d_z|6p\rangle^2$ is given by Julienne and Vigué (1991):

$$C^1_3 = C_3(0^+_u) = \frac{5}{3}C_3 \qquad C^2_3 = C_3(1_g) = \frac{\sqrt{7}+2}{3}C_3 \tag{54}$$

The fit allows us to identify the excited electronic states, and to obtain values for their dissociation energies and for the constant C_3 (see the reviews by Weiner *et al.*, 1999; Stwalley and Wang, 1999). In the cesium experiments not reviewed in the quoted papers, the following values are obtained: $D^{\text{fit}}(1_g) = -3 \pm 1$ GHz, $v^{\text{fit}}_D(1_g) = 212.9 \pm 0.5$ (this refers to numerotation $v = 0$ for $\delta_1 = -44.141\ cm^{-1}$) and $C^{\text{fit}}_3(1_g) = 15.72 \pm 0.05$ atomic units for the 1_g state and $D^{\text{fit}}(0^+_u) = -7.8 \pm 1.1$ GHz, $v^{\text{fit}}_D(0^+_u) = 214.0 \pm 1$ (this refers to numerotation $v = 0$ for $\delta_1 = -44.336\ cm^{-1}$, and $C^{\text{fit}}_3(0^+_u) = 16.1 \pm 0.4$ atomic units for the 0^+_u state. C_3 coefficients are in 4% and 9% agreement with the calculated values [$C_3(1_g) = 16.22$ a.u., $C_3(0^+_u) = 17.46$ a.u.] of Marinescu and Dalgarno (1995). But the atomic lifetime τ deduced from the fitted C_3 coefficients,

$$\tau = \left(\frac{\pi\hbar\epsilon_0}{\langle 6s|d_z|6p\rangle^2}\right)\left(\frac{\lambda}{2\pi}\right)^3 \tag{55}$$

is in 1% and 5% agreement with the experimental one, $\tau_{6p_{3/2}} = 30.5 \pm 0.1$ ns (Volz and Schomoranzer, 1996). Notice that the fits are performed in a range of detuning (larger than 4 cm^{-1}) where the hyperfine structure is not expected to perturb noticeably the $-C_3/R^3$ behavior. The uncertainty of the fitting coefficients illustrates their variation according to the number of lines included in the fit. Some more accurate fit, including the higher multipolar expansion in the asymptotic part of the potential, should give more accurate prediction. Other effects, such as predissociation of 0_u^+ (Kokoouline *et al.*, 2000b) should also be considered. As mentioned by Fioretti *et al.* (1998), the Le Roy–Bernstein approach does not work very well for fitting the asymptotic potential of 0_g^-, due to its particular double-well character, with smooth variation of the potential in the bump zone between the inner and outer wells. Similar conclusions were obtained by Fioretti *et al.* (2001) for the equivalent double-well in the Rb_2 case.

2. *Ion Spectrum*

The ion signal is more selective than the trap-loss one, only the vibrational progressions of the 0_g^- and 1_u states being present in the Cs_2^+ spectrum. The detection procedure can be optimized, for either 0_g^- or 1_u, by adjusting the wavelength of the pulsed laser used for the photoionization. The detection is here sensitive up to a detuning range of 80 cm^{-1} for the PA laser.

Cs_2 0_g^- Pure Long-Range State. The Cs_2^+ ion spectrum exhibits 133 well-resolved structures assigned as the vibrational progression in the outer well of the 0_g^- ($p_{3/2}$) state, starting at $v = 0$. The rotational structure, shown for $v = 10$ in the inset of Fig. 10, is resolved up to $J = 8$ for most of the vibrational levels below $v = 74$.[1] The energies of the spectral lines have been fitted with a Rydberg–Klein–Rees (RKR) and near-dissociation expansion (NDE) approach, giving, for the outer well, an effective potential curve with a 77.94 ± 0.01 cm^{-1} depth and an equilibrium distance $R_e = 23.36 \pm 0.10 a_0$ (Fioretti *et al.*, 1999). This provides good knowledge for the vibrational wavefunctions and for the inner and outer turning points of the classical vibrational motion up to $v = 74$. The 0_g^- long-range well filled potential of various alkali dimers has been characterized by photoassociation spectroscopy: the experimental values for the spectroscopic constants have been determined for Na_2 (Ratliff *et al.*, 1994), where hyperfine structure has to be included, for K_2 (Wang *et al.*, 1996), who obtain a well depth and position $D_e = 6.49\,cm^{-1}$, $R_e = 14.63 a_0$, Rb_2 (Cline *et al.*, 1994), where

[1]The large number of observed rotational levels is due to a cooperative effect between the cooling laser and the PA laser (Fioretti *et al.*, 1999). In fact, if the cooling is switched off during the PA phase, at a temperature $T \leq 30$ μK, only s-waves have to be considered in the experiment with excitation of only $J = 0$ and $J = 2$ rotational levels. At $T \simeq 200$ μK *s*-, *p*-, and *d*-waves are essentially present and the excitation of rotational state up to $J = 4$ is possible.

$D_e = 28.295\,\mathrm{cm}^{-1}$. As discussed in Section II.A, the well depth $D_e = 77.94\,\mathrm{cm}^{-1}$ found by Fioretti *et al.* (1999) is much larger for Cs_2.

Two giant structures at detunings $\delta_1 = 2.14\,\mathrm{cm}^{-1}$ and $\delta_2 = 6.15\,\mathrm{cm}^{-1}$ will be described in Section V.C. We remark that the variation of level spacing follows approximately the $\Delta^{5/6}$ scaling law as a function of detuning: in the vicinity of a 1-cm^{-1} detuning, the level spacing is $\sim 0.6\,\mathrm{cm}^{-1}$, whereas close to $\hbar\delta_L = 10\,\mathrm{cm}^{-1}$ the level spacing increases up to $\sim 3.6\,\mathrm{cm}^{-1}$, in qualitative agreement with the 6.8 factor predicted by the scaling law. More refined verification should take into account the derivative of the level energy, and the variation of the C_3^i coefficient as a function of distance R_v^i. The modulation of the line intensities, due to the nodal structure of the ground-state wavefunction, described in Section II.E, is clearly visible. It has been noticed (see, for instance, Côté *et al.*, 1995; Tiesinga *et al.*, 1996) that this modulation can be used for the determination of collision parameters such as scattering lengths. Up to six of the eight visible nodes could be used by Drag *et al.* (2000b) to fit the ground triplet scattering length a_T.

The slow variation of the maximum intensity as a function of detuning can be qualitatively explained by a compensation beween the $\Delta^{-7/6}$ variation of the photoassociation rate and the $\Delta^{5/6}$ variation of the bound–bound transition probability provided we may prove that the molecular ion signal is a signature of the presence of molecules in the $a^3\Sigma_u^+$ lower triplet state.

Cs_2 1_u Pure Long-Range State. The large structures in the Cs_2^+ ion spectrum in the range (3–6 cm^{-1}) are assigned to the 1_u state. The Cs_2^+ ion spectra, recorded as a function of the PA laser frequency for the MOT and the dark SPOT devices, are shown in Fig. 11. The MOT spectrum exhibits both the 0_g^- and the 1_u vibrational progressions, while the 0_g^- progression is dominated by the 1_u one in the dark SPOT spectrum. The observed intensities corresponding to the same vibrational levels are different for the MOT and the dark SPOT experiments, which is not surprising because the two spectra correspond to two different initial states of the collisional process [see Eqs. (49) and (50)], with two free atoms in either the $f = 4$ or $f = 3$ state. For the 1_u state, the intensities corresponding to the dark SPOT are on average 10 times larger. One notices also that the vibrational level, $v = 0$, appears in the dark SPOT spectrum but not in the MOT spectrum. Conversely, higher vibrational levels, up to $v = 12$, are observed in the MOT spectrum.

Figure 12 shows the well-resolved structures of the vibrational levels $v = 0$, 1, and 2 of the 1_u state. The spectrum does not exhibit any simple progression, neither hyperfine nor rotational. To interpret these complex structures, Comparat *et al.* (2000) have performed systematic asymptotic calculations including both hyperfine structure and molecular rotation, for all the electronic states involved in 1_u photoassociation. They had not to introduce exchange energy in the calculations since this quantity remains small at the position (about $25a_0$) of the inner wall of

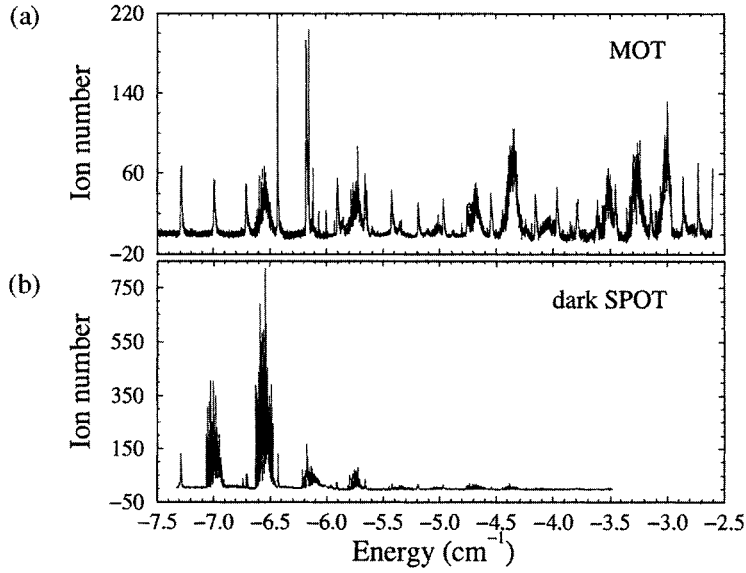

FIG. 11. Cs_2^+ ion signal versus detuning of the photoassociation laser in the dark SPOT device (a) and in the MOT (b). For the dark SPOT spectrum, the frequencies are shifted by 18.384 GHz.

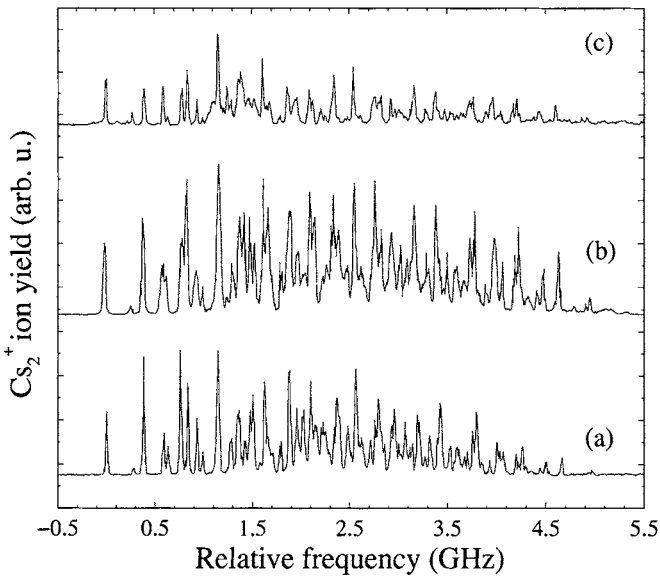

FIG. 12. Zoom of Cs_2^+ ion signal versus detuning of the PA laser in the dark SPOT device, for the 1_u vibrational levels $v = 0$ (a), $v = 1$ (b), and $v = 2$ (c).

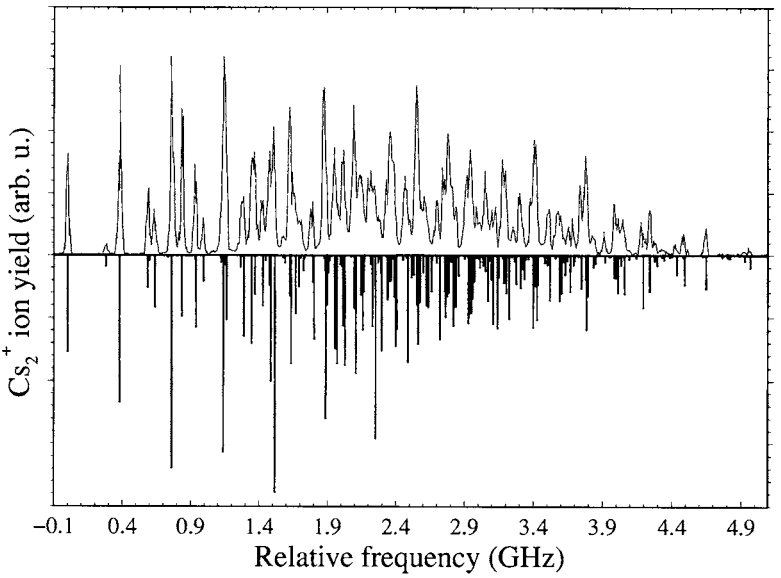

FIG. 13. Structure of the $v = 0$ line of the 1_u vibrational progression, compared in mirror with the calculated intensities. The frequency of the first observable line is arbitrarily taken as zero.

the 1_u potentials. The complete calculation of the positions and the intensities of the lines, in which the only adjustable parameters are the initial populations of the different partial waves (from s to g, here), agree very well with the experiment (see Fig. 13). More than the 0_g^- state, the 1_u state can really be labeled as a pure long-range state, corresponding to a pair of atoms, the cohesion of which is given by the electrostatic long-range multipole interaction (Stwalley *et al.*, 1978).

D. MECHANISM FOR COLD MOLECULE FORMATION

Up to now, although we have identified selective population of the $0_g^-(p_{3/2})$ and $1_u(p_{3/2})$ excited states in the ion spectrum, we have not yet proved the presence of ground-state ultracold molecules. Indeed, the molecular ions could be produced directly by photoionization of an excited state. To rule out this explanation, we analyze the Cs_2^+ ion signal by considering the following temporal sequence: first the PA laser beam is applied during 15 ms, then the ionizing laser pulse (7-ns width) is delayed compared to the switching on of the PA laser. We observe that the Cs_2^+ ion signal decreases with a characteristic time of the order of 10 ms (see Fig. 14). This time is five orders of magnitude larger than the radiative lifetime of any singly excited molecular state with electric-dipole allowed transition to the ground state. Indeed, this characteristic time is of the order of the time during

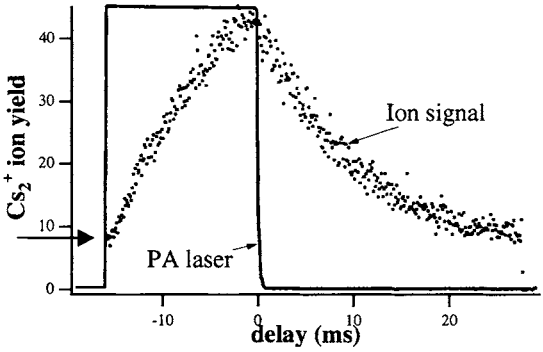

FIG. 14. Time evolution of the Cs_2^+ ion signal when the photoassociation laser is turned on and off. The exponential decrease corresponds to a characteristic time $T_d \approx 10$ ms, much larger than the radiative lifetime of the photoassociated molecules ($T_{sp} \approx 30$ ns). This result demonstrates that the photoionization scheme is indeed starting from long-lived ultracold molecules in the ground singlet or triplet state. The decrease of the signal is due to the fact that those molecules are falling down from the trap.

which molecules can move significantly out of the trap because of gravity. This result clearly indicates that ions are not produced by direct photoionization of PA excited molecules, but indeed by photoionization of the ground-state molecules.

Why, in contrast with earlier discussion, has reaction (52) a favorable branching ratio in the case of two particular symmetries? This can be explained by the very particular shape of the outer well for the two relevant potential curves, discussed in Section II.A. Due to the smooth $\sim R^{-3}$ behavior of the inner branch of the well, the vibrational motion is gradually slowed, and there is a non-negligible probability of presence at the inner turning point, as is manifested in Fig. 15, to be compared with Fig. 4 representing an "ordinary" vibrational wavefunction. The efficiency of the mechanism for the formation of cold molecules comes from the existence of a Condon point at intermediate distance, as shown schematically in Fig. 16. In all cases photoassociation occurs at long-range distance. The dissociation reaction (51) can always take place (i), but spontaneous emission may also occur at a short enough interatomic distance [case reaction (ii) or (iii)], forming cold ground-state (ii) or lower triplet-state (iii) molecules. This is due to the particular vibrational motion in the 0_g^- or 1_u external wells, where a long time delay is spent at both the outer and inner turning points. In contrast, in the case of the 1_g or 0_u^+ state, the reflection on the inner repulsive wall is very rapid, so that the vibration of the excited molecule keeps the two atoms at large interatomic distance most of the time.

Therefore, the formation of translationally cold molecules is attributed to the particular shape of some of the external potential wells in the heavy-alkali dimers, which offer at the same time an efficient photoassociation rate and a reasonable branching ratio for spontaneous emission toward the ground state. A confirmation of this mechanism has been demonstrated in rubidium by Gabbanini *et al.* (2000).

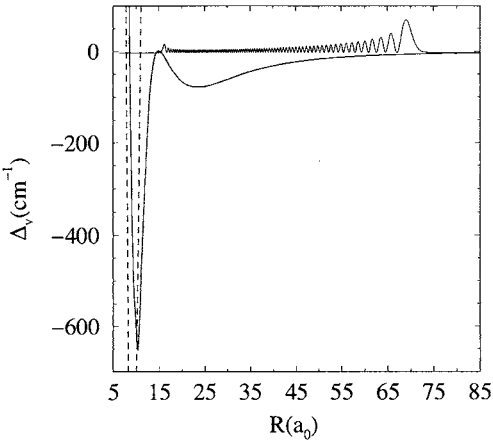

FIG. 15. Vibrational wavefunction in the outer well of the $0_g^-(6s + 6p_{3/2})$ potential of Cs_2, for a binding energy $\Delta_v = 6\,cm^{-1}$.

E. TRANSLATIONAL TEMPERATURE

These cold ground-state Cs_2 molecules are not trapped by the MOT and can be detected below the trap zone (Fioretti *et al.*, 1998; Comparat *et al.*, 1999). The spatial analysis of the ballistic expansion of the falling molecular cloud yields

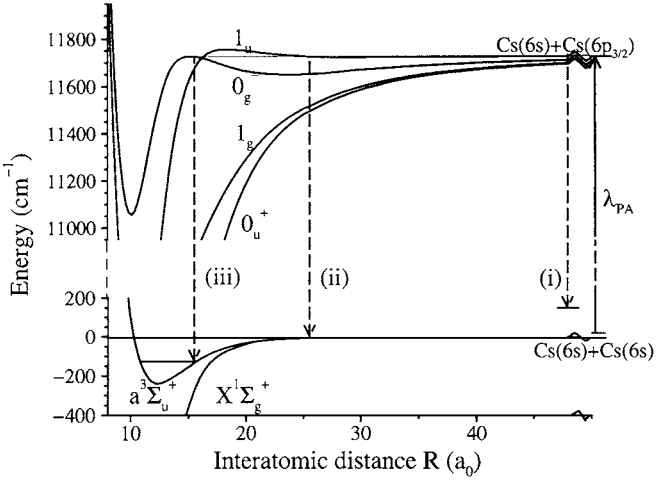

FIG. 16. Mechanism for the formation of ultracold molecules, from the relevant potential curves of Cs_2. The photoassociation process occurs at large distance. Line (i) represents spontaneous emission toward continuum states, with dissociation of the molecule; lines (ii) and (iii) represent spontaneous emission toward bound states, with formation of stable cold molecules.

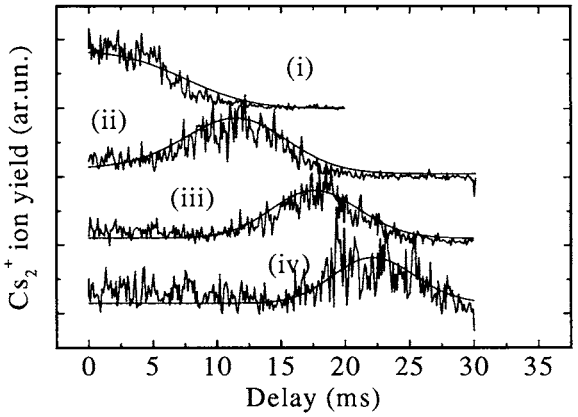

FIG. 17. Temperature measurement through time of flight: recordings (i–iv) correspond to the temporal analyzis of Cs_2^+ ion signal at the MOT position (i), and at 0.95 mm (ii), 1.90 mm (iii), and 2.85 mm (iv) below the MOT position.

a measure of the temperature of the molecular cloud. The ground-state cold Cs_2 molecules are photoionized into Cs_2^+ ions, using here the dye laser focused on spot of 300 μm diameter. Two kinds of measurements of the molecular temperature have been performed. The first one consists of photoassociating the cold atomic sample during a time of 3 ms. The fall of the molecular could is then temporally analyzed at different distances below the atomic trap. Figure 17 shows a time-of-flight analysis at different positions below the cold-atom trap. The theoretical fit of the experimental data gives access to the temperature, and also allows one to determine precisely the height of the fall. The other measurement of the temperature of the molecules relies on the analysis of the ballistic expansion for different heights, using the dye laser beam focussed on a spot with the same 300 μm diameter. Figure 18 depicts the spatial analysis of the falling molecular cloud. A model proposed by A. Lambrecht *et al.* (1996), taking into account the formation and the fall of the cold molecules, allows one to derive the molecular temperature from the data. A temperature as low as 20^{+15}_{-5} μK has been determined. The atomic temperature, measured similarly by photoionizing the cold Cs atoms into Cs^+ ions, lies in the range 20–30 μK, showing no difference with the molecular temperature.

F. PHOTOASSOCIATION RATE

The measurement of the rate of formation of cold molecules could be obtained directly by using the Cs_2^+ ion signal. Unfortunately, this signal is difficult to analyze, because the efficiency of the photoionization process is badly calibrated, probably not better than 10%. Taking into account the ion recollection and the detector efficiency, the global efficiency of the detection does not exceed a few percent.

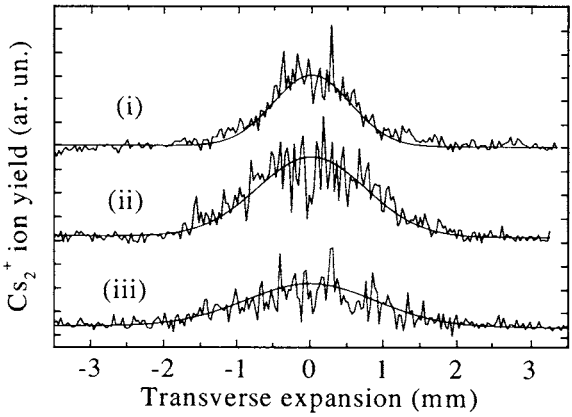

FIG. 18. Temperature measurement through ballistic expansion: recordings correspond to the spatial analyzis of Cs_2^+ ion signal at the MOT position (i), and at 1.90 mm (ii) and 3.80 mm (iii) below the MOT position.

This first estimation leads to a cold molecule formation rate of 0.1 per atom and per second in the conditions of a MOT. For a precise determination, it is preferable first to measure the PA rate by using the trap-loss signal and then to deduce the formation rate by using the calculated branching ratio between bound–bound and bound–free transitions of the photoassociated molecules.

Drag *et al.* (2000a) have so performed accurate trap-loss measurements for the two states 0_{it}^+ and 0_g^- $(6s + 6p_{3/2})$. To determine the experimental PA rates, they have considered the dynamic trap equation (Hoffmann *et al.*, 1994) expressing the balance between the loading rate Λ and the various loss rates, for a total number of trapped atoms N_{at} and a density n_{at},

$$\frac{dN_{\text{at}}}{dt} = \Lambda - \gamma N_{\text{at}} - (\beta + \beta_{\text{PA}}) \int_{\text{vol}} n_{\text{at}}^2(r)\, d^3r, \tag{56}$$

where γ is the loss rate due to background gas collisions, β is the loss rate due to binary collisions among the trapped atoms, and β_{PA} is the loss rate resulting from PA among the trapped atoms.[2] In the steady-state regime, the total number of trapped atoms is measured with or without the PA laser. In the former case, the resonance line intensity for the considered rovibrational level is recorded. Considering the Gaussian distribution of the atomic density and assuming that it is not too much affected by PA, determine the ratio

$$\frac{N_{\text{PA}}}{N_{\text{at}}} \simeq \frac{\gamma + \beta n_{\text{at}}}{\gamma + (\beta + \beta_{\text{PA}}) n_{\text{at}}}. \tag{57}$$

[2]The coefficient β_{PA} is weighted by a factor corresponding to the partial overlap between the cold atomic volume and the laser beam (see Fig. 8c).

Knowing the quantity $\gamma + \beta n_{at}$, one may deduce the parameter β_{PA}. The latter quantity corresponds to the inverse of the characteristic loading time of the MOT, which has been measured as $\tau \simeq 735$ ms, with the experimental conditions of the MOT $n_{at} = 10^{11}$ cm^{-3}, $T = 140\,\mu$K. They obtain in this way $n_{at}\beta_{PA}(0_u^+, 200\ \text{W cm}^{-2}) = 3.5 \pm 0.5\ \text{s}^{-1}$, for the level corresponding to a resonance line located at 14.35 cm^{-1} below the dissociation limit and for a PA laser intensity of 200 W cm^{-2}. They have measured the rate $n_{at}\beta_{PA}(0_g^-, 55\ \text{W cm}^{-2}) = 2.45 \pm 0.6\ \text{s}^{-1}$ for the $v = 77$, $J = 2$ level and for a PA laser intensity of 55 W cm^{-2}. More generally, in the Orsay experiments, for all the states observed in the energy range 5–10 cm^{-1} below both dissociation limits $6s + 6p_{3/2}$ and $6s + 6p_{1/2}$, PA rates measured through trap losses have values ranging roughly between 1 and 5 s^{-1} (Drag *et al.*, 2000a). The determination of the formation rate of cold molecules is discussed below in 5 V.B.

G. Rotational and Vibrational Temperatures

The molecules formed through PA are indeed translationally cold. But after spontaneous emission the cold molecular sample is found in a statistical mixture of a few rovibrational levels, determined by the Franck–Condon factors. To obtain ground-state molecules that are cold in all degrees of freedom (translation, vibration, and rotation) is still a challenge. Putting all the molecules in the same rovibrational level is a necessary step to get a molecular sample useful for further experiments. Stimulated Raman PA, where the emission on a given bound–bound transition is stimulated (see the scheme of the relevant levels in Fig. 19), offers such a possibility (Bohn and Julienne, 1996; Vardi *et al.*, 1997). Stimulated Raman PA has been used in a Rb condensate, where molecules should be formed, but up to now no direct evidence of their presence could be produced (Wynar *et al.*, 2000). It has been demonstrated for the cesium atom, by using a MOT device. (Laburthe-Tolra *et al.*, 2001)

The principle of the experiment consists, for a pair of colliding cold Cs atoms prepared in the hyperfine level $f = 3$, in having a Raman two-photon transition to form directly a ground-state $X^1\Sigma_g^+$ molecule in a well-defined final rovibrational level v, J. In fact, as the ground-state vibrational levels reached are located energy-wise in the vicinity of the dissociation limit, the gerade/ungerade symmetry is broken due to hyperfine coupling, and the electronic ground state corresponds to a superposition of singlet and triplet characters (Comparat *et al.*, 2000). The intermediate level, labeled 1 in Fig. 19, is a hyperfine-rotational component of the vibrational level $v = 0$ or 1 of the 1_u state, which will be specified later. The first laser, labeled L_1, is detuned by a value Δ on either the red side or the blue side of the resonance of the PA transition,

$$2\text{Cs}\,(6s,\ f = 3) + h\nu_1 \rightarrow \text{Cs}_2^*\,(1) \tag{58}$$

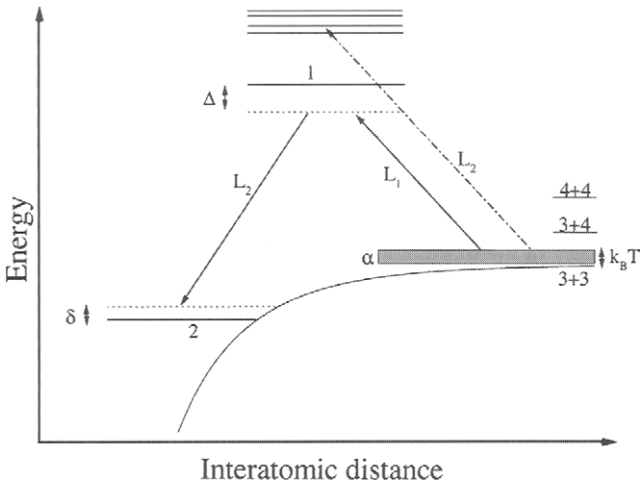

FIG. 19. Relevant energy levels of the stimulated Raman PA transition, from a continuum of states α of the two colliding atoms to a final bound level (2) of the ground state molecule. Δ and δ correspond to the detunings of lasers L_1 and L_2 compared to the PA transition $\alpha \rightarrow 1$ and to the stimulated Raman PA transition $\alpha \rightarrow 2$. The laser L_2 can also produce one-photon PA.

so that no PA due to the laser L_1 can be observed. We scan the frequency of the laser L_2 to make resonant ($\delta = 0$) the Raman transition toward the final ground-state level, labeled 2. One has

$$Cs_2^*(1) \rightarrow Cs_2(X^1\Sigma_g^+(6s, f' + 6s, f''); v, J) + h\nu_2 \tag{59}$$

Stimulated Raman PA is achieved by applying at $t = 0$, on the atomic cloud continuously illuminated by the laser beam L_2, a pulsed laser beam L_1 ($\tau = 2.5$ ms; this time is chosen to avoid a too significant decrease of the atomic density). The laser beam L_1 is provided by the Ti:sapphire laser with an available intensity in the MOT zone of 450 W cm^{-2}. A Pockels cell is used for switching. The laser beam L_2 is provided by a DBR diode laser (SDL 5712-H1, 100 mW) with a maximum available intensity of 50 W cm^{-2}.

Figure 20a shows the PA Cs_2^+ ion spectrum obtained by applying only the laser L_2 with an intensity of 30 W cm^{-2}, and by scanning its frequency around the resonance corresponding to one-photon excitation (process shown by the dot-dashed arrow in Fig. 19) of the vibrational level $v = 1$ of the $1_u(6s + 6p_{3/2})$ state. One has

$$2Cs(6s; f = 3) + h\nu_2 \tag{60}$$

$$\rightarrow Cs_2^*[1_u(6s + 6p_{3/2}); v = 1]. \tag{61}$$

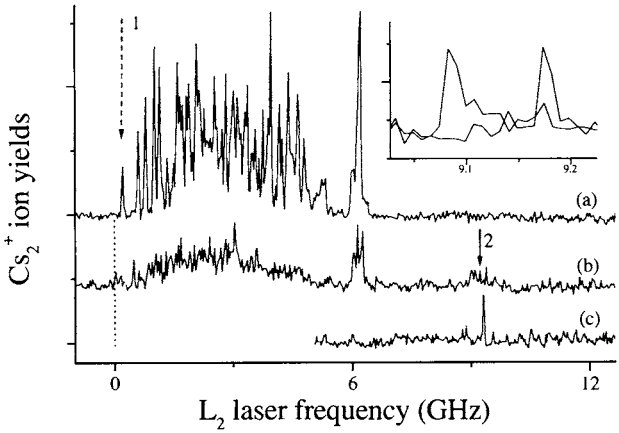

FIG. 20. (a) PA spectrum of the 1_u $v = 1$ level, by scanning laser L_2. (b) Same as (a) but in the presence of laser L_1. (c) Stimulated Raman PA resonance. The inset analyzes the Raman character of resonance (c).

The maximum of detected ions is here of the order of 100 per shot. The dashed arrow shows on this spectrum a very well resolved and isolated line. This resonance corresponds to the excitation of the hyperfine level, labeled 1, with a total angular momentum $F = 7$, and with a wave function close to

$$|(6s + 6p_{3/2})\, 1_u \Omega,\ I_t = 7, M_I = 7; F = 7, M_F\rangle. \tag{62}$$

I_t is the total nuclear spin, and M_I and Ω are respectively the projections of I_t and of the total electronic angular momentum, $J_t = 1$, on the molecular axis. The spectrum in Fig. 20b was obtained under the same conditions as previously, but by applying at the same time the Ti:sapphire laser (L_1). The frequency of laser L_1 (see the dotted line of Fig. 20) is now detuned by -20 MHz compared to the resonance 1. The Cs_2^+ ion signal is 1.5% of the ion signal with laser L_1 tuned to resonance 1, which means less than 10 ions per shot. This number is comparable to the Cs_2^+ ion background due to the presence of cold molecules in the MOT even without applying any PA laser (Fioretti *et al.*, 1998; Gabbanini *et al.*, 2000; Takekoshi *et al.*, 1998). Nevertheless, the presence of the laser L_1 perturbs the L_2 spectrum. This perturbation is not fully understood, but it probably corresponds to further excitation of the 1_u molecules toward highly excited states. Another characteristic of spectrum (b) compared to (a) is the appearance of new broad structures as shown by the full-line arrow. Reducing the intensity of the laser L_2 down to only 2 W cm^{-2} produces no more direct PA signal due to L_2, but maintains the existence of the extra structures which appear now as very narrow resonances (see Fig. 20c) corresponding to the formation of cold Cs_2 molecules

in a well-defined level of the ground state through stimulated Raman PA. The Raman character of the resonance has been tested by red- and then blue-detuning by quantities $\Delta \simeq \pm 40$-MHz laser L_1 from resonance 1. The inset in Fig. 20 shows the shift of the resonance by a quantity $\sim$80 MHz. It has been verified experimentally that the position of the line is fixed by the frequency difference of the two lasers. The stimulated Raman PA signal of Fig. 20c corresponds to about 50–100 detected ions, meaning a number of cold molecules of about 1000, within a factor of 3. The difficulty of a precise estimation of the cold-molecule number comes from the rough estimation for photoionization efficiency (Drag *et al.*, 2000a; Dion *et al.*, 2001).

H. Other Experiments

The case of the cesium atom is very demonstrative for the use of PA for the formation of cold molecules. We have already demonstrated the possibility to obtain cold molecules in the ground state or the lowest triplet state at temperature in the range 20–200 μK with a formation rate typically varying between 0.05 and 0.2 molecule per atom and per second for the experimental conditions in Orsay (atomic temperature 20–200 μK, density 4×10^{10} atoms/cm^3). For 50 million trapped atoms, 2.5 to 10 million ultracold molecules are formed per second. We can also form state-selected molecules with similar characteristics by using the stimulated Raman photoassociation. Is it possible to extend the case of the cesium atom and dimer to other species? The answer is not obvious, because the efficiency of the mechanisms is based on the particular double-well shape in the 0_g^- and $1_u\,(6s + 6p_{3/2})$ potentials curves, creating a Condon point at intermediate distance. Among other alkali atoms, only the rubidium present a similar characteristic for the $0_g^-\,(5s + 5p_{3/2})$ state. The formation of cold Rb_2 molecules in the lowest triplet state has been demonstrated by Gabbanini *et al.* (2000). The formation of translationally cold K_2 molecules in their singlet ground state has been demonstated via photoassociation of the $A^1\Sigma_u^+(4s + 4p_{3/2})$ state (Nikolov *et al.*, 1999). Here the molecular configuration does not correspond to a long-range outer well. The branching ratio for bound–bound transitions is not as important as for the cesium and rubidium experiments, and the rate for the formation of cold molecules is only 1000 per second for the considered experimental conditions. This number is nevertheless more important as compared to most of PA experiments, and is due to an accidentally non-negligible Franck–Condon factor for a given bound–bound transition. More complex schemes of formation of cold molecules have been proposed, with PA of highly excited molecular states (Band and Julienne, 1995; Bohn and Julienne, 1996). An efficient production of K_2 molecules has indeed been achieved by using a two-step excitation scheme. In this case, highly excited molecules radiate toward various vibrational levels of the X ground state, with a rate comparable to the one achieved for cesium atom

(Nikolov *et al.*, 2000). The supplementary difficulty is the use of a second photoassociation laser but the method is a general one.

The conclusion of this section is that the formation of cold molecules via PA can certainly be extended to any species which can be previously laser-cooled. The demonstration of novel mechanisms for the formation of ultracold molecules make this route very promising. However, a last difficulty in making these cold molecular samples useful for applications is to be able to trap them. The trapping of cold molecules with a CO_2 laser quasi-electrostatic trap has been demonstrated (Takekoshi *et al.*, 1998, 1999). These trapped cold molecules are not formed via PA, but are those naturally present in the MOT trap. This result should be extended to molecules formed directly by photoassociation in such a trap. Unpublished results obtained in Orsay have demonstrated the possibility of trapping cold molecules in the lowest triplet state by using a quadrupolar magnetic trap. Trap devices for molecules should show rapid developments in the next years. They should allow one to accumulate up to 10^4–10^6 ultracold molecules in a 10- to 100-μK temperature range, eventually in a well-defined rovibrational level of the ground state (or the lowest triplet state) if stimulated Raman PA is used. The PA experiments using a condensate should also show interesting developments (Wynar *et al.*, 2000). We did not develop in this review this kind of very exciting results, which should lead to the possibility of observing a molecular condensate or a molecule laser. The coherence of the Raman process is here a key point making the conception of these experiments a little different.

IV. Theoretical Methods

The theoretical treatment of cold-atom collisions has stimulated many new developments, which can be found, for instance, in the review of Weiner *et al.* (1999). In the present review we shall focus on progress that was specially motivated by the research on ultracold molecules, insisting upon the necessary accuracy in estimation of Franck–Condon overlap as described in Section II.D. The specific technical problems are:

- The dynamics of ultracold molecules is characterized by the large extension of the vibrational motion in regions where the potential is very weak. Accurate description of the nuclear motion requires methods capable of describing both the short-range region, where chemical potentials are acting, and the long-range region.
- In addition, the dynamics is very sensitive to the accuracy in the electronic potential curves, and the requirement is well beyond the present accuracy of

ab initio calculations. Methods to fit the potentials to accurate experimental data should be revisited for the present problem.

A. Dynamics: Determination of Vibrational Wavefunctions for Photoassociated Molecules

We have seen above that the estimation of the photoassociation rate is controlled by the matrix element of the electronic dipole moment between the continuum wavefunction in the ground state and the bound vibrational wavefunction in the excited state [see Eqs. (34) and (35)]. Numerical accuracy in the estimation of this quantity is a key for a good comparison between theory and experiment. Although well-established techniques have long been developed in molecular physics for that purpose, the problem of cold molecules presents some specific difficulties. We give in Fig. 4 an example of a typical vibrational wavefunction for a level close to the dissociation limit of the $Cs_2 1_g(p_{3/2})$. The local de Broglie wavelength $\lambda(R)$, in atomic units, with $\hbar = 1$, is

$$\lambda(R) = \frac{2\pi}{\sqrt{2\mu[V_\infty - V(R)]}}, \tag{63}$$

and depends on the value of the potential $V(R)$, which varies by several orders of magnitude from the short-range region to the asymptotic region. It is clearly visible in Fig. 4 that the local de Broglie wavelength is varying from a few tens of a_0 in the outer region to a value less than $1a_0$ in the inner region, i.e., by more than one order of magnitude from the short-range region to the long-range region. The numerical or analytical methods should be adapted to this situation, and the use of a radial coordinate adapted to the local de Broglie wavelength is the key for all developments.

1. Mapped Fourier Method

Grid numerical methods using fast Fourier transform have proved to be very efficient for quantum molecular dynamics (Kosloff, 1988, 1996). Wavefunctions and operators are represented on grids in both the momentum and coordinate spaces. It is convenient to use a constant grid step s, which is linked to the minimum value of the local de Broglie wavelength. For calculations of the vibrational levels of a diatomic molecule, a Fourier grid method, originally proposed by Marston and Balint-Kurti (1989) and by Colbert and Miller (1992), was further developed by Monnerville and Robbe (1994), Dulieu and Julienne (1995), and Dulieu *et al.* (1997), and proved to be very successful. The wavefunction may be represented by its values at a set of N equally spaced radial distances between the two distances

R_1 and $R_1 + N \times s = R_1 + L$,

$$\psi(R_i) = \sum_{k=(-N/2+1)}^{N/2} a_k g_k(R_i)(i,\ j = 1,\ N), \tag{64}$$

$$R_i = R_1 + (i-1)^s,\ s = \frac{L}{N} \tag{65}$$

where N is assumed to be an even number, provided we may define a set of delta functions at the grid points through the relation

$$\sum_{k=(-N/2+1)}^{N/2} g_k(R_i) g_k(R_j) = \delta(R_i - R_j) \qquad (i,\ j = 1,\ N). \tag{66}$$

(67)*

This can be achieved by a discrete Fourier expansion on a set of N ingoing and outgoing plane waves, with wavelength varying from $2s$ to L, choosing

$$g_k(R) = \frac{1}{\sqrt{N}} \exp\left(-i \frac{2k\pi R}{L}\right), \tag{68}$$

$$k \epsilon \left[-\frac{N}{2} + 1, \frac{N}{2}\right]. \tag{69}$$

The coefficients a_k are then readily calculated as

$$a_k = \frac{1}{\sqrt{N}} \sum_{k=1}^{N} \varphi(R_j) \exp\left(\frac{i2k\pi R_j}{L}\right), \tag{70}$$

and can be interpreted as the amplitude $a_k(p)$ of the wavefunction on equally spaced grid points in the momentum space, $p_k = 2k\pi/L$. The two representations are connected by Fourier transform, the basis set in momentum representation, conjugated to the coordinate representation basis set defined in Eq. (68), being

$$f_j(p) = \frac{1}{\sqrt{N}} \exp(-ipR_j). \tag{71}$$

The maximum value of momentum that can be represented in such a basis is

$$p_N = N\frac{\pi}{L} = \frac{\pi}{s}, \tag{72}$$

*Equation deleted in proof.

where s is the constant grid step defined in Eq. (65). It is then straightforward to represent all operators by $N \times N$ matrices either in coordinate or in momentum representation. The radial Schrödinger equation,

$$[\mathbf{T} + \mathbf{V}(R)]\psi(R) = E\psi(R), \tag{73}$$

involves two operators. The matrix $\mathbf{V}(R)$ is diagonal in the coordinate representation, while the kinetic energy operator $\mathbf{T}(p)$ is diagonal in the momentum representation and can be easily evaluated. After Fourier transform, it is written in the coordinate representation as

$$T_{ii} = \frac{\pi^2}{\mu L^2}\frac{N^2+2}{6}, \tag{74}$$

$$T_{ij} = (-1)^{i-j}\frac{\pi^2}{\mu L^2}\frac{1}{\sin^2[(i-j)\pi/N]}. \tag{75}$$

The eigenvalues are obtained by diagonalization of the $N \times N$ matrix $\mathbf{T} + \mathbf{V}(R)$. The computation effort involved in the diagonalization procedure scales as N^3. The choice of the constant step, and therefore of N, is linked to the maximum momentum in the physical problem or to the minimum value of the local de Broglie wavelength,

$$s \leq \frac{\lambda(R_e)}{2} = \frac{\pi}{\sqrt{2\mu(V_\infty - V_{R_e})}}, \tag{76}$$

obtained at the equilibrium distance R_e where the potential is minimum. In the example of the $v = 332$ excited wavefunction in the 1_g potential presented in Fig. 21, the calculations would require at least diagonalization of a 8200×8200 matrix. However, the grid step is unnecessarily small in the long-range region. Fattal *et al.* (1996) and Kosloff (1996) have proposed a mapping procedure in order to optimize the use of phase space in grid methods, with application to Coulomb potentials. This mapping procedure has been generalized to the present problem by Kokoouline *et al.* (1999), who have introduced a variable grid step adapted to the local de Broglie wavelength,

$$s(R) = \frac{\pi}{\sqrt{2\mu[V_\infty - V(R)]}} = \frac{\lambda(R)}{2}, \tag{77}$$

or more generally, depending on an enveloping potential $V_{\text{env}}(R)$ located below the physical potential for all internuclear distances, for instance, the analytical

asymptotic potential $-C_3^i/R^3$ or $-C_6^i/R^6$. The grid step is now

$$s_{\text{env}}(R) = \frac{\pi}{\sqrt{2\mu[V_\infty - V_{\text{env}}(R)]}}. \tag{78}$$

The number of grid points is markedly reduced when the step size is defined by Eq. (77) and the same accuracy can be obtained by diagonalization of a 564×564 matrix. This matrix is obtained by defining a grid in a new coordinate x such that the variable step in R corresponds to a constant step in x. We therefore use a Jacobian $J(x)$ such that

$$dR = J(x)\,dx, \tag{79}$$

$$J(x) = \frac{\lambda(R)}{\lambda(R_e)}. \tag{80}$$

The radial Schrödinger equation

$$\left\{-\frac{1}{2\mu J^2}\frac{d^2}{dx^2} + \frac{J'}{\mu J^3}\frac{d}{dx} + V + \frac{1}{2\mu}\left[-\frac{5}{4}\frac{(J')^2}{J^4} + \frac{1}{2}\frac{J''}{J^3}\right]\right\}\phi(x) = E\phi(x), \tag{81}$$

may be written in a symmetrical form by considering a new wavefunction $\phi(x)$,

$$\phi(x) = J^{+1/2}(x)\psi(x), \tag{82}$$

and by introducing a new potential, $\bar{v}(x)$ such that

$$\bar{V}(x) = V(x) + \frac{1}{2\mu}\left[\frac{7}{4}\frac{(J')^2}{J^4} - \frac{1}{2}\frac{J''}{J^3}\right]. \tag{83}$$

The calculation of the kinetic energy operator is then straightforward,

$$T_{i,j} = (-1)^{i-j}\frac{\pi^2}{2\mu L^2}\frac{1}{\sin^2[(i-j)\pi/N]}\left(\frac{1}{J_i^2} + \frac{1}{J_j^2}\right), \tag{84}$$

if $i \neq j$, while

$$T_{i,i} = \frac{\pi^2}{\mu L^2}\frac{N^2+2}{6}\frac{1}{J_i^2}. \tag{85}$$

Therefore calculations are performed in the working grid using the coordinate x with a constant grid step. The vibrational energies are then obtained by diagonalization of the Hamiltonian in the new representation. The wavefunctions have to be transformed making use of Eqs. (82) and (80) to obtain results in the physical grid R. If the potential $V(R)$ is given as a set of numerical values, the procedure is straightforward. However, as the derivation involves first and second derivatives of the Jacobian $J(x)$, care must be taken that such derivatives are well defined. In many applications, the potentials are obtained by matching short-range potentials computed by *ab initio* method to long-range asymptotic expansion, and interpolation procedures have to be carried out carefully. An alternative procedure consists of considering an enveloping analytical potential for the definition of the new variable x. Choosing, for instance, a potential $V_{\text{env}}(R) = -C_n/R^n$ with $n \neq 2$, the change of variable in Eq. (80) becomes analytical, and for a grid starting at distance R_{in} we may define an adaptative coordinate through the formula

$$x = \frac{2\sqrt{2\mu C_n}}{\pi(n-2)} \left(\frac{1}{R_{\text{in}}^{(n-2)/2}} - \frac{1}{R^{(n-2)/2}} \right). \tag{86}$$

The interpretation of this change of variable will be given on page 108.

As discussed by Kokoouline *et al.* (1999), this procedure is less efficient than the preceding one, making use of the real potential, as far as optimization of the phase space is considered, but the calculations now use analytic formulas, which may save computing time. Finally, we should note that the wavefunction defined at grid points can be interpolated without further loss of accuracy by use of the Fourier expansion,

$$\psi(q) = \sum_{j=i}^{N} \psi(q_j)\, \text{sinc}\left[\frac{\pi}{\Delta q}(q - q_j) \right], \tag{87}$$

where q_j is a working uniform grid (with or without mapping), q is any intermediate point, Δq is a grid step, and we have defined the function $\text{sinc}(z) = [\sin(z)/z]$. In Fig. 21 we display the wave function, computed with sinc interpolation at a large number ($N_{\text{interp}} = 10{,}000$) of q values, for the ($v = 332$) vibrational level of $Cs_2(1_g)$. Comparison with linear interpolation clearly illustrates the good quality of the second interpolation. Of course, we have checked the accuracy of the interpolated wavefunctions by comparing to standard methods. The wavefunction in the adaptative coordinate x is displayed in Fig. 22, illustrating the regularity of the oscillations.

The grid points can be used for the Fourier expansion of the wavefunction, yielding useful properties in numerical quadrature. It is possible to use MFGR representation with the same grid for the ground- and excited-state wavefunctions

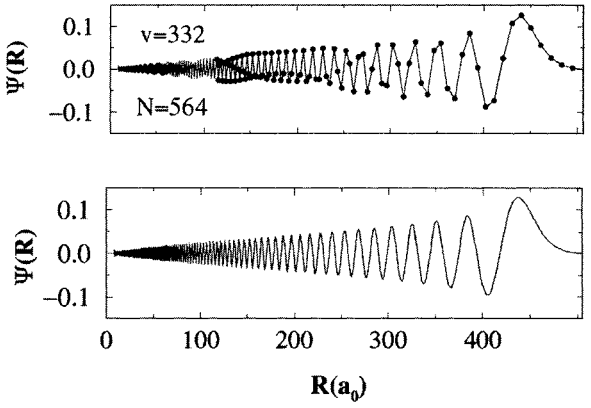

FIG. 21. (Upper) The $v = 332$ vibrational wavefunction for the $1_g(6s + 6p_{3/2})$ potential of Cs_2, with binding energy $\Delta_v = 0.0419\,\mathrm{cm}^{-1}$, computed at the grid points defined with the mapping of the Eq. (77). Here, the grid extends up to $500a_0$, and contains $N = 564$ points. (Lower) Interpolation procedure. The wave function $\psi(R)$, $R \neq R_j$, is interpolated as Eq. (87) in text.

so that excellent accuracy can be obtained for an overlap integral of the two functions; this seems one of the main advantages of a grid method. It can be easily generalized to double-well potentials, as will be discussed later in the example of tunneling effect, and to calculations with several channels, including predissociation problems where coupling between bound and continuum levels has to be considered (Kokoouline *et al.*, 2000b). In the method described above, all vibrational levels are computed up to a maximum energy. It may be convenient to limit the calculations to a given energy range by use of filtering techniques: in particular, in the vicinity of a dissociation limit, there is a large density of levels. A mapping procedure is introduced by Tiesinga *et al.* (1998) in a filtering method making use of Green-function operators to resolve the hyperfine structure for the levels close to the Na($3s$) + Na($3p$) asymptote.

The choice of the number of grid points is presently determined by optimization of the use of the classical phase space (Fattal *et al.*, 1996; Kokoouline *et al.*, 1999).

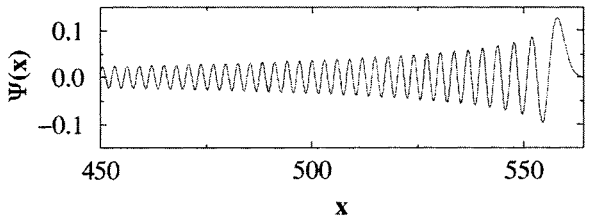

FIG. 22. Interpolated wavefunction in the x variable, adapted to the local de Broglie wavelength. The graph shows only the part corresponding to large R. Comparing with Fig. 21, one can appreciate the regularity of the oscillations in the mapped wavefunction.

For low-energy scattering, or for levels close to the dissociation limit, the extension of the wavefunction in the classically forbidden region increases, and this effect has been up to now empirically addressed by an increase of the number N of points. A proper treatment of the classically forbidden region, with *a priori* calculation of the number of points necessary to represent the classically forbidden region, still has to be implemented; it should benefit from the expertise developed by the groups working on analytical representation of the wavefunction (Boisseau *et al.*, 2000b).

2. *Numerov Approach and Other Methods*

Many groups working in the field of cold collisions and long-range molecules have used the well-known Numerov–Cooley algorithm (Cooley, 1971, and references therein), both for bound and continuum wavefunctions, often using the Blatt criterion (Blatt, 1967) to choose the step length by minimizing local truncation error. For bound and predissociated levels, the Cooley–Cashion–Zare routine SCHR has been regularly modified and improved by the group at the University of Waterloo (Canada), and the present version (Le Roy, 2000) includes variable steps. We should also mention introduction of a variable step in Numerov integration by Côté and Jamieson (1995), the step size being divided by a factor of 2 each time the local wavenumber becomes smaller than a given parameter. Comparison with the grid methods described above still has to be carefully done, in order to check accuracy and efficiency. The present situation is such that potentials data being usually given for a limited number of internuclear distances, with a large mesh size, results depend on the method chosen for interpolation. An accurate comparison should consider a potential in an analytical form, or implement the same interpolation procedure.

In the case of a two-channel problem, with both bound and continuum solutions, a recent paper by Rawitscher *et al.* (1999) compares various approaches to compute scattering wavefunctions and extract the scattering length and effective range. For two coupled potentials of Lennard–Jones type, with an exponential coupling term, equivalent results are obtained by

- A spectral-type integral equation based on Chebyshev expansions,
- A noniterative eigenchannel variant of the R-matrix method (Aymar *et al.*, 1996),
- A Gordon method (Gordon, 1969) as modified by Mies (1973).

The third one is easier to implement but necessitates a much larger number of points. In contrast, an improved Numerov method is shown to yield much poorer accuracy. The authors conclude with the necessity of performing similar comparison under more complex conditions.

3. Analytical Treatment

Analytical solutions of the radial Schrödinger equation have been proposed by many authors, mainly in the framework of the JWKB approximation. At zero scattering energy, Gribakin and Flanbaum (1993), in a paper which is considered one of the main references in cold collisions, obtained an analytical expression of the scattering length by transforming the radial equation into a Bessel equation. We should note that the change of variable is

$$x = \frac{2}{(n-2)} \frac{\sqrt{2\mu C_n}}{\hbar} \frac{1}{R^{(n-2)/2}}, \tag{88}$$

similar to the change of variable introduced in Eq. (86) at the limit $R_{in} \to \infty$, with $\hbar = 1$. Future work might benefit from this analogy. For the description of bound levels, many authors have worked within the framework of the semiclassical approximation defined above. Close to the dissociation limit, where the part of the wavefunction that extends into the nonclassical region becomes important, corrections to the first-order JWKB approximation have been implemented. Friedrich and Trost (1996a,b), Trost and Friedrich (1997); Trost *et al.* (1998) introduce a Maslov index modifying the $\pi/4$ reflexion phase at the outer turning point, and changing the Bohr–Sommerfeld quantization condition in Eq. (15). Another approach, by Boisseau *et al.* (1998, 2000a), considers second-order JWKB terms and numerical corrections to the quantization condition. The two derivations give the same results. Gao (2000) has discussed in detail the breakdown of Bohr's correspondence principle. As discussed above, numerical calculations can also be implemented in the region where the first-order semiclassical treatment fails.

B. The Need for Accurate Molecular Potential Curves and Electronic Dipole Transition Moments

One reason why the comparison between theory and experiment happened to be relatively easy in the case of K_2, Rb_2 and Cs_2 dimers is that accurate potentials were available at both short and long internuclear distances. We should cite, for short distances, the pseudo-potential *ab initio* calculations of Meyer's group (Spies, 1989) for Cs_2, of Foucrault *et al.* (1992) for Rb_2 and Cs_2, of Magnier and Millié (1996) for K_2 and NaK, and of Magnier *et al.* (1993) for Na_2. In addition, a lot of spectroscopic information is available, very accurate potentials being fitted to experimental spectra: let us cite, among many other examples, the recent fit of ground-state potential for the Rb_2 molecule by Seto *et al.* (2000), where 99.8% of the potential well can be deduced from a fit to 12,148 transition frequencies in a high-resolution A–X emission spectrum. For implementation of the detection scheme using absorption to an intermediate state, knowledge of excited potential curves and transition dipole moments is essential. In that case, the information

collected in the experiments of Pichler's group, who performed absorption experiments with dense alkali vapors in a heat pipe (Pichler *et al.*, 1983; Beuc *et al.*, 1982; Veza *et al.*, 1998), has also proved very helpful. In contrast, recent results on photoassociation of calcium (Zinner *et al.*, 2000) have not been fully interpreted due to the lack of theoretical information.

The matching between short-range *ab initio* calculations and long-range expansion (Marinescu and Dalgarno, 1995, 1996; Derevianko *et al.*, 1999), and references herein. Next must be performed (see Fig. 3). Discussion on the accuracy of long-range coefficients is beyond the scope of the present chapter, and can be found in various papers (Stivalley and Wang, 1999). The computed values either agree with experiment or must be modified by a few percentage. This can be verified on the values given in §C1 for the C_3 coefficients. Finally, it should be wise to remember from the two previous sections that when potentials are computed on a set of internuclear distances, the mesh size should be sufficiently small to avoid loss of accuracy due to the interpolation procedure.

V. Present Status of the Comparison between Experiment and Theory: Formation Rates

As examples of comparison between theory and experiment, we shall discuss the determination of photoassociation rates and absolute number of ultracold Cs_2 molecules obtained in Orsay, as well as the demonstration of a tunneling effect from analysis of the spectra.

A. Photoassociation Rates

Using for Cs_2 the set of potentials obtained by matching the *ab initio* calculations of Meyer's group (Spies, 1989) to asymptotic curves using the long-range coefficients of Marinescu and Dalgarno (1995), the photoassociation rates were computed with the numerical methods developed above and compared to experiment (Drag *et al.*, 2000a).

In Fig. 23 we display the quantities $\mathcal{R}_{PA}$ in s^{-1} (number of photoassociated molecules formed per second divided by the total number of atoms) defined in Eq. (36) and $\kappa_{PA} = \mathcal{R}_{PA}/n_{at}/(I/\hbar\omega_{PA})$, defined per photon and per unit density, for photoassociation into a vibrational level of the double-well 0_g^- $(6s + 6p_{3/2})$ curve, and of the long-range attractive 0_g^- $(6s + 6p_{1/2})$ curve. The detuning δ_L of the laser is relative to the D_2 and D_1 resonance lines, respectively, and is varied on the entire range covered by the 0_g^- $(6s + 6p_{3/2})$ external well. The photoassociation rate displays minima at detunings such that R_v^i corresponds to the nodes in the ground-state wavefunction, as discussed in Section II.E. The intensity of the maxima decreases as a function of the detuning of the laser: for photoassociation into a

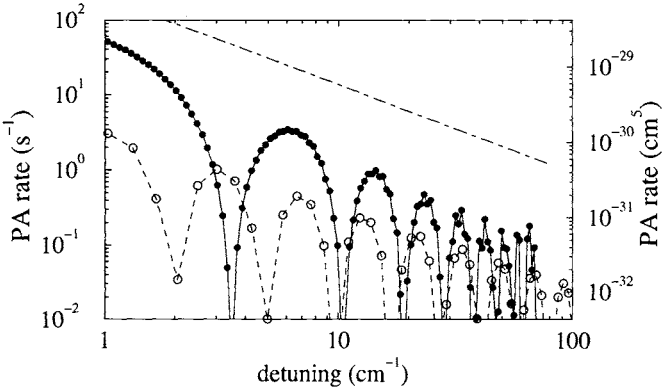

FIG. 23. Computed cesium photoassociation rates, $\mathcal{R}_{PA}$ (in s^{-1}) and κ_{PA} (in cm^{-5}), for molecular states of 0_g^- symmetry correlated to $6s + 6p_{3/2}$ (closed circles) and to $6s + 6p_{1/2}$ (open circles). Experimental parameters are chosen: $T = 140\,\mu K$, $n_{at} = 10^{11}$ cm^{-3}, $I = 55$ W/cm^2. We notice a modulation in the rates due to the nodal structure of the initial continuum state wavefunction (see text). The dot-dashed lines indicate the PA rate given with the approximate formula (55) in the work of Pillet *et al.* (1997), approximating the continuum wavefunction by its asymptotic sine behavior.

level of the $0_g^-(p_{3/2})$ state, the decrease verifies the $(\delta_L)^{-7/6}$ behavior predicted by the simple model described in Section II.F. We should notice the importance of the decrease, the rate varying by two orders of magnitude when the detuning increases from 1 cm^{-1} to 50 cm^{-1}.

In contrast, as the $0_g^-(p_{1/2})$ potential curve displays R^{-6} asymptotic behavior (due to cancellation of the C_3^i coefficient), the scaling law is different (Wang and Stwalley, 1998) and the decrease is slower. We notice that, despite the C_6 long-range behavior, the corresponding PA rates are not negligible, being roughly one order of magnitude smaller than in the previous case. This result is of some interest for future studies of PA in heteronuclear species, which also present R^{-6} long-range behavior (Wang and Stwalley, 1998).

An interesting result of the calculations is the importance of the correct determination of the correct ground-state wavefunction. In Fig. 23, we also display rates computed with a $\Psi_E(R)$ continuum wavefunction approximated by a free-wave sine function: the corresponding curve is overestimated by more than one order of magnitude, and of course does not represent the minima at the nodes of the real $\Psi_E(R)$ function. *This confirms that the bottleneck in the photoassociation process is the amplitude of the initial wavefunction, demonstrating the advantage of performing experiments at small detunings.*

Precise comparison between experiment and theory has been presented by Drag *et al.* (2000a) for photoassociation into the vibrational levels of the 0_g^- and $0_u^+(6s + 6p_{3/2})$ curves, at detunings 6.92 and 14.35 cm^{-1}, respectively, below the

$6s(f = 4) + 6p_{3/2}(f' = 5)$ limit, for which atomic loss rates have been measured. The main source of uncertainty lies in the experimental parameters (atomic density n_{at}, temperature T, laser intensity I) which have to be introduced in the calculations. The measured atom loss rates are determined under experimental conditions with $n_{at} = 10^{11}$ cm^{-3}, $T = 140 \pm 20$ μK, $I = 55$ W/cm^2 for 0_g^- and $I = 200$ W/cm^2 for 0_u^+. The calculations use $T = 140$ μK and $I = 55$ W/cm^2 in both cases. For the 0_g^- and 0_u^+ photoassociation rates, the theoretical values are, respectively, of 6.6 and 5.8 molecules s^{-1}, in good agreement with the experimental values of 2.4 and 3.5 molecules s^{-1} (assuming simply that the atom loss rate is twice the PA rate). Both calculated and experimental rates lie within the margin of 1–5 excited molecules formed per second and per atom, for a total number of atoms $N_{at} = 5 \times 10^7$, estimated within a factor of 2. *This means that all atoms in a MOT could be transformed into excited molecules in a time less than 1 s.*

B. Cold-Molecule Formation Rate

The next step is the estimation of the percentage of the photoassociated molecules that may be stabilized into long-lived molecules. The rate equation for the number $N_{exc}(v, J)$ (or simply N_{exc}) of molecules photoassociated in a rovibrational state (v, J) by the laser can be written as

$$\frac{d}{dt} N_{exc} = \mathcal{R}_{PA} N_{at} - \Gamma_{exc} N_{exc}, \tag{89}$$

where Γ_{exc} is the spontaneous emission probability of level (v, J) and N_{at} is the number of atoms in the trap at time t. Provided that $\mathcal{R}_{PA} \ll \Gamma_{exc} \approx \Gamma$, the number of atoms N_{at} is assumed to be constant, as the trap loading time is longer ($\sim$700 ms) than all other characteristic times in the problem. In such conditions, the system reaches within a time Γ_{exc}^{-1} a stationary state with a constant number $\bar{N}_{exc}$ of excited molecules,

$$\bar{N}_{exc} = \frac{\mathcal{R}_{PA}}{\Gamma_{exc}} N_{at}(0). \tag{90}$$

The number of long-lived ultracold molecules $N_{cold}(t)$ produced at time t by spontaneous emission can be estimated as

$$N_{cold}(t) = \Gamma_{exc}^{bound} \bar{N}_{exc} t, \tag{91}$$

where Γ_{exc}^{bound} is the spontaneous emission probability of the excited level v toward all levels v_0 of the molecular ground and lower triplet states. One can write,

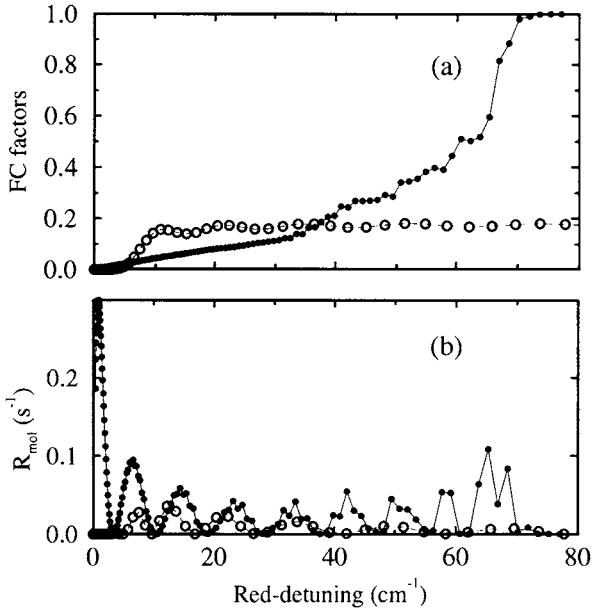

FIG. 24. (a) Probability of populating vibrational levels of the ultracold molecules in the $a^3\Sigma_u^+$ state, after spontaneous decay from the photoassociated levels lying in the external well of the $0_g^-(6s + 6p_{3/2})$ state (black circles) or in the $0_g^-(6s + 6p_{1/2})$ curve. (b) Number of ultracold molecules formed in the $a^3\Sigma_u^+$ state after photoassociation and spontaneous emission.

according to Eq. (90),

$$N_{\text{cold}}(t) = \Gamma_{\text{exc}}^{\text{bound}} \frac{\mathcal{R}_{\text{PA}}}{\Gamma_{\text{exc}}} N_{\text{at}}(0) t. \tag{92}$$

Neglecting the R dependence of the transition dipole moment, the ratio between bound–bound and total spontaneous emission probabilities in Eq. (82) can be approximated by

$$\frac{\Gamma_{\text{exc}}^{\text{bound}}}{\Gamma_{\text{exc}}} = \sum_{v_0} |\langle v_0 | v \rangle|^2 = S(v \to g), \tag{93}$$

where the sum runs over all bound vibrational levels v_0 of the molecular ground or (metastable triplet) state g. Selection rules for the PA rate are the same as for spontaneous emission. We present in Fig. 24 the $S(v \to g)$ sums computed for the transitions $0_g^-(6s + 6p_{3/2}; v, J = 0) \to a^3\Sigma_u^+$ over detunings covering the entire energy range of the 0_g^- external well. In the calculations of Drag *et al.* (2000a), the

vibrational levels v_0 in the ground triplet state have been considered up to a binding energy of 0.4 cm^{-1}, the upper ones being not detected in the experiment. As expected, the variation of S as a function of detuning is opposite to the variation of the PA rate, due to the $\Delta_v^{5/6}$ dependence of the normalization factor N_v^2 [see Eq. (29)]. The decay occurs by vertical transition at intermediate distance, and the probability increases at large detuning due to the increase of the normalization factor. The lowest levels of the $0_g^-(6s + 6p_{3/2})$ long-range well are shown to decay almost completely into bound levels. For comparison we have also reported the bound–bound branching ratios for the $0_g^-(6s + 6p_{1/2};\ v, J = 0)$ state, where, due to a different scaling law, the dependence on detuning is much weaker. At all detunings, the weakness of $S[0_g^-(6s + 6p_{1/2};\ v, J = 0) \rightarrow a^3\Sigma_u^+]$ population transfer, due to the lack of a Condon point at intermediate distance, confirms the difficulty of identifying the vibrational levels of the $0_g^-(6s + 6p_{1/2})$ state in the ion spectra, since the probability of forming metastable $a^3\Sigma_u^+$ molecules is small.

When the photoassociation rate is multiplied by the probability of decay into a bound level, we obtain the curves given in Fig. 24b, where the number of ultracold molecules formed per second in the trap is given as a function of detuning. The minima correspond to the zeros in the photoassociation rate at nodes of the ground-state wavefunction. The maxima display a slow decrease as a function of detuning, due to the balance between the $\Delta_v^{-7/6}$ decrease of the photoassociation rate and the $\Delta_v^{5/6}$ increase of the probability of spontaneous decay into a bound level.

This result explains an interesting feature in the Cs_2^+ photoassociation spectrum for the 0_g^- (Fioretti *et al.*, 1999) double-well long-range state (see Fig. 10), where, apart from the intensity minima already discussed in previous works (Côté *et al.*, 1995; Fioretti *et al.*, 1998; Drag *et al.*, 2000b), the average number of detected molecular ions is roughly constant over the entire energy range investigated ($\sim$80 cm^{-1}). Assuming comparable ionization efficiency for all vibrational levels v_0, this would indicate that the formation rate of ultracold molecules for this particular double-well state in Cs_2 is nearly independent of the choice of v in the photoassociation process. This has been predicted in Section II from the balance between the two scaling laws: a level v close to the dissociation limit of the excited state will be populated efficiently (due to favorable Franck–Condon factors at large distances), but will poorly emit toward bound levels v_0 of the lowest electronic states, due to the low probability amplitude in the vibrational wavefunction $\phi_{v,J}^i(R)$ at intermediate distance. The situation is exactly opposite for the lowest levels v of the excited state: the very large branching ratio for decay to bound levels in the $^3\Sigma_u^+$ curve is associated with a very small PA rate, such that the calculations predict no formation of cold molecules, as is effectively observed (Fioretti *et al.*, 1999). The conclusion is that, *in order to get a large rate for ultracold-molecule formation, one needs a good compromise between the PA rate and the branching ratio for the bound–bound spontaneous emission.*

Except at very low detunings, the calculations yield an average theoretical rate oscillating beween 0.1 and 0 triplet ultracold molecules per second and per atom. This number is in reasonable agreement with the rates obtained directly from trap-loss measurements, where a number of 0.05 to 0.2 molecule per second and per atoms seems a good estimate (Drag, 2000). It is also compatible with the values deduced from the measured number of ions: a global rate for the formation of cold molecules is between 2×10^5 and 10^6 molecules per second, in a trap containing $N_{at} \approx 50$ million atoms.

Concerning other alkali atoms, only rubidium offers a similar outer well in its $0_g^-(5s + 5p_{3/2})$ state. The number of cold Rb_2 molecules is found to be smaller than for Cs_2 as the outer well is located at a greater distance, reducing by a factor of 3 the bound–bound branching ratio (Fioretti *et al.*, 2001). The number of cold K_2 molecules obtained by Nikolov *et al.* (1999) by one-step photoassociation is only about 1000 molecules per second, due to the absence of a similar external well. In contrast, the two-step scheme of Nikolov *et al.* (2000) produces 10^5 molecules per second and per vibrational level, or 10^6 molecules per second when summing over all vibrational levels, which is the same formation rate as in the cesium case. The time delay to transform half the atoms into molecules is therefore estimated to be less than 1 minute in all the present experiments, showing that the process is indeed very efficient.

An even better efficiency might be obtained if the photoassociation process was simultaneously populating a large number of levels, using, for instance, broad-band pulsed laser excitation: at low detunings, the small value of the amplitude of the vibrational wavefunction of each individual level in the excited state would be compensated by the number of levels, increasing the flux toward the ground state.

C. Tunneling Effect

Another scheme for formation of ultracold molecules in low vibrational levels of the $a^3\Sigma_u^+$ Cs_2 state was identified in the photoassociation spectrum of Fioretti *et al.* (1999), manifested by detection of a large number of molecular ions. In the experimental ion spectrum displayed in Fig. 10, we can see two "giant" lines, corresponding to binding energies $\Delta_1 = 2.14\,\mathrm{cm}^{-1}$, $\Delta_2 = 6.153\,\mathrm{cm}^{-1}$ relative to the $6s + 6p_{3/2}$ dissociation limit. Details of the observed spectrum are given in Fig. 25. The "giant" structures have a well-resolved rotational structure in contrast to the neighboring lines identified as vibrational levels of the outer well of the $0_g^-(6s + 6p_{3/2})$ potential curve. Vatasescu *et al.* (2000) have analyzed the data showing that the rotational constants $B_v^1 = 137\,\mathrm{MHz}$ and $B_v^2 = 189\,\mathrm{MHz}$ associated to vibrational levels of the two structures are typical of motion in the inner well. This can be deduced from the definition of the rotational constant as $B_v = \langle \hbar^2/2\mu R^2 \rangle$ with $\mu = 121135.83$ a.u., giving an estimate of the mean value of the internuclear distance $\bar{R} = \hbar/(2\mu B_v)^{1/2}$. For G_1 and G_2 structures, respectively,

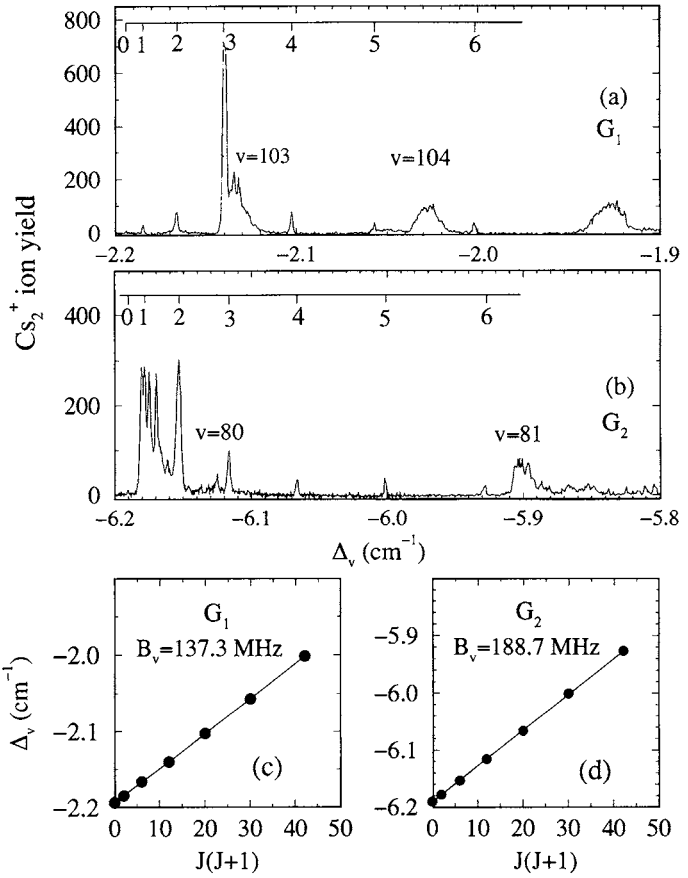

FIG. 25. Details of the photoassociation spectra in the region of the (a) G_1 and (b) G_2 structures, with their J labeling. Such structures are embedded in the vibrational progression of regular levels (a) $v = 102$–105, (b) $v = 79$–81 with unresolved rotational structure. The rotational constants of the giant structures G_1 and G_2 are obtained from the slopes of the lower curves giving the variation of the binding energy as a function of $J(J + 1)$.

this yields $\bar{R}_1 \approx 14a_0$ and $\bar{R}_2 \approx 12a_0$, whereas the hump in the double-well potential is located at a distance $R_b \approx 15a_0$. The spectroscopy results could be reproduced by theoretical calculations, and we show in Fig. 26 an example of a vibrational wavefunction with tunneling. In the inner region, coupling with vibrational motion in the potential curve $0_g^-(6s + 5d)$ has to be considered, so that the function displays several Condon points favorable to spontaneous decay toward low-lying bound levels of the $a\ ^3\Sigma_u^+$ Cs_2 state. The large intensity of the ion signal at the detunings corresponding to Δ_1 and Δ_2 binding energies could be an

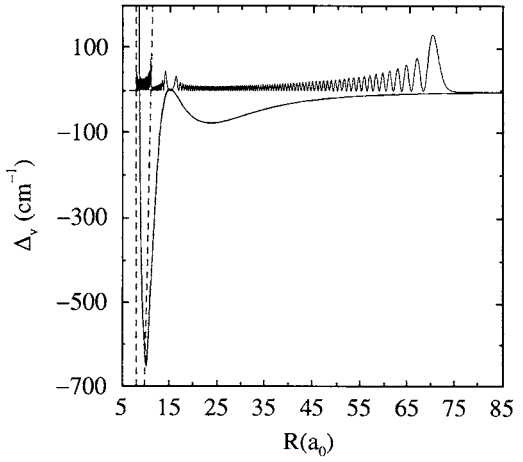

FIG. 26. Tunneling effect: vibrational wavefunction extending both in the outer well of the $0_g^-(6s + 6p\,^2p_{3/2})$ potential curve of Cs_2 and in the inner well. In the inner region, coupling with the $0_g^-(6s + 5d)$ vibrational series has to be considered.

indication of a good efficiency for this scheme, but better analysis of the detection efficiency as a function of the vibrational number v_0 of the final molecule has to be performed.

VI. New Schemes for Making Ultracold Molecules

Due to the complexity of potential curves in a given molecule, it seems that many new schemes can be proposed owing to collaboration between theory and experiment. If we stay within the present scheme of photoassociation with continuous laser light, it seems wise to perform photoassociation at large internuclear distances and to look for situations where the vibrational motion is gradually stopped at intermediate distance, providing opportunity to populate bound levels in the ground-state potential curve by spontaneous emission. Besides potential barriers with a gentle slope, which are not easily encountered, a more general mechanism is offered by resonant coupling. In many situations, the excited-state potential curve i is dynamically coupled to another one, i'. Looking for resonances beweeen the two vibrational series, one can transfer population from a level v_i of the first series to a level $v_{i'}$ of the other one. Dion *et al.* (2001) have recently shown that a large number of ground-state Cs_2 molecules are indeed observed in experiments where a loosely bound level v_i of the $0_u^+(6s + 6p_{1/2})$ curve is populated by photoassociation, and the population transferred to a level $v_{i'}$ of the narrower $0_u^+(6s + 6p_{3/2})$ curve, which is has good Franck–Condon overlap with bound levels of the ground state. This scheme is summarized in Fig. 27 (see Addendum on p. 120). Two-step photoassociation, with transfer of population to bound levels of the lowest $Na_2\ ^1\Pi_u$ Rydberg

excited curve, has been discussed by Band and Julienne (1995), while Almazor *et al.* (1999) proposed to populate a double-well curve in the Na_2 (6) $^1\Sigma_g^+$ excited state.

Another possibility consists of considering photoassociation with pulsed lasers, and trying to control the formation of molecules. This has been discussed by several authors (Vardi *et al.*, 1997; Vala *et al.*, 2001), but no absolute rate has been given up to now in the condition of the experiments. Vala *et al.* (2001) propose to enhance the photoassociation rate by use of chirped pulses. In the work of Vardi *et al.*, two nanosecond pulses are used, one for photoassociation, another one for population transfer by induced emission to a precise bound level v_0 in the ground excited curve. The estimation of 6×10^{-6} molecules formed per pulse and per atom indicates that this process is much less efficient that the present schemes using CW lasers. Half the atoms could be converted to molecules in ~25 mn, whereas the CW experiments predict times of the order of a few seconds. However, all long-lived molecules would be produced in the same vibrational level v_0, which is not the case in the present experimental schemes with CW lasers. The main advantage of pulsed excitation is that a large number of levels can be photoassociated at the same time, increasing at low detunings the flux to bound levels of the ground state as discussed in Section V.B. We have shown in Section II.B that at low binding energies all photoassociated vibrational levels have a similar wave function at short and intermediate internuclear distance, and therefore similar spontaneous emission probabilities toward levels of the ground state.

VII. Conclusion

While direct laser cooling of molecules is not at present a promising technique, this chapter shows that an efficient way of making ultracold molecules is to start from a sample of laser-cooled atoms, and to implement a two-step process: first, a photoassociation reaction creates, out of two atoms, a bound molecule in an excited electronic state, and second, this short-lived molecule decays by spontaneous emission to bound levels of the ground electronic state (or lower triplet state).

The photoassociation process, first suggested by Thorsheim *et al.* (1987), uses laser light slightly red-detuned with respect to an atomic resonance line, and can be understood as a vertical (Franck–Condon) transition at large distance R_v^i between a continuum level (two colliding atoms) and a bound level v in an excited electronic curve i of the molecule. The photoassociated molecule can be viewed as a pair of distant atoms, weakly bound by dipole–dipole interaction: for loosely bound vibrational levels, the two atoms are most of the time moving in the asymptotic region of weak interaction, the outer classical turning point R_v^i being a decreasing function of the detuning. The dynamics is similar to that of a Rydberg electron, the binding energy of a level being linked to its vibrational number by the Le Roy–Bernstein formula generalizing the Rydberg formula. Scaling laws are

found, showing that the photoassociation process is favored at very small detunings, corresponding to vertical transitions at large distances. In such conditions, the photoassociated molecule usually decays back into a pair of ground-state atoms. Indeed, the ground-state potential curve, with asymptotic R^{-6} behavior, is much narrower than the excited curve, and bound levels can be efficiently populated by spontaneous emission only when the nuclei are at short or intermediate distance. In most cases, the vibrational motion of the photoassociated molecule is such that the amount of time spent in the short-range region is too small, making the branching ratio between stabilization and dissociation negligible.

However, experiments by Fioretti *et al.* (1998, 1999), using photoassociation in a cesium sample and detection of molecular ions by a REMPI scheme, have demonstrated for some symmetries (0_g^-, 1_u) of the photoassociated molecule, an efficient mechanism for population of bound levels in the ground (or lower-triplet)-state potential curve. This can be explained by the double-well structure of the 0_g^- and 1_u curves, where a barrier at intermediate distance is gently slowing down the vibrational motion, increasing the time spent at distances where spontaneous emission can efficiently populate a bound level of a ground (or lower triplet) state of the molecule. A similar mechanism exists for rubidium, and was demonstrated by Gabbanini *et al.* (2000). At present, in a cesium trap containing 50 million atoms, at a density $n_{at} = 10^{11}$ cm^{-3} and temperature $T = 140\ \mu$K, using continuous photoassociation lasers with intensity ≤ 1 kW/cm^2, it is possible to create from 10^5 to 10^6 molecules per second, that is, to transform 10% of the atoms into molecules in a time of a few seconds. Similar results were obtained by Nikolov *et al.* (2000) for K_2 using another mechanism where the photoassociated molecule is excited by a second laser to a Rydberg state which decays by spontaneous emission to bound levels of the ground electronic state. Presently, we should note that only a few molecules ($\sim$5%) thus formed are detected. The sensitivity of the REMPI detection should be improved, and the ionization step optimized, in collaboration with molecular spectroscopy groups. Once most molecules are detected, the formation of ultracold molecules will appear as a very strong effect.

The interpretation of experiments and design of new schemes relies on close collaboration between theory and experiment. New theoretical methods have been developed to treat ultracold molecules, and their comparison with more traditional methods has to be implemented. There is good agreement between measured photoassociation rates and theoretical calculations performed in the framework of a perturbative treatment. An important result is the rapid decrease of the photoassociation rate as a function of detuning, interpreted by scaling laws, and by the behavior of the initial continuum-state wavefunction, which has a reduced probability amplitude at small internuclear distances. The photoassociation process is thus more efficient at low detuning. In contrast, the branching ratio for stabilization into bound levels by the spontaneous emission process is decreasing at low detuning, due to a smaller amplitude of the vibrational wavefunctions of the photoassociated molecule in the intermediate distance region where vertical transition to bound

levels is possible. Present experiments have to choose a compromise between the efficiency of the photoassociation step and the efficiency of the stabilization step. Some new schemes that rely on tunneling effect, resonant coupling, or two-step excitation were also shown to be efficient, and must be further explored.

The photoassociation rate is presently estimated in the framework of a perturbative treatment, and comparison with more sophisticated theoretical studies using time-dependent formalism still has to be implemented. Photoassociation using pulsed lasers has been little explored as yet experimentally (Boesten *et al.,* 1996, 1998) but seems a promising route. The conclusions of the present chapter concern photoassociation rates for population of individual vibrational levels. Different conclusions would be drawn if broad-band excitation was used in the photoassociation process, as the population of a large number of levels, with similar wavefunctions in the short- and intermediate-distance region, would increase the efficiency of the stabilization process. The discussion of pulsed laser experiments connects the subject of cold-molecule formation to the general problem of coherent control.

Current results could be extended to all homonuclear systems provided a dense enough sample can be obtained. Formation of heteronuclear molecules, although presenting smaller photoassociation rates, would have the advantage of making the trapping process easy with a dipole trap. Indeed, at present the molecules stay for roughly 10 s inside the trap, and then fall down. The next important step is to trap them. A CO_2 laser, used in the experiments of Takekoshi *et al.* (1998, 1999) seems promissing. Magnetic trapping has been used for triplet molecules, and first demonstration has been achieved recently in Orsay. The rotational temperature of the ultracold molecules is low, but they are formed in a large number of vibrational levels, so a Raman scheme to lower the vibrational temperature should be implemented. Coherent control techniques (Bartana *et al.,* 1993, 1997) also offer interesting possibilities.

The optimization of the rate of molecule formation should be searched for in an increase of the atomic density rather than an increase of the laser intensity, which may lead to saturation or reexcitation. We are reaching there the field of atomic condensates, which is beyond the scope of the present review but offers very interesting opportunities: the choice between two routes toward molecular condensates, either creating molecules within an atomic condensate (Wynar *et al.,* 2000) or bringing a dense ensemble of ultracold molecules to conditions where Bose condensation can take place, is an interesting perspective. The molecule laser would be an important application.

Other applications lie in threshold laws for collisions (atom–molecule, Rydberg atom–molecule, molecule–molecule collisions), very little explored at present (Forrey *et al.,* 1998, 1999a,b), on the formation of more complex species (trimers small clusters). Ultracold molecular sources would be ideal for molecular interferometry experiments (Bordé *et al.,* 1994; Chapman *et al.,* 1995; Lisdat *et al.,* 2000). In short, a new research field is open.

VIII. Acknowledgments

This review relies on work done within the team *Molécules et atomes froids* in Laboratoire Aimé Cotton, so we are very indebted to Ph.D. students Cyril Drag, Bruno Laburthe Tolra, Salah Boussen, and Nathalie Hoang for experiments, Marie-Laure Almazor, Viatcheslav Kokoouline, Philippe Pellegrini, Benoit T'Jampens, and Mihaela Vatasescu for theory, to former or present postdocs Andrea Fioretti, Wilson de Souza Melo, Ricardo Gutteres, and Claude Dion, and to our young or senior colleagues Daniel Comparat, Olivier Dulieu, Samuel Guibal, Claude Amiot, and Anne Crubellier. Special thanks are due to Olivier Dulieu and Claude Dion for their help in preparing the manuscript and figures. Stimulating collaboration is gratefully acknowledged with R. Kosloff in Jerusalem, (owing to the Arc en Ciel-Keshet cooperation program and to invitation of F. M-S by the Fritz Haber Institute where part of the paper has been written), with E. Tiemann, University of Hannover, (within the Procope Franco-German cooperation program), and with the group of W. Stwalley in Storrs, University of Connecticut, (within CNRS-NSF cooperation). We thank T. F. Gallagher (Virginia), G. Pichler (Zagreb), E. Luc-Koenig (Orsay), V. N. Ostrovsky (St. Petersburg) for collaboration. Finally, we are grateful to M. Allegrini, R. Côté, A. Dalgarno, J. Dalibard, C. Gabbanini, Ph. Gould, P. Lett, J. Pinard, L. Pruvost, C. Salomon, and C. Williams for useful discussions.

Addendum

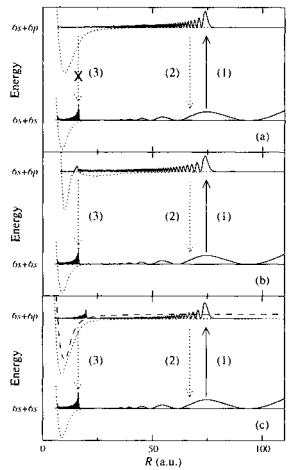

FIG. 27. Photoassociation (arrow (1)) from the Cs ($6s$) + Cs ($6s$) continuum towards a vibrational level in an excited electronic state of the Cs_2 molecule with (a) a typical potential; (b) a double-well potential [e.g. $0_g^-(6s + 6p_{3/2}]$; (c) two coupled potentials [e.g. $0_u^+(6s + 6p_{1/2})$ and $0_u^+(6s + 6p_{3/2})$ as discussed by Dion *et al* (2001)]. The system decays by spontaneous emission either back to the continuum (*dissociation,* arrow (2), see Eq. (51) in text) or to a bound level of the ground state (*stabilization,* arrow (3), see Eq. (52) in text.)

IX. References

Abraham, E. R. I., Ritchie, N. W. M., McAlexander, W. I., and Hulet, R. G. (1995). Photoassociative spectroscopy of long-range states of ultracold $^6Li_2$ and $^7Li_2$. *J. Chem. Phys.* **103,** 7773–7778.

Almazor, M.-L., Dulieu, O., Elbs, M., Tiemann, E., and Masnou-Seeuws, F. (1999). How to get access to long range states of highly excited molecules. *Eur. Phys. J. D* **5,** 237–242.

Aubert-Frécon, M., Hadinger, G., Magnier, S., and Rousseau, S. (1998). Analytical formulas for long range energies of the 16 $\Omega_{g,u}^{(+/-)}$ states of alkali dimers dissociating into M(ns) + M(np). *J. Mol. Spectrosc.* **188,** 182–189.

Avila, G., Gain, P., deClercq, E., and Cerez, P. (1986). New absolute wavenumber measurement of the D_2 line of caesium. *Metrologia* **22,** 11–14.

Aymar, M., Greene, C. H., and Luc-Koenig, E. (1996). Multichannel Rydberg spectroscopy of complex atoms. *Rev. Mod. Phys.* **68,** 1015–1124.

Bahns, J. T., Gould, P. L., and Stwalley, W. (1997). Laser cooling of molecules: A sequential scheme for rotation, translation and vibration. *J. Chem. Phys.* **104,** 9689.

Bahns, J. T., Stwalley, W. C., and Gould, P. L. (2000). Formation of cold ($T \leq 1$ K) molecules. *Adv. Atomic Mol. Opt. Phys.* **42,** 171–224.

Band, Y. B., and Julienne, P. S. (1995). Ultracold-molecule production by laser-cooled atom photoassociation. *Phys. Rev. A* **51,** R4317–R4320.

Bartana, A., Kosloff, R., and Tannor, D. J. (1993). Laser cooling of molecular internal degrees of freedom by a series of shaped pulses. *J. Chem. Phys.* **99,** 196–210.

Bartana, A., Kosloff, R., and Tannor, D. J. (1997). Laser cooling of internal degrees of freedom II. *J. Chem. Phys.* **106,** 1435–1448.

Bethlem, H. L., Berden, G., and Meijer, G. (1999). Decelerating neutral dipolar molecules. *Phys. Rev. Lett.* **83,** 1558–1561.

Bethlem, H. L., Berden, G., Crompvoets, F. M. H., Jongma, R. T., van Roij, A. J. A., and Meijer, G. (2000a). Electrostatic trapping of ammonia molecules. *Nature* **406,** 491–494.

Bethlem, H. L., Berden, G., van Roij, A. J. A., Crompvoets, F. M. H., and Meijer, G. (2000b). Trapping neutral molecules in a traveling potential well. *Phys. Rev. Lett.* **84,** 5744–5747.

Beuc, R., Milosevic, S., Movre, M., Pichler, G., and Veza, D. (1982). Satellite bands in the far blue wing of the potassium first resonance doublet. *Fizika (Yu)* **14,** 345–349.

Blatt, J. M. (1967). *J. Comput. Phys.* **1,** 382.

Boesten, H., Tsai, C. C., Verhaar, B. J., and Heinzen, D. J. (1996). Observation of a shape resonance in cold-atom scattering by pulsed photoassociation. *Phys. Rev. Lett.* **77,** 5194.

Boesten, H., Tsai, C. C., Heinzen, D. J., moonen, A. J., and Verhaar, B. J. (1999). Time-independent and time-dependent photoassociation of rubidium. *J. Phys. B* **32,** 287–308.

Bohn, J. L., and Julienne, P. S. (1996). Semianalytic treatment of two-color photoassociation spectroscopy and control of cold atoms. *Phys. Rev. A* **54,** R4637–R4640.

Boisseau, C., Audouard, E., and Vigué, J. (1998). Quantization of the highest levels in a molecular potential. *Europhys. Lett.* **41,** 349–354.

Boisseau, C., Audouard, E., Vigué, J., and Flanbaum, V. V. (2000a). Analytical corrections to the JWKB quantization conditions for the highest levels in a molecular potential. *Eur. Phys. J. D* **12,** 199–209.

Boisseau, C., Audouard, E., Vigué, J., and Julienne, P. S. (2000b). Reflection approximation in photoassociation spectroscopy. *Phys. Rev. A* **62,** 052705.

Bordé, C. J., Courtier, N., du Burck, L., Goncharov, A. N., and Gorlicki, M. (1994). Molecular interferometry experiments. *Phys. Lett.* **A188,** 187–190.

Bussery, B., and Aubert-Frécon, M. (1985a). Multipolar long-range electrostatic, dispersion and induction energy terms for the interaction between two identical alkali atoms Li, Na, K, Rb and Cs in various electronic states. *J. Chem. Phys.* **82,** 3224–3234.

Bussery, B., and Aubert-Frécon, M. (1985b). Potential energy curves and vibration-rotation energies for the two purely long-range bound states 1_u and 0_g^- of the alkali dimers M_2 dissociating to $M(ns^2S_{1/2}) + M(np^2P_{3/2})$ with M = Li, Na, K, Rb, and Cs. *J. Mol. Spectrosc.* **113,** 21–27.

Chapman, M. S., Ekstrom, C. R., Hammond, T. D., Rubinstein, R. A., Schiedmayer, J., Wehinger, S., and Pritchard, D. E. (1995). Optics and interferometry with Na_2 molecules. *Phys. Rev. Lett.* **74,** 4783–4786.

Child, M. S. (1991). "Semiclassical Mechanics with Molecular Applications." Clarendon Press, Oxford.

Cline, R. A., Miller, J. D., and Heinzen, D. J. (1994). Study of Rb_2 long-range states by high resolution photoassociation spectroscopy. *Phys. Rev. Lett.* **73,** 632–635.

Colbert, D. T., and Miller, W. H. (1992). A novel discrete variable representation for quantum mechanical reactive scattering via the *S*-matrix Kohn method. *J. Chem. Phys.* **96,** 1982–1991.

Comparat, D., Drag, C., Fioretti, A., Dulieu, O., and Pillet, P. (1999). Photoassociative spectroscopy and formation of cold molecules in cold cesium vapor: Trap-loss spectrum versus ion spectrum. *J. Mol. Spectrosc.* **195,** 229–235.

Comparat, D., Drag, C., Laburthe Tolra, B., Pillet, P., Crubellier, A., Dulieu, O., and Masnou-Seeuws, F. (2000). Formation of cold Cs_2 ground state molecules through photoassociation in the 1_u^- long range state. *Eur. Phys. J. D* **11,** 59–71.

Condon, E. U. (1926). A theory of intensity distribution in band systems. *Phys. Rev.* **28,** 1182–1201.

Condon, E. (1928). Nuclear motions associated with electron transitions in diatomic molecules. *Phys. Rev.* **32,** 858–872.

Cooley, J. W. (1961). An improved eigenvalue corrector formula for solving the Schrödinger equation for central fields. *Math. Comput.* **15,** 363.

Côté, R., and Dalgarno, A. (1997). Mechanism for the production of vibrationally excited ultracold molecules of $^7Li_2$. *Chem. Phys. Lett.* **279,** 50–54.

Côté, R., and Dalgarno, A. (1998). Photoassociation intensities and radiative trap loss in lithium. *Phys. Rev. A* **58,** 498–508.

Côté, R., and Dalgarno, A. (1999). Mechanism for the production of $^6Li_2$ and $^7Li_2$ utracold molecules. *J. Mol. Spectrosc.* **195,** 236–245.

Côté, R., and Jamieson, M. J. (1995). comparison of phaseshift calculations by asymptotic fit and quadrature in ultra-low temperature scattering. *J. Comput. Phys.* **118,** 388–391.

Côté, R., Dalgarno, A., Sun, Y., and Hulet, R. G. (1995). Photoabsorption by ultra-cold atoms and the scattering length. *Phys. Rev. Lett.* **74,** 3581–3583.

Dashevskaya, E., Voronin, A. I., and Nikitin, E. E. (1969). Theory of excitation transfer between identical alkali atoms. I. Identical partners. *Can. J. Phys.* **47,** 1238–1248.

deCarvalho, R., Doyle, J. M., Friedrich, B., Guillet, T., Kim, J., Patterson, D., and Weinstein, J. D. (1999). Buffer-gas loaded magnetic traps for atoms and molecules: A primer. *Eur. Phys. J. D* **7,** 289–309.

Derevianko, A., W. R, J., Safronova, M. S., and Babb, J. F. (1999). High-precision calculations of dispersion coefficients, static dipole polarizabilities and atom-wall interaction constants for alkali-metal atoms. *Phys. Rev. Lett.* 3589–3592.

Dion, C. M., Drag, C., Dulieu, O., Laburthe Tolra, B., Masnou-Seeuws, F., and Pillet, P. (2001). Resonant coupling in the formation of ultracold ground state molecules via photoassociation. *Phys. Rev. Lett.* **86,** 2253–2256.

Djeu, N., and Whitney, W. T. (1981). Laser cooling by spontaneous anti-Stokes scattering. *Phys. Rev. Lett.* **46,** 236.

Doyle, J. M., Friedrich, B., Kim, J., and Patterson, D. (1995). Buffer-gas loading of atoms and molecules into a magnetic trap. *Phys. Rev. A* **52,** R2515–R2518.

Doyle, R. (1968). The continuous energy spectrum of the hydrogen quasi-molecule. *J. Quant. Spectrosc. Radiat. Transfer* **8,** 1555–1569.

Drag, C. (2000). Photoassociation d'atomes de césium froids. Formation et caractérisation d'un nuage froid de molécules diatomiques de césium. Ph.D. thesis, Université Paris-Sud, Centre d'Orsay.

Drag, C., Laburthe Tolra, B., Dulieu, O., Comparat, D., Vatasescu, M., Boussen, S., Guibal, S., Crubellier, A., and Pillet, P. (2000a). Experimental versus theoretical rates for photoassociation and formation of cold molecules. *IEE Quantum Electron.* **36,** 1378–1388.

Drag, C., Tolra, B. L., T'Jampens, B., Allegrini, M., Crubellier, A., and Pillet, P. (2000b). Photoassociative spectroscopy as a self-sufficient tool for the determination of the Cs triplet scattering length. *Phys. Rev. Lett.* **85,** 1408–1411.

Dulieu, O., and Julienne, P. S. (1995). Coupled channel bound states calculations for alkali dimers using the Fourier grid method. *J. Chem. Phys.* **103,** 60–66.

Dulieu, O., Kosloff, R., Masnou-Seeuws, F., and Pichler, G. (1997). Intermediate long range molecules: Bound and quasibound states for alkali dimers. *J. Chem. Phys.* **107,** 10633–10642.

Fatemi, F. K., Jones, K. M., and Lett, P. D. (2000). Observation of optically induced Feschbach resonances in collisions of cold atoms. *Phys. Rev. Lett.* **85,** 4462–4465.

Fattal, E., Baer, R., and Kosloff, R. (1996). Phase space approach for optimizing grid representations: The mapped Fourier method. *Phys. Rev. E* **53,** 1217–1227.

Fioretti, A., Comparat, D., Crubellier, A., Dulieu, O., Masnou-Seeuws, F., and Pillet, P. (1998). Formation of cold Cs_2 molecules through photoassociation. *Phys. Rev. Lett.* **80,** 4402–4405.

Fioretti, A., Comparat, D., Drag, C. Amiot, C., Dulieu, O., Masnou-Seeuws, F., and Pillet, P. (1999). Photoassociative spectroscopy of the Cs_2 0_g^- long range state. *Eur. Phys. J. D* **5,** 389–403.

Fioretti, A., Amiot, C., Dulieu, O., Mazzoni, M., and Gabbanini, C. (2001). Cold rubidium molecule formation through photoassociation: A spectroscopic study of the 0_g^- long range state of Rb_2. *Eur. Phys. J. D.* **15,** 189–198.

Forrey, R. C., Balakrishnan, N., Karchenko, V., and Dalgarno, A. (1998). Feshbach resonances in ultracold atom-diatom scattering. *Phys. Rev. A* **58,** R2645–R2647.

Forrey, R. C., Balakrishnan, N., Dalgarno, A., Haggerty, M. R., and Heller, E. J. (1999a). Quasiresonant energy transfer in ultracold atom-diatom collisions. *Phys. Rev. Lett.* **82,** 2657–2660.

Forrey, R. C., Karchenko, V., Balakrishnan, N., and Dalgarno, A. (1999b). Vibrational relaxation of trapped molecules. *Phys. Rev. A* **59,** 2146–2152.

Foucrault, M., Millié, P., and Daudey, J. P. (1992). Non-perturbative method for core-valence correlation in pseudopotential calculations: Application to the Rb_2 and Cs_2 molecules. *J. Chem. Phys.* **96,** 1257–1264.

Franck, J. (1925). *Trans. Faraday Soc.* **21,** 536.

Friedrich, H. (1998). "Theoretical Atomic Physics." Springer-Verlag, Berlin.

Friedrich, H., and Trost, J. (1996a). Phase loss in WKB waves due to reflection by a potential. *Phys. Rev. Lett.* **76,** 4469–4473.

Friedrich, H., and Trost, J. (1996b). Non integral Maslov indexes. *Phys. Rev. A* **54,** 1136–1145.

Friedrich, B., deCarvalho, R., Kim, J., Patterson, D., Weinstein, J. D., and Doyle, J. M. (1998). Towards magnetic trapping of molecules. *J. Chem. Soc. Faraday Trans.* **94,** 1783–1791.

Friedrich, B., Weinstein, J. D., deCarvalho, R., and Doyle, J. M. (1999). Zeeman spectroscopy of CaH molecules in a magnetic trap. *J. Chem. Phys.* **110,** 2376–2383.

Gabbanini, C., Fioretti, A., Lucchesini, A., Gozzini, S., and Mazzoni, M. (2000). Observation of translationally cold ground state rubidium molecules. *Phys. Rev. Lett.* **84,** 2814–2817.

Gao, B. (2000). Breakdown of Bohr's correspondence principle. *Phys. Rev. Lett.* **83,** 4225–4228.

Gardner, J., Cline, R. A., Miller, J. D., Heinzen, D. J., Boesten, H. J. M., and Verhaar, B. J. (1995). Collisions of doubly spin-polarized, ultracold ^{85}Rb atoms. *Phys. Rev. Lett.* **74,** 3764–3767.

Gerstenkorn, S., Vergès, J., and Chevillard, J. (1982). Atlas du spectre d'absorption de la molécule d'iode. Tech. Rep., Laboratoire Aimé Cotton, Orsay, France.

Gordon, R. G. (1969). New methods for constructing wavefunctions for bound states and scattering. *J. Chem. Phys.* **51,** 14–25.

Gouédard, G., Girard, B., Billy, N., and Vigué, J. (1989). ω_l scaling law near a molecular dissociation limit: Theory and experimental tests in Cl_2 B state. *Chem. Phys.* **132,** 385–390.

Gray, S. K., and Rice, S. A. (1985). A scattering resonance description of very low energy collision induced vibrational relaxation. *J. Chem. Phys.* **83,** 2818–2828.

Gribakin, G. F., and Flanbaum, V. V. (1993). Calculation of the scattering length using the semiclassical approximation. *Phys. Rev. A* **48,** 546–553.

Herman, A., Leutwyler, S., Woste, L., and Schumacher, E. (1979). Molecular spectroscopy by photodeflection of Na_2 in a supersonic beam. *Chem. Phys. Lett.* **62,** 44–47.

Herschbach, N., Tol, P. J. J., Wassen, W., Hogervorst, W., Woestenenk, G., Thomsen, J. W., der Straten,

P. V., and Niehaus, A. (2000). Photoassociation spectroscopy of cold He(2^3s) atoms. *Phys. Rev. Lett.* **84,** 1874–1877.

Hinds, E. A., and Sangster, K. (1992). Testing time-reversal symmetry with molecules. *AIP Conf. Proc.* **270,** 77–83.

Hoffmann, D., Feng, P., and Walker, T. (1994). Measurements of Rb trap-loss collision spectra. *J. Opt. Soc. Am. B* **11,** 712–720.

Jablonski, A. (1945). General theory of pressure broadening in spectral lines. *Phys. Rev. A* **68,** 78–93.

James, H. M., and Coolidge, A. S. (1939). Continuous spectra of H_2 and D_2. *Phys. Rev.* **55,** 84.

Javanainen, J., and Mackie, M. (1998). Probability of photoassociation from a quasi-continuum approach. *Phys. Rev. A* **58,** R789–R792.

Julienne, P. S. (1996). Cold binary collisions in a light field. *J. Res. Natl. Inst. Std. Technol.* **101,** 487–503.

Julienne, P. S., and Vigué, J. (1991). Cold collisions of ground- and excited-state alkali metal atoms. *Phys. Rev. A* **44,** 4464–4485.

Julienne, P., Burnett, K., Band, Y., and Stwalley, W. (1998). Stimulated Raman molecule production in Bose-Einstein condensation. *Phys. Rev. A* **58,** R797–R800.

Kastler, A. (1950). Quelques suggestions concernant la production optique et la détection optique d'une inégalité de population des niveaux de quantification spatiale des atomes. application à l'expérience de Stern et Gerlach et à la résonance magnétique. *J. Phys. France* **11,** 255.

Ketterle, W., Davies, K. B., Joffe, M. A., Martins, A., and Pritchard, D. E. (1993). High density of cold atoms in a dark spontaneous-force optical trap. *Phys. Rev. Lett.* **70,** 2253–2256.

Kokoouline, V., Dulieu, O., Kosloff, R., and Masnou-Seeuws, F. (1999). Mapped Fourier methods for long range molecules: Application to perturbations in the $Rb_2(0_u^+)$ spectrum. *J. Chem. Phys.* **110,** 9865–9876.

Kokoouline, V., Dulieu, O., Kosloff, R., and Masnou-Seeuws, F. (2000a). Theoretical treatment of channel mixing in excited Rb_2 and Cs_2 ultra-cold molecules: Determination of predissociation lifetimes with coordinate mapping. *Phys. Rev. A* **62,** 032716.

Kokoouline, V., Dulieu, O., and Masnou-Seeuws, F. (2000b). Theoretical treatment of channel mixing in excited Rb_2 and Cs_2 ultra-cold molecules. Perturbations in 0_u^+ photoassociation and fluorescence spectra. *Phys. Rev. A* **62,** 022504.

Kosloff, R. (1988). Time dependent methods in molecular dynamics. *J. Phys. Chem.* **92,** 2087–2100.

Kosloff, R. (1996). Quantum molecular dynamics on grids. *In* "Dynamics of Molecules and Chemical Reactions" (R. H. Wyatt and J. Z. H. Zhang, Eds.), p. 185. Marcel Dekker, New York.

Koštrun, M., Mackie, M., Côté, R., and Javanainen, J. (2000). Theory of coherent photoassociation of a Bose-Einstein condensate. *Phys. Rev.* **A62,** 063616.

Kozlov, M. G., and Ezhov, V. F. (1994). Enhancement of the electric dipole moment of the electron in the YbF molecule. *Phys. Rev. A* **49,** 4502–4507.

Laburthe-Tobra, B., Drag, C., and Pillet, P. (2001). Observation of cold state-selected cesium molecules formed by stimulated Raman photoassociation, PRA in press.

Lambrecht, A., Giacobino, E., and Reynaud, S. (1996). Atomic number fluctuations in a falling cold atomic cloud. *Quantum Semiclass.* **8,** 457.

Landau, L. D., and Lifshitz, E. M. (1977). "Quantum Mechanics (Non-Relativistic Theory)". Pergamon, Oxford.

Le Roy, B. (1980). Applications of Bohr quantization in diatomic molecule spectroscopy in "Semiclassical methods in molecular scattering and spectroscopy" M. S. Child editor, 1980 Reidel Publ. Dordredt, Holland.

Le Roy, R. J. (2000). A computer program for solving the radial Schrödinger equation for bound and quasi-bound levels. Univ. Waterloo Chem. Phys. Res. Rep. CP 642 R **1.**

Le Roy, R. J., and Bernstein, R. B. (1970). Dissociation energy and long-range potential of diatomic molecules from vibrational spacings of higher levels. *J. Chem. Phys.* **52,** 3869–3879.

Lefebvre-Brion, H., and Field, R. W. (1986). "Perturbations in the Spectra of Diatomic Molecules." Academic Press, New York.

Lett, P. D., Helmerson, K., Philips, W. D., Ratliff, L. P., Rolston, S. L., and Wagshul, M. E. (1993). Spectroscopy of Na_2 by photoassociation of laser-cooled Na. *Phys. Rev. Lett.* **71,** 2200–2203.

Lisdat, C., Franck, M., Knöckel, H., Almazor, M.-L., and Tiemann, E. (2000). Realization of a Ramsey-Bordé matter wave interferometer on the K_2 molecule. *Eur. Phys. J. D* **12,** 235–240.

Mackholm, M., Giusti-Suzor, A., and Mies, F. H. (1994). Photoassociation of atoms in ultracold collisions probed by wavepacket dynamics. *Phys. Rev. A* **50,** 5025–5036.

Mackie, M., and Javanainen, J. (1999). Quasi-continuum modeling of photoassociation. *Phys. Rev. A* **60,** 3174–3187.

Magnier, S., and Millié, P. (1996). Potential curves for the ground and numerous excited electronic states of the K_2 and NaK molecule. *Phys. Rev. A* **54,** 204–218.

Magnier, S., Millié, P., Dulieu, O., and Masnou-Seeuws, F. (1993). Potential curves for the ground and excited states of the Na_2 molecule up to the $(3s + 5p)$ dissociation limit. *J. Chem. Phys.* **98,** 7113–7125.

Marinescu, M., and Dalgarno, A. (1995). Dispersion forces and long-range electronic transition dipole moments of alkali-metal dimer excited states. *Phys. Rev. A* **52,** 311–320.

Marinescu, M., and Dalgarno, A. (1996). Analytical interaction potentials of the long range alkali-metal dimers. *Z. Phys. D* **36,** 239–248.

Marston, C. C., and Balint-Kurti, G. (1989). The Fourier grid Hamiltonian method for bound state eigenvalues and eigenfunctions. *J. Chem. Phys.* **91,** 3571–3576.

Mies, F. H. (1973). Molecular theory of atomic collisions: Calculated croos sections for $H^+ + F(^2P)$. *Phys. Rev. A* **7,** 957–967.

Miller, J. D., Cline, R. A., and Heinzen, D. J. (1993). Photoassociation spectrum of ultracold Rb atoms. *Phys. Rev. Lett.* **71,** 2204–2207.

Miller, W. H. (1968). Uniform semiclassical approximations for elastic scattering and eigenvalue problems. *J. Chem. Phys.* **48,** 464–467.

Monnerville, M., and Robbe, J. M. (1994). Optical potential coupled to discrete variable representation for calculations of quasibound states: Application to the $CO(B\ ^1\Sigma^+ - D'\ ^1\Sigma^+)$ predissociating interaction. *J. Chem. Phys.* **101,** 7580–7581.

Monroe, C., Swann, W., Robinson, H., and Wieman, C. (1990). Very cold trapped atoms in a vapor cell. *Phys. Rev. Lett.* **65,** 1571–1574.

Mosk, A. P., Reynolds, M. W., Hijmans, T. W., and Walraven, J. T. M. (1999). Photoassociation of spin-polarized hydrogen. *Phys. Rev. Lett.* **82,** 307–310.

Movre, M., and Pichler, G. (1977). Resonance interaction and self-broadening of alkali resonances lines I: Adiabatic potential curves. *J. Phys. B: At. Mol. Opt. Phys.* **10,** 2631–2638.

Napolitano, R., Weiner, J., Williams, C. J., and Julienne, P. S. (1994). Line shapes of high resolution photoassociation spectra of optically cooled atoms. *Phys. Rev. Lett.* **73,** 1352–1355.

Nikolov, A. N., Eyler, E. E., Wang, X., Li, J., Wang, H., Stwalley, W. C., and Gould, P. (1999). Observation of translationally ultracold ground state potassium molecules. *Phys. Rev. Lett.* **82,** 703–706.

Nikolov, A. N., Ensher, J. R., Eyler, E. E., Wang, H., Stwalley, W. C., and Gould, P. (2000). Efficient production of ground-state potassium molecules at sub-mK temperatures by two-step photoassociation. *Phys. Rev. Lett.* **84,** 246–249.

Ostrovsky, V. N., Kokoouline, V., Luc-Koenig, E., and Masnou-Seeuws, F. (2001). *J. Phys. B: At. Mol. Opt. Phys.* **34,** L27–L38.

Pichler, G., Milosevic, S., Veza, D., and Beuc, R. (1983). Diffuse bands in the visible absorption spectra of dense alkali vapors. *J. Phys. B: Atomic Mol. Opt. Phys.* **16,** 4619–4631.

Pillet, P., Crubellier, A., Bleton, A., Dulieu, O., Nosbaum, P., Mourachko, I., and Masnou-Seeuws, F.

(1997). Photoassociation in a gas of cold alkali atoms. I: Perturbative quantum approach. *J. Phys. B* **30,** 2801–2820.

Raab, E. L., Prentiss, M., Cable, A., Chu, S., and Pritchard, D. E. (1987). Trapping of neutral sodium atoms with radiation pressure. *Phys. Rev. Lett.* **59,** 2631.

Ratliff, L. P., Wagshul, M. E., Lett, P. D., Rolston, S. L., and Phillips, W. D. (1994). Photoassociative ionization of the 1_g, 0_u^+ and 0_g^- states of Na_2. *J. Chem. Phys.* **101,** 2638–2641.

Rawitscher, G. H., Esry, B. D., Tiesinga, E., J. P. Burke, J., and Koltracht, I. (1999). Comparison of numerical methods for the calculation of cold atom collisions. *J. Chem. Phys.* **111,** 10418–10426.

Sauer, B. E., Wang, J., and Hinds, E. A. (1994). YbF—A new way to measure the electron dipole moment. *Bull. Am. Phys. Soc. Ser. H.* **39,** 1060.

Seaton, M. J. (1983). Quantum defect theory. *Rep. Prog. Phys.* **46,** 167–257.

Seto, J., Vergès, L. J., and Amiot, C. (1995). Direct potential fit analysis of the $X^1\Sigma_g^+$ state of Rb_2: Nothing else will do. *J. Chem. Phys.* **113,** 3067–3076.

Shaffer, J. P., Chalupezak, W., and Bigelow, N. P. (1999). Photoassociative ionization of heteronuclear molecules in a novel two-species magneto-optical trap. *Phys. Rev. Lett.* **82,** 1124–1127.

Spies, N. (1989). Ph. D. thesis. Fachbereich Chemie, Universitat Kaiserslautern.

Stwalley, W. C. (1973). Expectation values of the kinetic and potential energy of a diatomic molecule. *J. Chem. Phys.* **58,** 3867–3870.

Stwalley, W., and Wang, H. (1999). Photoassociation of ultracold atoms: A new spectroscopic technique. *J. Mol. Spectrosc.* **195,** 194–228.

Stwalley, W., Uang, Y., and Pichler, G. (1978). Pure long-range molecules. *Phys. Rev. Lett.* **41,** 1164–1167.

Takekoshi, T., Patterson, B. M., and Knize, R. J. (1999a). Observation of cold ground state cesium molecules produced in a magneto-optical trap. *Phys. Rev. A* **59,** R5–R7.

Takekoshi, T., Patterson, B. M., and Knize, R. J. (1999b). Observation of optically trapped cold cesium molecules. *Phys. Rev. Lett.* **81,** 5105–5108.

Tellinghuisen, J. (1985). The Franck–Condon principle in bound-free transitions. *In* "Photodissociation and Photoionization". (K. P. Lawley, Ed.), pp. 299–369. John Wiley and Sons Ltd. *Advances in Chemical Physics* **60,** 299–369.

Thorsheim, H. R., Weiner, J., and Julienne, P. S. (1987). Laser-induced photoassociation of ultracold sodium atoms. *Phys. Rev. Lett.* **58,** 2420.

Tiesinga, E., Williams, C. J., and Julienne, P. S. (1996). A spectroscopic determination of scattering lengths for sodium atom collisions. *J. Res. Natl. Inst. Std. Technol.* **101,** 505–520.

Tiesinga, E., Williams, C. J., and Julienne, P. S. (1998). Photoassociative spectroscopy of highly excited vibrational levels of alkali dimers: Green's function approach for eigenvalues solvers. *Phys. Rev. A* **57,** 4257–4267.

Timmermans, E., Tommasini, P., Côté, R., Hussein, M., and Kerman, A. (1999a). Rarefied liquid properties of hybrid atomic-molecular Bose-Einstein condensates. *Phys. Rev. Lett.* **88,** 2691–94. 199–230.

Timmermans, E., Tommasini, P., Hussein, M., and Kerman, A. (1999b). Feshbach resonances in atomic Bose-Einstein condensates. *Phys. Rep.* **315,** 199–230.

Townsend, C., Edwards, N., Cooper, C., Zetie, K., Foot, C., Steane, A., Szriftgiser, P., Perrin, H., and Dalibard, J. (1995). Phase-space density in the magneto-optical trap. *Phys. Rev. A* **52,** 1423–1440.

Townsend, C. G., Edwards, N. H., Zetie, K. P., Cooper, C. J., and Foot, C. J. (1996). High density trapping of cesium atoms in a dark magneto-optical trap. *Phys. Rev. A* **53,** 1702–1714.

Trost, J., and Friedrich, H. (1997). WKB and exact wave functions for inverse power-law potentials. *Phys. Lett.* **A228,** 127–133.

Trost, J., Eltschka, C., and Friedrich, H. (1998). Quantization in molecular potentials. *J. Phys. B* **31,** 361–374.

Vala, J., Dulieu, O., Masnou-Seeuws, F., Pillet, P., and Kosloff, R. (2001). Coherent control of cold molecule formation through photoassociation using chirped pulsed laser field. *Phys. Rev. A* **63,** 013412.

Vardi, A., Abrashkevich, D., Frishman, E., and Shapiro, M. (1997). Theory of radiative recombination with strong laser pulses and the formation of ultracold molecules via stimulated photorecombination of cold atoms. *J. Chem. Phys.* **107,** 6166–6174.

Vatasescu, M., Dulieu, O., Amiot, C., Comparat, D., Drag, C., Kokoouline, V., Masnou-Seeuws, F., and Pillet, P. (2000). Multichannel tunneling in the Cs_2 0_g^- photoassociation spectrum. *Phys. Rev. A* **61,** 044701-1-4.

Vatasescu, M., Dulieu, O., Kosloff, R., and Masnou-Seeuws, F. (2001). Toward optimal control of photoassociation of cold atoms and photodissociation of long range molecules: Characteristic times for wavepacket propagation. *Phys. Rev. A* **63,** 033407-1-13.

Veza, D., Beuc, R., Milosevic, S., and Pichler, G. (1998). Cusp satellite bands in the spectrum of Cs_2 molecule. *Eur. Phys. J. D* **2,** 45–52.

Vigué, J. (1982). Semiclassical approximation applied to the vibration of diatomic molecules. *Ann. Phys. Fr* **3,** 155–192.

Volz, U., and Schomoranzer, H. (1996). Precision lifetime measurements on alkali atoms and on helium by beam gas laser spectroscopy. *Physica Scripta* **65,** 48–56.

Wang, H., Gould, P. L., and Stwalley, W. (1996). Photoassociative spectroscopy of ultracold ^{39}K atoms in a high density vapor-cell magneto-optical trap. *Phys. Rev. A* **53,** R1216–R1219.

Wang, H., Gould, P. L., and Stwalley, W. (1997). Long-range interaction of the $^{39}K(4s)+^{39}K(4p)$ asymptote by photoassociativespectroscopy. I. the 0_g^- pure long-range state and the long-range potential constants. *J. Chem. Phys.* **106,** 7899–7912.

Wang, H., and Stwalley, W. (1998). Ultracold photoassociative spectroscopy of heteronuclear alkali-metal diatomic molecules. *J. Chem. Phys.* **108,** 5767–71.

Wang, X., Wang, H., Gould, P. L., Stwalley, W., Tiesinga, E., and Julienne, P. S. (1998). First observation of the pure long range 1_u state of an alkali dimer by photoassociative spectroscopy. *Phys. Rev. A* **57,** 4600–4603.

Weiner, J., Bagnato, V. S., Zilio, S. C., and Julienne, P. S. (1999). Experiments and theory in cold and ultracold collisions. *Rev. Mod. Phys.* **71,** 1–86.

Weinstein, J. D., deCarvalho, R., Guillet, T., Friedrich, B., and Doyle, J. M. (1998). Magnetic trapping of calcium monohydride molecules at millikelvin temperatures. *Nature* **395,** 148.

Winans, J., and Stueckelberg, E. C. G. (1928). The origin of the continuous spectrum of the hydrogen molecule. *Proc. Natl. Acad. Sci. USA* **14,** 867–871.

Wynar, R., Freeland, R. S., Han, D. J., Ryu, C., and Heinzen, D. J. (2000). Molecules in a Bose-Einstein condensate. *Science* **287,** 1016.

Zinner, G., Binnewies, T., Riehle, F., and Tiemann, E. (2000). Photoassociation of cold Ca atoms. *Phys. Rev. Lett.* **85,** 2292–2295.